Università degli Studi di Catania

Facoltà di Scienze Matematiche, Fisiche e Naturali

Dipartimento di Matematica e Informatica

Dottorato di ricerca in Matematica Applicata

XXV Ciclo

Subbands models for semiconductors based on the Maximum Entropy Principle

Vito Dario Camiola

Advisor
Prof. Vittorio Romano

Anno Accademico 2011-2012

UNIVERSITÁ DI CATANIA

Subbands model for semiconductors based on the Maximum Entropy Principle

by

Vito D. Camiola

A thesis submitted in partial fulfillment for the degree of Doctor of Philosophy

in the

Dipartimento di Matematica ed Informatica

December 2012

"Cum fulminis impetus uires suas expandere dedignetur in uirgulam, uerum audaces prouectarum arborum expugnet excessus, imperiosa uenti rabies iras non expendat in calamum, uerum in altissimarum supercilia reurum uesani flatus inuectiones excitet furiosas, per uitiosam nostri operis humilitatem inuidie flamma non fulminet, nostri libelli depressa pauperiem detractionis flatus non deprimat, ubi potius miserie naufragium, misericordie portum expostulat , quam felicitas liuoris exposcat aculeum. In quo lector non latratu corrixationis insaniens, uerum limam correctionis emendans, circumcidat superfluum et compleat diminutum quatenus illimatum revertatur ad limam, impolitum reducatur ad fabricam, inartificiosum suo referatur artifici, male tortum proprie reddatur incudi. Sed quamuis artificii enormitas imperitiam accuset artificiis, in adulterino opere imperitie uestigium manus relinquat opificis, opus tamen sui ueniam deprecatur erroris, cum tenuis humane rationis igniculus multis ignorantie obnubiletur erroribus, humani ingenii scintilla multas erroris euanescat in nebulas. "

Alanus de Insulis, Anticlaudianus

"Whenever I look at any quantum-mechanical calculation, the basic craziness of what we are doing rises in my gorge and I have to stop and try to find some different way of looking at the problem, that makes physical sense."

E.T. Jaynes

"Probability theory is nothing but common sense reduced to calculation."

Laplace

Acknowledgements

First of all I want to thank my advisor Prof. Vittorio Romano for his scientific competence, for his ability to teach and, above all, for his patience. Without his trust, I would not have ever begun my PhD studies.
I want to thank Dr. Giovanni Mascali for his professionalism. It was a pleasure to work together.
Thanks to Prof. Ferdinand Schürrer and to all members of his group for the hospitality at the Institute of Theoretical an Computational Physics of the University of Graz.
Special thanks to Dr. Jole Costanza who has made our office a better place in these last years.
I thank my family for the moral support during the long period of studies and, at the end but not the less important, thanks to my little four years old nephew Giordana who permitted me to write this thesis during my homework.

Contents

List of Figures

List of Tables

Dedicated to Giordana

Preface

In 1948 W. Shockley, W. Brattain and J. Bardeen realized the first transistor at the Bell laboratories and in 1958 Jack Kilby, an engineer at the Texas Instrument, announced the creation of the first integrated circuit. From then on progressing in electronic engineering means miniaturizing.

By continuing to shrink the dimension of electronic devices, effects of quantum confinement becomes more and more relevant. In particular, in this thesis, I will deal with double gate MOSFETs (hereafter DG-MOSFETs) and MOSFETs.

In a DG-MOSFETs the potential between the two gates and the oxide layers confines the electrons in the transversal direction, producing a quantum well whose length is comparable with the de Broglie wavelength. A similar effect is also present in hetero-structures like AlGa-Ga. For a comprehensive review the reader is referred to [28, 63, 65].

In a purely quantum approach, electric properties of nanoscale devices, like current-voltage curves, can be computed via the non-equilibrium Green function [44, 45]. Another way to tackle the problem is in the framework of quantum kinetic theory via the Wigner function, which gives the macroscopic physical quantities of interest as expectation values [46–48]. Other approaches are based on the master equation [49]. However, in structures like DG-MOSFETs, one has a confining effect in one direction, that transversal to the oxide, while in the other directions the electrons flow from the source to the drain. The electron transport can be treated semiclassically when the typical longitudinal length is of the order of a few tenths of nanometers. In fact, in these conditions the electrons as waves achieve equilibrium along the confining direction in a time which is much shorter than the typical transport time, so that one can adopt a quasi-static description along the confining direction by a coupled Schrödinger-Poisson system which leads to a subband decomposition. The transport along the longitudinal direction is described by a semiclassical Boltzmann equation for each subband. Numerical integration of the Boltzmann-Schrödinger-Poisson system has been performed with Monte-Carlo methods or deterministic schemes for solving the transport part [30, 31, 33–35, 66], but they are very expensive, from a computational point of view, for computer aided design (CAD) purposes. This has prompted to substitute the Boltzmann equations with

macroscopic models like drift-diffusion or energy-transport ones [36, 38].
Here, in order to describe the electron transport, we use an energy transport model which is deduced, under a suitable diffusion scaling, from a system of equations derived from the Boltzmann equations by using the moment method. The moment equations are closed by resorting to the maximum entropy principle (MEP) [19], and take into account scattering of electrons with acoustic and non polar optical phonons. The results fit into the framework of extended thermodynamics [67, 68]. After the formulation of an appropriate numerical scheme for the energy transport-Schrödinger-Poisson system, the simulation of a nanoscale silicon DG-MOSFET is presented in order to validate the model and the robustness of the numerical scheme. DG-MOSFET with its extra gate is considered as one of the most appropriate structures for minimizing the short channel effects in nanometer devices, which deteriorate the transistor performance. This is due to the enhanced gate control (two gates) over the channel and to the reduced silicon layer thickness.
The results have been published and can be found in

- Camiola, V.D., Mascali, G., Romano, V.: Numerical simulation of a double-gate MOSFET with a subband model for semiconductors based on the maximum entropy principle, Continuum Mechanics and Thermodynamics, **24** (2012)
- Camiola, V.D., Mascali, G., Romano, V.: Simulation of a double-gate MOSFET by a non-parabolic energy-transport subband model for semiconductors based on the maximum entropy principle, Mathematical and Computer Modelling (2012)

The other device examined in this thesis by the method reviewed above is the MOSFET. At variance with DG-MOSFET the symmetry of the geometric disposition of the oxide at the two gates is no longer present. Under the gate oxide, in the channel of the device, there is still a quantization in the transversal direction forming a 2D electron gas but far from such a region electrons are 3D. Therefore one has to include the coexistence of both 2D and 3D electron gas inside the channel and only 3D electrons in the remaining part.
A crucial point is how to take into account the transition of electrons from the 3DEG to the 2DEG. In principle one should calculate the relative transition rate by using the Fermi golden rule, but this requires to solve the Schrödinger equation and becomes too involved to be applied in the formulation of a hydrodynamical or energy-transport model.
I overcome such a problem inspired by the procedure used in [18]. If an electron belonging to the 2DEG gains an energy above a threshold value after a scattering, it is considered as 3D and vice versa if a 3D electron gets an energy below a threshold value after an

emission process it is considered into the 2DEG.
The model here exposed has been extracted by the preprint

- Camiola, V.D., Romano, V.: 2DEG-3DEG charge transport model for mosfet based on the Maximum Entropy Principle, (submitted)

The plan of the thesis is the following. In chapter 1 an overview of semiconductor band structure and of the Boltzmann equation is given. In chapter 2 the Maximum Entropy Principle (MEP) is presented in a general way focusing the attention on its meaning as method of inference. The original part is exposed in chapters 3 and 4. In Chapter 3 the transport model for the DG-MOSFET is developed taking into account both parabolic and Kane dispersion relations for energy. In chapter 4 the MOSFET is examined.

Chapter 1

Band structure and Boltzmann equation

In this chapter I will give a short overeview regarding the solid state physics of the semiconductors and some properties of the Boltzmann equation that is the start point for describing the semi classic transport. The reader is referred to the bibliography for more details [1–3].

1.1 Crystal structure

The structure of a solid is given by a periodic repetition of a set of atoms, named *basis*, in the three dimensional space. In this way a three dimensional crystal lattice is formed and its translational periodicity is defined by three non complanar vectors $\mathbf{a}_1, \mathbf{a}_2, \mathbf{a}_3$ such that the crystal remains identical if translated by a vector

$$\mathbf{T} = n_1\mathbf{a}_1 + n_2\mathbf{a}_2 + n_3\mathbf{a}_3, \quad n_1, n_2, n_3 \in \mathbb{Z}.$$

The vectors $\mathbf{a_1}, \mathbf{a_2}, \mathbf{a_2}$ and the set

$$L = \{\mathbf{T} = n_1\mathbf{a}_1 + n_2\mathbf{a}_2 + n_3\mathbf{a}_3 : n_1, n_2, n_3 \in \mathbb{Z}\} \subset \mathbb{R}^3$$

are called respectively *primitive vectors* and *Bravais Lattice*.
The *primitive cell* of L is a connected set $D \subset \mathbb{R}^3$ whose volume equals the volume of the parallelepiped spanned by the basis vectors $vol(D) = \mathbf{a}_1\dot{(}\mathbf{a}_2 \times \mathbf{a}_3)$ [1] and the whole space occupied by the solid is covered by the union of translates of D by the primitive

[1] the symbol "$\times$" denotes the vector product

vectors. In particular, the special primitive cell

$$D = \left\{ x \in \mathbb{R}^3 : x = \sum_{n=1}^{3} \alpha_n \mathbf{a}_n, \alpha_n \in \left[-\frac{1}{2}, \frac{1}{2} \right] \right\}$$

is called *Wigner-Seitz cell*.

The *reciprocal lattice* L^* of L is defined by

$$L^* = \{ \mathbf{G} = n_1 \mathbf{a}_1^* + n_2 \mathbf{a}_2^* + n_3 \mathbf{a}_3^* : n_1, n_2, n_3 \in \mathbb{Z} \}$$

where the *primitive vectors* $\mathbf{a}_1^*, \mathbf{a}_2^*, \mathbf{a}_3^* \in \mathbb{R}^3$ are the dual basis given by

$$\mathbf{a}_1^* = 2\pi \frac{\mathbf{a}_2 \times \mathbf{a}_3}{\mathbf{a}_1 \cdot \mathbf{a}_2 \times \mathbf{a}_3}; \quad \mathbf{a}_2^* = 2\pi \frac{\mathbf{a}_3 \times \mathbf{a}_1}{\mathbf{a}_1 \cdot \mathbf{a}_2 \times \mathbf{a}_3}; \quad \mathbf{a}_1^* = 2\pi \frac{\mathbf{a}_1 \times \mathbf{a}_2}{\mathbf{a}_1 \cdot \mathbf{a}_2 \times \mathbf{a}_3}$$

satisfying the relation $\mathbf{a}_m \mathbf{a}_n^* = 2\pi \delta_{mn}$ with $m, n = 1, 2, 3$.

According to the previous definitions, the volume of the reciprocal primitive cell is $vol(D) = \mathbf{a}_1^* \dot{(} \mathbf{a}_2^* \times \mathbf{a}_3^*)$, while the Wigner-Seitz cell of the reciprocal lattice is

$$B = \left\{ \mathbf{k} \in \mathbb{R}^3 : \mathbf{k} = \sum_{n=1}^{3} \beta_n \mathbf{a}_n^*, \beta_n \in \left[-\frac{1}{2}, \frac{1}{2} \right] \right\} \tag{1.1}$$

and is called the first *Brillouin zone*.

To understand these definitions it is useful to review the physics of X-waves diffraction used to investigate the crystal structure.

Because of the periodicity of the crystal, the electron number density $n(\mathbf{r})$ is a periodic function of the position $\mathbf{r}$

$$n(\mathbf{r} + \mathbf{T}) = n(\mathbf{r})$$

so it is possible a Fourier expansion

$$n(\mathbf{r}) = \sum_{\mathbf{G}} n_{\mathbf{G}} \exp(i \mathbf{G} \cdot \mathbf{r})$$

where G's are points in the reciprocal lattice and

$$n_{\mathbf{G}} = \frac{1}{vol(D)} \int_D n(\mathbf{r}) \exp(-i \mathbf{G} \cdot \mathbf{r}) \, d^3\mathbf{r}.$$

Now let us consider the X-ray reflections by the crystal lattice.

Let $\mathbf{k}$ and $\mathbf{k}'$ be the wavevectors of the incoming and outgoing beams. In general the amplitude of the electric or magnetic field vectors in the scattered electromagnetic wave is proportional to the following *scattering amplitude*

$$F = \int n(\mathbf{r}) \exp(-i \Delta \mathbf{k} \cdot \mathbf{r}) \, d^3\mathbf{r}$$

where $\Delta\mathbf{k} = \mathbf{k} - \mathbf{k}'$.
Replacing $n(\mathbf{r})$ with its Fourier expansion, one obtains

$$F = \sum_{\mathbf{G}} \int n_{\mathbf{G}} \exp[i(\mathbf{G} - \Delta\mathbf{k}) \cdot \mathbf{r}] \, d^3\mathbf{r}.$$

F is negligible when $\Delta\mathbf{k}$ differs significantly from any reciprocal lattice vector and has its maximum when

$$\Delta\mathbf{k} = \mathbf{G}. \tag{1.2}$$

Considering elastic scattering, the phonon energy $\hbar\omega$ is conserved so the frequency $\omega' = ck'$ of the emergent beam is equal to the frequency of the incident beam and $k^2 = k'^2$. From 1.2 the *diffraction condition* is written as $(\mathbf{k} + \mathbf{G})^2 = k^2$ or

$$2\mathbf{k} \cdot \mathbf{G} + G^2 = 0. \tag{1.3}$$

Considering that if $\mathbf{G}$ is a reciprocal lattice vector, so is $-\mathbf{G}$, from 1.3 we obtain the general form of the well known *Bragg condition*

$$2\mathbf{k} \cdot \mathbf{G} = G^2.$$

Starting from this relation, it is possible to construct the *first Brillouin zone* 1.1 that is *the smallest volume entirely enclosed by planes that are the perpendicular bisectors of the reciprocal lattice vectors drawn from the origin* (see [1] for the details).

1.2 The energy band structure

Because of the quantum wave behavior, the energy structure of the semiconductors, as the X-rays diffraction, is strictly correlated with the periodicity of the crystal lattice.
In semiconductors the dynamics of one electron is described by the time dependent Schrödinger equation

$$i\hbar \frac{\partial}{\partial t} \Psi(\mathbf{r}, t) = H\Psi(\mathbf{r}, t)$$

with

$$H = -\frac{\hbar^2}{2m}\Delta - qV(\mathbf{r}).$$

where $V(\mathbf{r})$ is the potential due to the crystal displacement. Impurities and many particles effects are necessary for a more realistic description in the case of low temperatures and high densities and not will be considered here.
Assuming the ansatz $\Psi(\mathbf{r}, t) = \psi(\mathbf{r})e^{-i\frac{Et}{\hbar}}$, the *time indipendent* or *stationary* Schrödinger

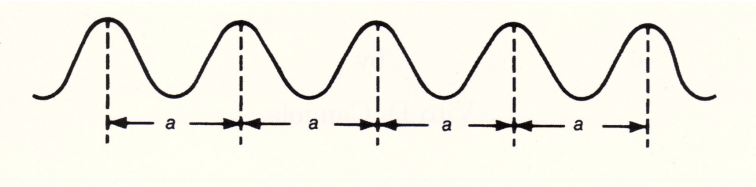

FIGURE 1.1: schematic one dimensional representation of the potential in a crystal lattice.

equation is obtained

$$H\psi(\mathbf{r}) = E\psi(\mathbf{r}) \tag{1.4}$$

with $E \in \mathbb{R}$.

Regarding $V(\mathbf{r})$, let us consider a one dimensional periodic potential (fig. 1.1), so

$$V(x \pm a) = V(x).$$

We will adopt the Dirac notation and the translation operator $\tau(a)$ which satisfies

$$\tau^\dagger(a)x\tau(a) = x + a, \quad \tau(a)|x' >= |x' + a >$$

and

$$\tau^\dagger(a)V(x)\tau(a) = V(x + a) = V(x)$$

The whole hamiltonian is invariant for translational operation

$$\tau^\dagger(a)H\tau(a) = H \quad \text{or} \quad [H, \tau(a)] = 0,$$

hence H and τ can be diagonalized together. Observing that τ is unitary but non hermitian, it is possible to conclude that its eigenvalues will be complex numbers with modulus equals to one.

Let $|n >$ be the ket for an electron in the n-th cell (see fig. 1.1) with the property $\tau(a)|n >= |n + 1 >$ $(n \in \mathbb{Z})$ so that the wave function $< x'|n >$ is not zero in the n-th cell and in its neighbors. Let us suppose that

$$< n|H|n >= E_0, \qquad E_0 \in \mathbb{R}$$

and

$$< n'|H|n > \neq 0 \iff n' = n \quad \text{or} \quad n' = n \pm 1.$$

In particular we assume the *tight binding approximation* and define

$$< n \pm 1|H|n >= -\delta, \qquad \delta \in \mathbb{R}$$

it follows

$$H|n>= E_0|n> -\delta|n+1> -\delta|n-1> .$$

The ket

$$|\theta>= \sum_{n=-\infty}^{+\infty} e^{in\theta}|n>,$$

with $\theta \in [-\pi, \pi]$, is an eigenket of $\tau(a)$ and H, in fact

$$\begin{aligned} \tau(a)|\theta> &= \sum_{n=-\infty}^{+\infty} e^{in\theta}|n+1>= \sum_{n=-\infty}^{+\infty} e^{i(n-1)\theta}|n>= e^{-i\theta}|\theta> \\ \text{and} & \\ H|\theta> &= E_0 \sum_{n=-\infty}^{+\infty} e^{in\theta}|n> -\delta \sum_{n=-\infty}^{+\infty} e^{in\theta}|n+1> -\delta \sum_{n=-\infty}^{+\infty} e^{in\theta}|n-1>= \\ &= E_0 \sum_{n=-\infty}^{+\infty} e^{in\theta}|n> -\delta \sum_{n=-\infty}^{+\infty} \left(e^{in\theta-i\theta} + e^{in\theta+i\theta}\right)|n>= \\ &= (E_0 - 2\Delta\cos\theta) \sum_{n=-\infty}^{+\infty} e^{in\theta}|n> \end{aligned}$$

Let us observe that

$$< x'|\tau(a)|\theta >=< x'-a|\theta >$$

and

$$< x'|\tau(a)|\theta >=< x'|\theta > e^{-i\theta}.$$

so $< x'-a|\theta >=< x'|\theta > e^{-i\theta}$.
The solution of this equation is

$$< x'|\theta >= e^{ikx'} u_k(x')$$

with $\theta = ka$ and $u_k(x')$ a periodic function with period a.
At the end it is possible to conclude that the solution of 1.4 is a plane wave function modulated by u_k with $k \in \left[-\frac{\pi}{a}, \frac{\pi}{a}\right]$ and the eigenvalue of the energy $E(k)$ depends on k. This discussion, developed in [4], can be considered a motivation for the following

Theorem 1.1. *Bloch theorem [2]*
Let V_L be a a periodic potential, i.e.,$V_L(\mathbf{x}+\mathbf{y}) = V_L(\mathbf{x})$ for all $x \in \mathbb{R}^3$ and $\mathbf{y} \in L$ (the Bravais lattice). Then the eigenvalue problem for the Schrödingier operator

$$H = -\frac{\hbar^2}{2m}\Delta - qV_L(x), \quad x \in \mathbb{R}^3,$$

can be reduced to an eigenvalue problem of the Schrödingier equation on the primitive cell D of the lattice, indexed by $k \in B$ (the Brillouin zone),

$$H\Psi = E\Psi \quad in\, D, \quad \Psi(x+y) = e^{ik\cdot y}\Psi(x), \quad x \in D,\, y \in L. \tag{1.5}$$

For each $k \in B$, there exist a sequence $E_n(k)$, $n \geq 1$, of eigenvalues with associated eigenfunctions $\Psi_{n,k}$. The eigenvalues $E_n(k)$ are real function of k and periodic and symmetric on B. The spectrum of H is given by the union of the closed intervals $\left\{E_n(k) : k \in \bar{B}\right\}$ for $n \geq 1$ (with $\bar{B}$ being the closure of B).

The eigenfunction, called *Bloch functions*, of 1.5 can be written as

$$\Psi_{n,k}(x) = e^{ik\cdot x}u_{n,k}(x), \quad x \in D,\, k \in B$$

and they are plane waves modulated by the periodic function $u_{n,k}$. k is termed *pseudo-wave vector*.
Inserting the above expression in the Schrödingier equation, it is possible to see that $u_{n,k}$ is solution of

$$-\frac{\hbar^2}{2m}\left(\nabla u_{n,k} + 2ik\cdot\Delta u_{n,k}\right) + \left(\frac{\hbar^2}{2m}k^2 - qV_L(x)\right)u_{n.k} = E_n(k)u_{n,k}$$

with the periodic boundary conditions

$$u_{n,k}(x+y) = u_{n,k}(x), \quad x \in \mathbb{R}^3,\, y \in L.$$

$E_n(k)$ is an even function of k called the *dispersion relation* and the set $\{E_n(k) : k \in B\}$ the nth *energy band*. The union of ranges of E_n over $n \in \mathbb{N}$ is not necessary the whole real line $\mathbb{R}$, i.e. there may exist energies E^* for which there is non number $n \in \mathbb{N}$ and no vector $k \in B$ such that $E_n(k) = E^*$. The connected components of the set of energies with this non-existence property are called *energy gaps*.
It is important to remark that the quantity $\hbar\mathbf{k}$ is not in general the momentum of the electron, but reduces to it only in the free case ($V_L = 0$). Because its relation to the periodicity of the crystal, $\hbar\mathbf{k}$ is called *crystal momentum*.
The collection of the bands gives the band structure of the material.
In general ,on account of the Pauli exclusion principle, N electrons inside the crystal are distributed occupying different states corresponding to those with the lowest available energies. In the single electron approximation each state is an eigenstate corresponding to a $\Psi_{n,\mathbf{k}}$ solution of the Schrödinger equation.
At zero temperature the N electrons occupy the N lowest energy states (indeed we should take into account also the spin, but for simplicity we ignore it). The Fermi

energy ε_F at zero temperature is the energy of the highest occupied energy state in the single electron scheme.
Two cases may occur:

- A certain set of bands is completely filled while the remaining ones are empty, that is the Fermi energy does not fall inside a band. In this case the differences between the energy of the highest occupied level and the energy of the lowest unoccupied level is known as *band gap* ε_G. If ε_G is of order of 2 to few eV the solid is an *insulator* while if ε_G is between 0.1 and 2 eV the solid is a *semiconductors*. Of course the distinction between insulator and semiconductors is not sharp. The energy bands below ε_F are called valence bands because determine the chemical bindings, those above ε_F are called conduction bands because are responsible for the electrical conduction property of the material .

- Some bands are partially filled, that is the Fermi energy, lies within the range of one or more bands. The electrons have infinite states which are available with an energy close to ε_F. In this case the solid is a *conductor*.

Semiconductors therefore are characterized by a sizable energy gap between the valence and the conduction bands, which are almost fully filled at the thermal equilibrium. Upon thermal excitation electrons from the valence band can jump to the conduction band leaving behind vacancies in the valence bands. These vacancies are in turn available free states, the electrons in the valence bands may move to. This generates a motion of vacancies similar to that of positively charged particles that are named *holes* in the language of quasi-particles. Thus the transport of charge is achieved through both negatively charged (electrons) and positively charged (holes) carriers.
The creation of electron-hole pairs by thermal excitations increases with the temperature and as consequence the conductivity is an increasing function of the temperature.
Usually in the crystal are present impurities, a small percentage of foreign atoms. If these can be positively ionized additional free electron are provided to the conduction band while if these are negatively ionized additional holes are created in the valence bands. The impurities of the first type are called *donors*, those of the second type are called *acceptors*.
A semiconductor with a negligible presence of impurities is said *intrinsic*. Instead we speak about extrinsic semiconductor of *n-type* or *p-type* if the impurities are prevalently donors or acceptors.
The energy band structure of crystals depend on the explicit form of the potential V_L whose determination is one of the most stringent problem in solid state physics. For the most common semiconductors the energy band structure has been obtained at the cost

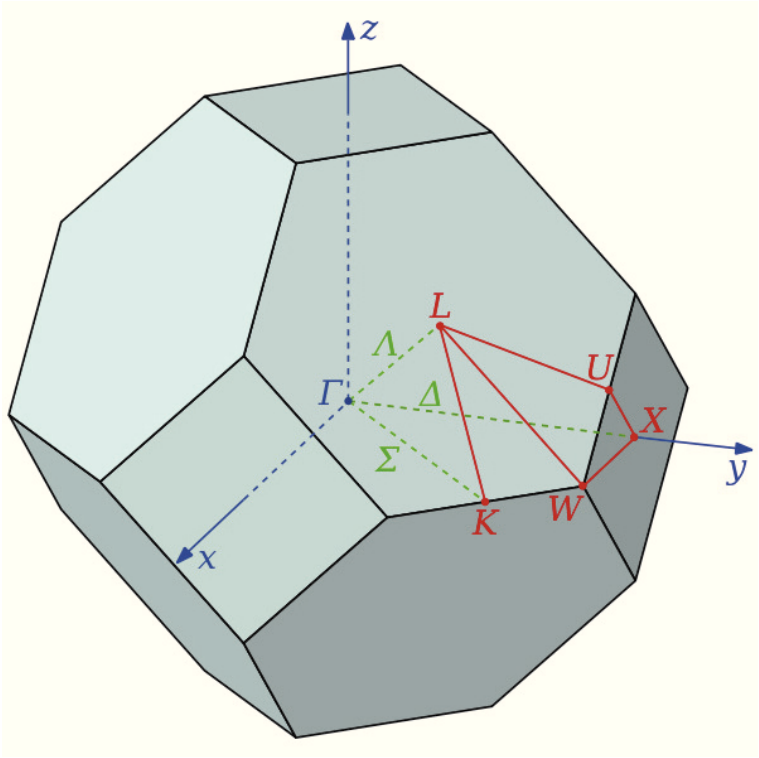

FIGURE 1.2: Silicon Brillouin zone.

of intensive numerical calculations and also semiphenomenologically by quantum theory of solids, e.g. with the pseudo potentials.
In the next section the energy band structure of the Si will be examined in view of the application in this thesis.

1.3 The Si band structure and the semi-classical picture

The crystal has the diamond structure with cubic symmetry and therefore the first Brillouin zone has the shape of a truncated octahedron (fig 1.2). There are essentially three conduction bands and three valence bands (fig. 1.3). The energy gap is about 1.1 eV. The lowest conduction band has six related minima along the main crystallographic directions Δ at about 85% from the center of the first Brillouin zone, near the X points [1]. The valence band minimum occurs at $k = 0$, where two degenerates bands meet giving rise to *light holes* and *yeavy holes*. The third valence band (the split-off band) has a maximum at 0.044 eV below the valence band maximum.
However, in order to describe electron transport, for most applications, a simplified description of the energy bands is adopted. It based on a simple analytical approximations. Let us consider only the conduction bands. At normal operating device conditions, it is sufficient to take into account only the lowest conduction band, because the others

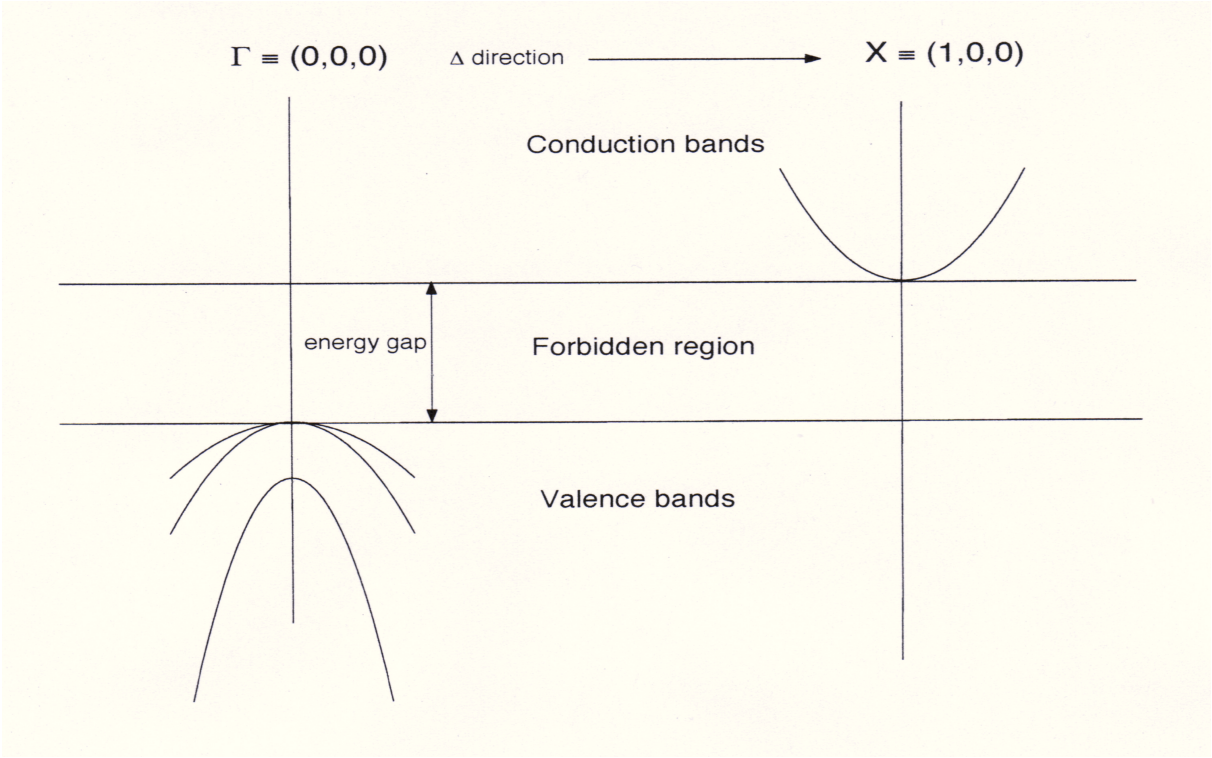

FIGURE 1.3: A schematic representation of the silicon band structure along some crystallographic directions ($E(k)$ versus k in arbitrary units). There are reported the valence bands and the valley of the condition bands around the minima near the X points. For reason of symmetry the band structure presents six X-balley. Note the presence of the maximum at the Γ point in the valence bands. The conduction bands for holes are obtained from those of valence by reversing the sign.

are scarcely populated. Moreover, the electrons in this band are essentially located in the neighboroods of the lowest energy local minima, the so-called *valleys*, e.g. Si has six valleys termed as X-valleys.

The energy-wavevector relation in the neighborhood of the A-th extremum can be approximated by a quadratic form. Assuming k_0 as a minimum point, $\nabla_k E_n(k_0) = 0$, and that the energy values are shifted in such a way that $E_n(k_0) = 0$. Let us also suppose $E_n(0) = 0$, the Taylor expansion is

$$\begin{aligned} E_n(k) &= E_n(0) + \nabla E_n(0) \cdot \mathbf{k} + \frac{1}{2}\mathbf{k}^T \left(\frac{d^2 E_n}{dk^2}(0) \right) \mathbf{k} + O(k^3) \\ &= \frac{\hbar^2}{2} \left(\frac{k_1^2}{m_1^*} + \frac{k_2^2}{m_2^*} + \frac{k_3^2}{m_3^*} \right) + O(k^3) \quad \text{for} \quad k \to 0 \end{aligned}$$

where $k = (k_1, k_2, k_3)^T$ and $O(k^3)$ denotes terms of order k^3. m^* is the *effective mass tensor* defined by

$$\frac{1}{m^*} = \frac{1}{\hbar^2} \frac{d^2 E_n}{dk^2}.$$

In this thesis it is assumed that $m^* = m_1^* = m_2^* = m_3^*$.
In the *parabolic band approximation* the dispersion relation is assumed to be

$$E(k) = \frac{\hbar^2}{2m^*}k^2$$

where now $\mathbf{k}$ is assumed to vary in all $\mathbb{R}^3$.
In order, if one considers higher applied field in the Si-devices, the electron energy is more appropriately described by the *Kane dispersion relation*

$$E(k)[1 + \alpha E(k)] = \frac{\hbar^2 k^2}{2m^*}$$

where α is the *non-parabolicity* parameter (for Silicon $\alpha = 0.5eV^{-1}$ for each X-valley).
The anisotropic version is

$$E(k)[1 + \alpha E(k)] = \frac{\hbar^2}{2}\left[\frac{k_1^2}{m_1^*} + \frac{k_2^2}{m_2^*} + \frac{k_3^2}{m_3^*}\right].$$

In the semiclassical picture considered in this thesis the wave packets are assumed to be highly localized and the electron is considered as a particle whose velocity is identified with the group velocity of the wave packet. It is possible to show that the electron velocity $\mathbf{v}(\mathbf{k})$ in a generic band depends on the energy $E(k)$ measured from the conduction band minimum by the relation

$$\mathbf{v}(\mathbf{k}) = \frac{1}{\hbar}\nabla_{\mathbf{k}}E.$$

Explicitly in the conduction band we get in the parabolic case

$$\mathbf{v} = \frac{\hbar\mathbf{k}}{m^*}$$

while for the Kane dispersion relation

$$\mathbf{v} = \frac{\hbar\mathbf{k}}{m^*\left[1 + 2\alpha E(k)\right]}.$$

1.4 The Boltzmann equation

The Boltzmann equation has been the first function to describe the evolution of a distribution in the history of the science and is the background for the development of the semiclassical charge transport model that is going to be described.
Let us consider an electron gas of N particles. The distribution function $f(\mathbf{r}, \mathbf{k}, t)$ furnishes the the number of particles in the space volume $d\mathbf{r}$ around $\mathbf{r}$ and in the moment

volume $d\mathbf{k}$ around $\mathbf{k}$. Assuming the normalization condition

$$\int d\mathbf{r} \int d\mathbf{k} f(\mathbf{r}, \mathbf{k}, t) = N,$$

$\int d\mathbf{k} f(\mathbf{r}, \mathbf{k}, t) = n(\mathbf{r}, t)$ is the particle density at time t.
The semiclassical Boltzmann equation for electrons in the conduction band is

$$\frac{\partial f}{\partial t} + \mathbf{v}(\mathbf{k}) \nabla f - \frac{e}{\hbar} \mathbf{E} \nabla_{\mathbf{k}} f = C[f] \tag{1.6}$$

where $\mathbf{v}$ is the velocity of the electron, $\mathbf{E}$ the electric field and $C[f]$ is the collisional term that describes the electrons scattering.
The scattering mechanism we will deal with is only the electron-phonon interaction, non considering electron-electron interaction, impurities and roughness effects.
At nonzero temperature the crystal ions vibrate around the equilibrium position represented by the point of the ideal Bravais lattice. Several normals modes can be exited in the lattice. The modes with a dispersion relation like that of the acoustic wave form the acoustic branches. The modes that can interact with electromagnetic radiation and characterize the optical properties of the material form the optical branches [3]. The transport of energy in the dielectric solid is described in the quantum theory of crystal as quasi-particle called phonons. At equilibrium, they obeys the Bose-Einstein distribution

$$N_B = \frac{1}{e^{\frac{\hbar\omega}{K_B T_L}} - 1}$$

where $T_L$is the lattice temperature and $\hbar\omega$ stands for the phonon energy.
The interaction with the phonons produce a change in the energy and momentum of the electrons. Therefore if initially an electron had a wave vector $\mathbf{k}$, after the collision its wave vector will be $\mathbf{k}'$. The exchange of energy can leave the electron in the same band (*intraband transition*) or pull it into another band (*inter band transition*).
In the conduction bands the electrons are essentially located in the valleys. After a collision the electron can remain in the same valley (*inter valley scattering*) or be drawn in another valley (*inter valley scattering*).
The expression for the collision term is obtained by the *Fermi's golden rule*.
For a generic intravalley or intraband interaction $C[f]$ can be written as

$$C[f] = \int_B \left[P(\mathbf{k}', \mathbf{k}) f(\mathbf{k}')(1 - f(\mathbf{k})) - P(\mathbf{k}, \mathbf{k}') f(\mathbf{k})(1 - f(\mathbf{k}')) \right] d^3\mathbf{k} \tag{1.7}$$

B is the first Brillouine zone, $P(\mathbf{k}, \mathbf{k}')$ is the transition probability from the state $\mathbf{k}$ to the state $\mathbf{k}'$. The first term in (1.7) represents the gain, that is the number of electron that are scattered in the state of wave vector $\mathbf{k}$. It is assumed to be proportional to $f(\mathbf{k}')$ and to $1 - f(\mathbf{k})$ on account of the Pauli exclusion principle. With analogous meaning,

the second term is the loss.
Under the assumption that the electron gas is dilute the collision operator can be linearized with respect to f and becomes

$$C[f] = \int_B \left[P(\mathbf{k}', \mathbf{k}) f(\mathbf{k}) - P(\mathbf{k}, \mathbf{k}') f(\mathbf{k}')\right] d^3\mathbf{k}. \tag{1.8}$$

At equilibrium the electron distribution must obey the Fermi-Dirac statistic

$$f_{eq} = \left[\exp\left(-\frac{E-\mu}{K_B T_L}\right) + 1\right]^{-1}.$$

Substituting it in (1.8), one obtains

$$\int \left[P(\mathbf{k}', \mathbf{k}) f_{eq}(\mathbf{k}') - P(\mathbf{k}, \mathbf{k}') f_{eq}(\mathbf{k})\right] d^3\mathbf{k}' = 0.$$

The *detailed balance principle* affirms that this integral is zero because the integrand is zero, so

$$P(\mathbf{k}', \mathbf{k}) f_{eq}(\mathbf{k}') = P(\mathbf{k}, \mathbf{k}') f_{eq}(\mathbf{k})$$

from which one obtains

$$\frac{P(\mathbf{k}, \mathbf{k}')}{P(\mathbf{k}, \mathbf{k}')} = a^{-\frac{E(\mathbf{k}')-E(\mathbf{k})}{K_B T}}.$$

This result is true in the equilibrium case, but it is assumed true also in the non equilibrium situation.
The transition probabilities for the phonons are given by the following expression:

$$P^{(ac)} = \frac{K_B T_L \Xi_d^2}{4\pi^2 \hbar \rho v_s^2} \delta(E(\mathbf{k}) - E(\mathbf{k}')) \tag{1.9}$$

$$P^{(no)} = Z_f \frac{(D_T K)^2}{8\pi^2 \rho \omega} (N_q + \frac{1}{2} \mp \frac{1}{2}) \delta(E(\mathbf{k}') - E(\mathbf{k}) \mp \hbar\omega) \tag{1.10}$$

respectively for acoustic and non polar optical phonons and with N_q the Bose-Einstein distribution for phonons (for the values of the others parameter see the appendix A).
The minus $(-)$ sign refers to absorption phenomena and plus $(+)$ to emission.
The Boltzmann equation is an integro-differential equation and is a very hard task to solve it both analytically and numerically. In general one is interested not in distribution function but in macroscopic quantity as average electron density, energy velocity etc. and macroscopic models are used to obtains equations for such microscopic quantity.
For this purpose, let us consider a function $\mu_A(\mathbf{k})$, and define the momentum

$$M_A(\mathbf{r}, t) = \int_B \mu_A(\mathbf{k}) f(\mathbf{r}, \mathbf{k}, t) d^3\mathbf{k}. \tag{1.11}$$

By multiplying the equation (1.6) by the function $\mu_A(\mathbf{k})$ and integrating over B, one finds the moment equation

$$\frac{\partial M_A}{\partial t} + \int_B \mu_A(\mathbf{k})\mathbf{v}(\mathbf{k})\nabla_{\mathbf{r}} f d^3\mathbf{k} - \frac{e}{\hbar}\mathbf{E}\int_B \mu_A(\mathbf{k})\nabla_{\mathbf{k}} f d^3\mathbf{k} = \int_B \mu_A(\mathbf{k})C[f]d^3\mathbf{k} \tag{1.12}$$

Since

$$\int_B \mu_A(\mathbf{k})\nabla_{\mathbf{k}} d^3\mathbf{k} = \int_{\partial B} \mu_A(\mathbf{k}) f\mathbf{n} d\sigma - \int_B f\nabla_{\mathbf{k}}\mu(\mathbf{k})d^3\mathbf{k}$$

with $\mathbf{n}$ outward unit normal vector field on the boundary ∂B of the domain B and $d\sigma$ surface element of ∂B, equation (1.12) becomes

$$\frac{\partial M_A}{\partial t} + \nabla_{\mathbf{r}}\int_B f\mu_A(\mathbf{k})\mathbf{v}(\mathbf{k})d^3\mathbf{k} + \frac{e}{\hbar}\mathbf{E}\left[\int_B f\nabla_{\mathbf{k}}\mu_A(\mathbf{k})d^3\mathbf{k} - \int_{\partial B}\mu_A(\mathbf{k})f\mathbf{n}d\sigma\right] \tag{1.13}$$

$$= \int_B \mu_A(\mathbf{k})C[f]d^3\mathbf{k}. \tag{1.14}$$

The last term on the r.h.s. vanishes either when B is expanded to $\mathbb{R}^3$ (because in order to guarantee the integrability condition f must tend to zero sufficiently fast as $k \to \infty$) or when B is compact and $\mu_A(\mathbf{k})$ is periodic and continuos on ∂B. This latter condition is a consequence of the periodicity of f on B and symmetry of B with respect to the origin.

Various models employ different expression of $\mu_A(\mathbf{k})$. For example, let us consider $\mu_A(\mathbf{k}) = 1$,

$$\int_B \frac{\partial f}{\partial t}d^3\mathbf{k} = \frac{\partial}{\partial t}\int_B f d^3\mathbf{k} = \frac{\partial n(\mathbf{r},t)}{\partial t}$$

$$\int_B \nabla_{\mathbf{r}} f(\mathbf{k})\mathbf{v}(\mathbf{k})d^3\mathbf{k} = \nabla_{\mathbf{r}}\int_B f(\mathbf{k})\mathbf{v}(\mathbf{k})d^3\mathbf{k} = \nabla\left(n(\mathbf{r},t)\mathbf{V}(\mathbf{r},t)\right)$$

$$\int_B fC[f]d^3\mathbf{k} = 0$$

wherefrom the continuity equation

$$\frac{\partial n(\mathbf{r},t)}{\partial t} + \nabla\left[n(\mathbf{r},t)\mathbf{V}(\mathbf{r},t)\right] = 0$$

where $\mathbf{V}$ is the *macroscopic (average) velocity*.

Setting $\mathbf{J} = en\mathbf{V}$ (*electric current*) one has the charge conservation

$$\frac{\partial n(\mathbf{r},t)}{\partial t} - \frac{1}{e}\nabla\mathbf{J} = 0. \tag{1.15}$$

Defining other moments it is possible to obtain a system of equations for all the macroscopic quantity which one is interested in.

However other complications emerge from these equations because there are more unknowns than equations (*the closure problem*). For example in 1.15 one has one equation

and two unknowns ($\mathbf{J}$ and n).

The strategy used in this thesis to tackle the problem will be explained in the next chapter.

Chapter 2

Maximum Entropy Principle

The description of a physical system requires the knowledge of some informations, for example the motion of a point particle in classical mechanics requires the knowledge of its instantaneous position and momentum. In the case of a great quantity of particle, i.e. of the order of Avogadro's number ($6,022 \cdot 10^{23}$), the information for a detailed description of the motion of every particle is no more available, so the distribution functions are introduced and statistical methods describe the behavior of the complex systems.
In the context of the Bayesian interpretation of the probability, Jaynes [21, 22] showed as it is possible to develop the Maximum Entropy Principle (hereafter MEP) as an inference method to obtain the results achieved in the context of the statistical mechanics or, in more general terms, in all cases where all the informations useful for a detailed description are lost or not available.

2.1 The Entropy

The term *entropy* was introduced for the first time in classical thermodynamics by Clausius in 1865. It was coined by the old greek $\epsilon\nu$ (inside) and $\tau\rho o\pi\eta$ (transformation) and was used to indicate a thermodynamical potential. Boltzmann, by his famous expression $S = KlogW$, linking the entropy S to a quantity W proportional to the number of micro states of the system, furnished a physical interpretation of the entropy and built a bridge between the macroscopic and the microscopic world.
In 1948 Shannon [23] used the same term to indicate the amount of ignorance about a system in the context of communication theory. The formal expression for this quantity is the same of the statistical Boltzmann entropy in the canonical ensemble and in 1957 Jaynes showed that it is possible to obtain all the expression of the statistical mechanics by maximizing it.

To better understand this last statement it is important to underline that Clausius-Boltzmann entropy is a property of the system while in Shannon-Jaynes point of view it is a property of the knowledge of the observer, so the maximum state of entropy for a system means "the maximum state of ignorance of the observer".

2.1.1 Properties of the Shannon-Jaynes Entropy

Let x be a discrete random variable, $\mathbb{X}$ the countable set of its values $x_1, x_2, ..., x_N$ ($N \in \mathbb{N}$), $p(x_i) = p_i$ ($i = 1, 2, ..., N$) the probability that x assumes the value x_i satisfying of course the condition $\sum_{i=1}^{N} p_i = 1$. The Shannon entropy is

$$S[p] = -k \sum_{i=1}^{N} p_i \log p_i \text{[1]} \tag{2.1}$$

with the assumption $0 \log 0 = 0$ and $k \in \mathbb{R}^+$ a constant depending on the unit to be used [2].
Since the entropy represents the amount of ignorance, it has to satisfy the following properties (or *desiderata* in Jaynes terms [22]):

1. *Entropy is a maximum for equals probabilities*, i. e.

$$S\left(\frac{1}{N}, \frac{1}{N}, ..., \frac{1}{N}\right) \geq S(p_1, p_2, ..., p_N), \quad \text{unless} \quad p_i = \frac{1}{N} \quad \text{for all} \quad i$$

   This means that observer's ignorance must be maximal if all the N outcomes have equal likelihood.

2. *Entropy is unaffected by extra states of zero probability.*

$$S(p_1, p_2, ..., p_{N-1}, 0) = S(p_1, p_2, ..., p_{N-1})$$

   If there is no possibility that an event occurs, then the ignorance is no larger than it would have been if the observer had not included the event in the list of possible outcomes.

3. *The entropy of a system is correlated to the entropy of its parts.*
   This property needs a bit longer explanation.
   Let us consider another random variable y taking its values in the set $\mathbb{X}$ by the

[1] indeed Shannon used $\log_2$ in his definition because he had in mind the two binary states (0 and 1) of the information so that entropy is measured in *bits*, but this detail is not important for the purpose of this thesis

[2] In this paragraph $k = 1$

probability $q(y_l) = q_l$. Let $r_{kl} = P(x_k, y_l)$ be the joint probability for two outcomes x_k and y_l and

$$c_{kl} = P(x_k|y_l) = \frac{P(x_k, y_l)}{q(y_l)} = \frac{r_{kl}}{q_l}$$

the conditional probability. Naturally $\sum_k P(x_k|y_l) = \sum_k c_{kl} = 1$.
If we suppose that the two random variables x and y describe some properties of two interacting systems A and B, the ignorance function related to the the compound system is given by

$$\begin{aligned} S_{(AB)} &= S_{(AB)}(r_{11}, r_{12}, ..., r_{1M}, r_{21}, ..., r_{NM}) \\ &= S_{(AB)}(c_{11}q_1, c_{12}q_2, ..., c_{1M}q_M, c_{21}q_1, ..., c_{NM}q_M) \end{aligned}$$

and the knowledge of one outcome y_l connected with the system B modifies the ignorance regarding the system A by the amount

$$S_{(A|B_l)} = S_{(A|B_l)}(c_{1l}, ..., c_{Nl})$$

so the combined ignorance decreases from $S_{(AB)}$ to $S_{(A|B_l)}$.
At the end the expected ignorance after all the outcomes have been obtained is furnished by the average

$$\langle S_{(A|B)} \rangle_B = \sum_l q_l S_{(A|B_l)}.$$

Introducing the conditional entropy

$$S_{(A|B_l)} = -\sum_l c_{kl} \log c_{kl}$$

one is led to the following result

$$\begin{aligned} S_{(AB)} &= -\sum_{kl} c_{kl}q_l \log(c_{kl}q_l) \\ &= -\left[\sum_{kl} c_{kl}q_l \log(c_{kl}) + \sum_{kl} c_{kl}q_l \log(q_l)\right] \\ &= \sum_l q_l \left[-\sum_k c_{kl} \log(c_{kl})\right] - \sum_l q_l \log(q_l) \left(\sum_k c_{kl}\right) \\ &= \sum_l q_l S_{(A|B_l)} + S(B) = \langle S_{(A|B)} \rangle_B + S_{(B)}, \end{aligned}$$

so

$$S_{(AB)} = \langle S_{(A|B)} \rangle_B + S_{(B)}$$

that is the mathematical expression of the property (3).
In other words taking measures on the system B modifies the observer's knowledge of the system A.

If A and B are uncoupled, the probabilities are uncorrelated so $S_{(A|B_l)} = S_{(A)}$ and $S_{(AB)} = S_{(A)} + S_{(B)}$. The ignorance regarding two uncoupled systems is additive, i. e. *entropy is extensive* (a well know property of the Clausiu-Boltzmann entropy).
If x is a continuous variable one has to substitute the probability p_i with a probability density function $p(x)$ so $p(x)dx$ is the probability that the random variable assumes values in the range $(x, x + dx)$.
An extension of the definition of entropy in the continuum case is the following:

$$S[p(x)] = -\int_{+\infty}^{-\infty} p(x) \log p(x) dx. \tag{2.2}$$

However, this expression is not invariant under a transform of the coordinates systems. To overcome this problem a measure $m(x)$ is introduced in the definition of entropy

$$S[p(x)] = -\int_{+\infty}^{-\infty} p(x) \log \left[\frac{p(x)}{m(x)}\right] dx \tag{2.3}$$

Now, let us consider the transformation $x = f(t)$ the distribution and the measure change according to

$$q(t) = p(x)|f_t'|, \qquad n(t) = m(x)|f_t'|$$

and therefore

$$\begin{aligned} S[p(x)] &= -\int_{-\infty}^{+\infty} q(t) \log \left[\frac{p(x)|f_t'|}{m(x)|f_t'|}\right] dt \\ &= -\int_{-\infty}^{+\infty} q(t) \log \left[\frac{q(t)}{n(t)}\right] dt = S[q(t)] \end{aligned}$$

so the value of S remains unchanged.
Entropy in this last expression is named *relative entropy* [50] and $m(x)$ is considered a probability distribution, in particular Jaynes considers it as " the prior distribution describing the complete ignorance of x" [22] (this last statement will be clear as soon as the maximum entropy principle will be expained).
Another important difference between the continuum and discrete case is given by the fact that 2.1 furnishes the absolute value of the uncertainty, while 2.3 can be used only to calculate the change (increase or decrease) of the uncertainty.

After these considerations, also the discrete form 2.1 is changed in

$$S[p] = -\sum_{i=1}^{n} p_i \log \frac{p_i}{m_i}.$$

2.2 Maximum-entropy inference of a distribution

The properties enumerates before permit to solve the following problem.
Let us consider a random variable x having n possible outcomes $x_1, x_2, ..., x_n$. We know some averages $\langle f_r(x) \rangle = \sum_{i=1}^{n} p_i f_r(x_i), r = 1, 2, .., m$ and want to estimate the corresponding unknown propabilities $p(x_1), p(x_2), ..., p(x_n)$. The solution is given by the maximization of the entropy $S = -\sum_i p_i \log(p_i/m_i)$ under the costraints

$$\sum_i p_i = 1, \quad \text{(normalization condition)}$$
$$\langle f_r(x) \rangle = \sum_i p_i f_r(x_i), \quad r = 1, 2, ..., m$$

Introducing the Lagrange multipliers $\lambda_0, \lambda_r, r = 1, 2, ..., m$, the function to maximize is

$$S' = -\sum_i p_i \log p_i - \lambda_0 \left(\sum_i p_i - 1 \right) - \sum_{r=1}^{m} \lambda_r \left[\sum_i p_i f_r(x_i) - \langle f_r(x_i) \rangle \right].$$

It is simple to proof that the solution is

$$p_i = m_i e^{-\lambda_0 - \sum_{r=1}^{m} \lambda_r f_r(x_i)}.$$

Using the normalizing condition and the other costraints

$$p_i = \frac{m_i}{Z} e^{-\sum_{r=1}^{m} \lambda_r f_r(x_i)},$$
$$\lambda_0 = \log Z$$

where

$$Z = \sum_i e^{-\sum_{r=1}^{m} \lambda_r f_r(x_i)}$$

is the partition function.
Now, assuming x to be some microscopic quantity of a macroscopic physical system, it will be shown how it is possible to obtain all the distributions of the statistical mechanics.

2.3 Distribution function

2.3.1 Maxwell-Boltzmann distribution

Let us consider a system at thermodynamical equilibrium having N particles and a total energy E, our purpose is to determine the number of particle n_i ($\sum_i n_i = N$) occupying the energy level ε_i ($\sum_i \varepsilon_i n_i = E$). In the case of Maxwell-Boltzmann distribution the particles are considered identical and distinguishable, i.e. they obey with a good approximation to the laws of classical mechanics or, in other terms, their wavelength is greater than the Deby wavelenght.
Considering the previous expression, p_i is now the probability that a particle is found to be in one of the G_i energy levels ε_i. Defining the average energy as $\overline{\varepsilon} = E/N$, the constraints read

$$\sum_i p_i = 1$$
$$\sum_i p_i \varepsilon_i = \overline{\varepsilon}.$$

The MEP solution is

$$p_i = \frac{G_i}{Z} e^{\lambda \varepsilon_i} \tag{2.4}$$

whit the partition function

$$Z = \sum_i G_i e^{\lambda \varepsilon_i}$$

I have used the expression of entropy $S = -K_B \sum_i p_i \log p_i$, where K_B is the Boltzmann constant. If $\lambda = 1/K_B T$, 2.4 is the Maxwell-Boltxmann distribution.

2.3.2 Fermi-Dirac and Bose-Einstein distributions

For the quantum statistical distributions the discussion is a little more involved. Here the particles are identical and indistinguishable and the fermions have to obey to Pauli's exclusion principle.
p_{ijn} is the probability that the j-th quantum state of energy level ε_i contains n particles. The average energy particles in energy level ε_i is

$$\langle n_i \rangle = \sum_{j=1}^{G_i} \sum_n p_{ijn} n.$$

The entropy used is

$$S = -\sum_i \sum_{j=1}^{G_i} \sum_n p_{ijn} \log p_{ijn}$$

and the costraints

$$\sum_n p_{ijn} = 1, \quad i = 1, 2, ... \quad j = 1, 2, ..., G_i,$$

$$\sum_i \sum_{j=1}^{G_i} \sum_n p_{ijn} n = N$$

$$\sum_i \sum_{j=1}^{G_i} \sum_n p_{ijn} n p_{ijn} n \varepsilon_i = E$$

The MEP solution is

$$p_{ijn} = \frac{e^{-(\lambda_1 + \lambda_2 \varepsilon_i) n}}{\sum_n e^{-(\lambda_1 + \lambda_2 \varepsilon_i) n}}$$

Now one has to distinguish two cases:

- *Fermi-Dirac distribution.* According to Pauli's exclusion principle, $n = 0, 1$ and

$$\begin{aligned} \langle n_i \rangle &= \frac{\sum_{j=1}^{G_i} \sum_{n=0}^{1} n e^{-(\lambda_1 + \lambda_2 \varepsilon_i) n}}{\sum_{n=0}^{1} e^{-(\lambda_1 + \lambda_2 \varepsilon_i) n}} \\ &= \frac{G_i e^{-(\lambda_1 + \lambda_2 \varepsilon_i)}}{1 + e^{-(\lambda_1 + \lambda_2 \varepsilon_i)}} \\ &= \frac{G_i}{1 + e^{\lambda_1 + \lambda_2 \varepsilon_i}} \end{aligned}$$

- *Bose-Einstein distribution.* Here Pauli's exclusion principle does not hold and $n = 0, 1, ...$

$$\langle n_i \rangle = \frac{\sum_{j=1}^{G_i} \sum_{n=0}^{+\infty} n e^{-(\lambda_1 + \lambda_2 \varepsilon_i) n}}{\sum_{n=0}^{+\infty} e^{-(\lambda_1 + \lambda_2 \varepsilon_i) n}}$$

  Applying the formulae

$$\sum_{n=0}^{+\infty} e^{-an} = \frac{1}{1 - e^{-a}}, \quad \sum_{n=0}^{+\infty} n e^{-an} = \frac{e^{-a}}{(1 - e^{-a})^2}, \quad a > 0$$

  the above expression becomes

$$< n_i >= \frac{G_i}{e^{\lambda_1 + \lambda_2 \varepsilon_i} - 1}$$

If we impose

$$\lambda_1 = \alpha = -\frac{\mu}{K_B T}$$
$$\lambda_2 = \beta = \frac{1}{K_B T}$$

where μ is the chemical potential, the results obtained are the same of the statistical mechanics.
These examples mane clear the use of the MEP as inference method and it is remarkable to observe that the well known results in the context of the statistical mechanics are obtained without any physical assumption (molecular chaos, ergodic hypothesis, etc.).

2.4 The Boltzmann equation and the Maximum Entropy Principle

The MEP has been used with great success to solve the closure problem touched on in the previous chapter.
Let us consider again the Boltzmann equation 1.6, the moments 1.11 and the derived moment equations 1.12. Let us also assume the following expression for the entropy

$$S = -K_B \int_B (f \log f - f)\,.$$

Introducing the Lagrangian multipliers λ_A, the problem to maximize S under the constrains () is equivalent to maximize

$$S' = S - \sum_A \lambda_A \left(\int_B \mu_A(\mathbf{k}) f(\mathbf{r}, \mathbf{k}, t) d^3\mathbf{k} - M_A(\mathbf{r}, t) \right)$$

Imposing $\delta S' = 0$ gives

$$\left(\log f + \frac{1}{K_B} \sum_A \lambda_A \mu_A \right) \delta f = 0$$

since this relation must hold for arbitrary δf, it follows

$$f_{ME} = e^{-\frac{1}{K_B} \sum_A \lambda_A \mu_A}. \tag{2.5}$$

In order to complete the procedure, one has to express the multipliers λ_A's as functions of the moments M_A by inverting the constrains 1.11.
Once the Lagrangian multipliers have been expressed in terms of the moments, one finds the closure relations for fluxes and production terms by replacing the original set

of moment equations 1.12 with

$$\begin{aligned}\frac{\partial M_A}{\partial t} &+ \nabla_{\mathbf{r}} \int_B f_{ME}\mu_A(\mathbf{k})\mathbf{v}(\mathbf{k})d^3\mathbf{k} + \frac{e}{\hbar}\mathbf{E}\int_B f_{ME}\nabla_{\mathbf{k}}\mu_A(\mathbf{k})d^3\mathbf{k} = \\ &= \int_B \mu_A(\mathbf{k})C[f_{ME}]d^3\mathbf{k}.\end{aligned}$$

This method will be used in the next chapter and will be discussed in detail in the application. The reader interested in mathematical problem concerning the existence of the solution for the MEP method applied to semiconductors transport problem is referred to [61] , [62].

Chapter 3

The Double-Gate MOSFET

In this chapter the energy-transport model for the DG-MOSFET will be described and the simulation showed. The results here exposed has been extracted from

- Camiola, V.D., Mascali, G., Romano, V.: Numerical simulation of a double-gate MOSFET with a subband model for semiconductors based on the maximum entropy principle, Continuum Mechanics and Thermodynamics, **24** (2012)
- Camiola, V.D., Mascali, G., Romano, V.: Simulation of a double-gate MOSFET by a non-parabolic energy-transport subband model for semiconductors based on the maximum entropy principle, Mathematical and Computer Modelling (2012)

3.1 The simulated device

The main aim of this chapter is to simulate the nanoscale silicon DG-MOSFET reported in Fig. 3.1. The length of the diode is L_x= 40 nm, the width of the silicon layer is $L_z = 8$ nm and the oxide thickness is $t_{ox} = 1$ nm. The n^+ regions are 10 nm long. The gate contacts have the same length as the n region and are above it. The device is supposed to be infinite in the y direction.

The doping in the n^+ regions is $N_D(x) = N_D^+ = 10^{20}$ cm^{-3} and in the n region is $N_D(x) = N_D^- = 10^{15}$ cm^{-3}, with a regularization at the two junctions by a hyperbolic tangent profile

$$N_D(x) = N_D^+ - d\left(\tanh\frac{x-x_1}{s} - \tanh\frac{x-x_2}{s}\right),$$

where $s = 0.1$ nm, $d = \dfrac{N_D^+}{2}\left(1 - \dfrac{N_D^-}{N_D^+}\right)$, $x_1 = 10$ nm and $x_2 = 30$ nm.

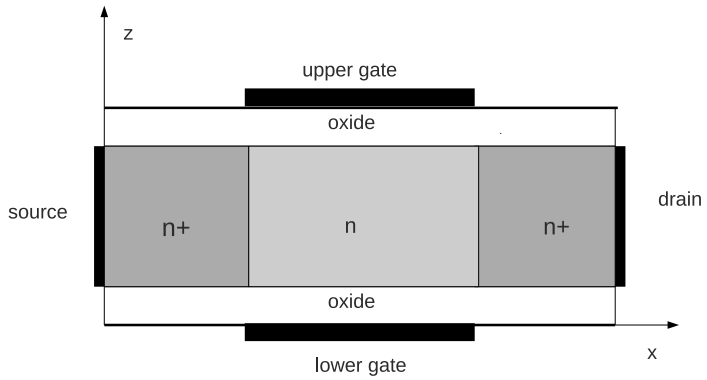

FIGURE 3.1: Simulated double gate MOSFET. Along the y axis the device is considered as infinite.

Due to the symmetries and dimensions of the device, the transport is, within a good approximation, one dimensional and along the longitudinal direction with respect the two oxide layers, while the electrons are quantized in the transversal direction. We assume that the oxide gives rise to an infinitely deep potential barrier; in fact realistic values of the potential barrier are more than 3 V high and it is very unlikely to find electrons with such an energy in the device under consideration. Six equivalent valleys are considered with a single effective mass $m^* = 0.32m_e$, m_e being the free electron mass. A possible generalization could include both longitudinal and transverse masses.

3.2 Quantum confinement and transport equations

Since electrons are quantized in the z direction and free to move in the x-y plane, it is natural to assume the following ansatz for their wave function

$$\psi(\mathbf{k}, \mathbf{r}) = \psi(k_x, k_y, k_z, x, y, z) = \frac{1}{\sqrt{\mathcal{A}}}\, \varphi(z) e^{i\mathbf{k}_{||}\cdot\mathbf{r}_{||}},$$

with $\mathbf{k}_{||} = (k_x, k_y)$ and $\mathbf{r}_{||} = (x, y)$ denoting the longitudinal components of the wave-vector $\mathbf{k}$ and the position vector $\mathbf{r}$, respectively, and $\mathcal{A}$ symbolizing the area of the xy cross-section.

Inserting the previous expression of ψ into the Schrödinger equation in the effective mass approximation

$$\left[-\frac{\hbar^2}{2m^*}\,\Delta + E_C(\mathbf{r})\right]\psi = E\,\psi,$$

gives the following equation for the envelope function $\varphi(z)$

$$\left[-\frac{\hbar^2}{2m^*}\frac{d^2}{dz^2} + E_C\right]\varphi(z) = \varepsilon\varphi(z), \quad t_{ox} \leq z \leq t_{ox} + L_z, \tag{3.1}$$

where $\hbar$ is the reduced Planck constant, E_C is the conduction band minimum, and ε is the energy associated with the confinement in the z-direction. In (3.1) $E_C = -q(V_C+V)$, where V_C is the confining potential and V is the self-consistent electrostatic potential. Under the assumption that the confining potential gives rise to an infinite barrier at the oxide/silicon interfaces, we solve eq. (3.1) only in the silicon region setting $\varphi = 0$ at $z = t_{ox}$ and $z = t_{ox} + L_z$ and taking $E_C = -q\,V$.

One finds a countable set of eigen-pairs (subbands) $(\varphi_\nu, \varepsilon_\nu), \nu = 1, 2...$ while V is obtained from the Poisson equation

$$\nabla \cdot (\epsilon\,\nabla V) = -q(N_D(\mathbf{r}) - n), \tag{3.2}$$

where q is the absolute value of the electron charge, ϵ is the dielectric constant, $N_D(\mathbf{r})$ is the doping concentration, and n is the electron density given by

$$n(\mathbf{r}, t) = \sum_{\nu=1}^{+\infty} \rho_\nu(x, y, t)|\varphi_\nu(z, t)|^2,$$

with the areal density of electrons ρ_ν of the νth subband. Of course the Schrödinger and Poisson equations are coupled and must be solved simultaneously.

The above Schrödinger-Poisson model is able to describe only the ballistic case, because the scattering is not included. In order to take into account this latter, several approaches are available. One can add in the Hamiltonian a term describing the electron-phonon interaction and solve the corresponding Schrödinger equation for the wave function in the electron-phonon space or use a Green density function method. However for devices with characteristic length of a few tenths of nanometers, which is the case we are going to simulate, the transport of electrons in the longitudinal direction is semi-classical within a good approximation. Electrons in each subband are considered as different populations whose dynamics is described by a semiclassical distribution function. Therefore the description of the electron transport along the longitudinal direction is included by adding to the Schorödinger-Poisson model the system of coupled Boltzmann equations for the distributions $f_\nu(x,y,k_x,k_y,t)$ of electrons in each subband

$$\frac{\partial f_\nu}{\partial t} + \frac{1}{\hbar}\nabla_{\mathbf{k}_{||}} E_\nu \cdot \nabla_{\mathbf{r}_{||}} f_\nu - \frac{q}{\hbar}\mathbf{E}_\nu^{eff} \cdot \nabla_{\mathbf{k}_{||}} f_\nu = \sum_{\mu=1}^{\infty} C_{\nu,\mu}[f_\nu, f_\mu], \quad \nu = 1, 2, \ldots \tag{3.3}$$

where $\mathbf{E}_\nu^{eff} = \frac{1}{q}\nabla_{\mathbf{r}_{||}}\varepsilon_\nu(\mathbf{r}_{||})$. ρ_ν is expressed in terms of f_ν by

$$\rho_\nu = \int_{B_2} f_\nu(\mathbf{r}_{||}, \mathbf{k}_{||}, t) d^2\mathbf{k}_{||},$$

with B_2 indicating the 2D Brillouin zone, which will be approximated with $\mathbb{R}^2$ consistently with the effective mass approximation.

In each subband the energy is the sum of a transversal contribution ε_ν and a longitudinal (kinetic) contribution $\varepsilon_{||}$

$$E_\nu = \varepsilon_\nu + \frac{\hbar^2}{2m^*}\left(k_x^2 + k_y^2\right) \equiv \varepsilon_\nu + \varepsilon_{||},$$

where a parabolic band approximation has been used for the longitudinal contribution. Consequently the longitudinal electron velocity is

$$\mathbf{v}_{||} = \frac{1}{\hbar}\nabla_{\mathbf{k}_{||}}\varepsilon_{||} = \frac{\hbar\mathbf{k}_{||}}{m^*}.$$

For more details the interested reader is referred to [19].

In the non degenerate approximation, each term contributing to the collision operator has the general form

$$C_{\nu,\mu}[f_\nu, f_\mu] = \int_{B_2}\left[S_{\mu\nu}(\mathbf{k}'_{||}, \mathbf{k}_{||})\, f'_\mu - S_{\nu\mu}(\mathbf{k}_{||}, \mathbf{k}'_{||})\, f_\nu\right] d^2\mathbf{k}'_{||}.$$

When $\mu = \nu$ we have intra-subband scatterings; when $\mu \neq \nu$ we have inter-subband scatterings. $S_{\mu\nu}(\mathbf{k}'_{||}, \mathbf{k}_{||})$ is the transition rate from the longitudinal state with wave-vector $\mathbf{k}'_{||}$, belonging to the μth subband, to the longitudinal state with wave-vector $\mathbf{k}_{||}$, belonging to the νth subband, and $f'_\mu \equiv f_\mu(\mathbf{r}_{||}, \mathbf{k}'_{||}, t)$. The relevant 2D scattering mechanisms in Si are acoustic phonon scattering, and nonpolar phonon scattering. Scattering with impurities will be not considered in this paper, but it is relevant only at low temperature or low field [63].

For the acoustic phonon scattering in the elastic approximation, the transition rate is given by

$$S_{\nu\mu}^{(ac)}(\mathbf{k}_{||}, \mathbf{k}'_{||}) = A^{(ac)} G_{\nu\mu}\delta(E_\mu(\mathbf{k}'_{||}) - E_\nu(\mathbf{k}_{||})),$$

with

$$A^{(ac)} = \frac{k_B T_L \Xi_d^2}{4\pi^2\hbar\rho v_S^2},$$

where k_B is the Boltzmann constant, T_L the lattice temperature, which will be kept constant in this paper, ρ the silicon density, Ξ_d the acoustic phonon deformation potential

and v_S the longitudinal sound speed. Their values are reported in the appendix A. The $G_{\nu\mu}$'s are the interaction integrals

$$G_{\nu\mu} = \int_{-\infty}^{\infty} |I_{\nu\mu}(q_z)|^2 dq_z, \quad I_{\nu\mu}(q_z) = \int_{t_{ox}}^{L_z+t_{ox}} \overline{\varphi_\nu(z)} \varphi_\mu(z) e^{iq_z z}\, dz,$$

with $\mathbf{q}$ denoting the 3D-phonon wave vector, and the bar indicating complex conjugation. We note that $G_{\nu\mu} = G_{\mu\nu}$ holds.

Similarly for non-polar optical phonon scattering one has

$$S^{(no)}_{\nu\mu}(\mathbf{k}_{||}, \mathbf{k}'_{||}) = A^{(no)} G_{\nu\mu} \left(N_q + \frac{1}{2} \mp \frac{1}{2} \right) \delta(E_\mu(\mathbf{k}'_{||}) - E_\nu(\mathbf{k}_{||}) \mp \hbar\omega),$$

where

$$A^{(no)} = \frac{(D_t K)^2}{8\pi^2 \rho \omega},$$

N_q is the Bose-Einstein distribution of phonons, $D_t K$ is the non-polar optical phonon deformation potential, and $\hbar\omega$ is the phonon energy. Their values are reported in the appendix A.

3.3 The moment system and its closure by the MEP

The system (3.1),(3.2),(3.3) furnishes a complete mathematical model for the simulation of the DG-MOSFET of Fig. 3.1 (see for example [33–35]). However solving it is a daunting computational task. This has prompted the development of simpler macroscopic models for CAD purposes. These models can be obtained as moment equations of the Boltzmann transport equations under suitable closure relations. The moment of the νth subband distribution with respect to a weight function $a(\mathbf{k}_{||})$ reads

$$M^\nu_a = \int_{B_2} a(\mathbf{k}_{||}) f_\nu(\mathbf{r}_{||}, \mathbf{k}_{||}, t) d^2\mathbf{k}_{||}.$$

In particular we take as basic moments

$$\begin{aligned}
\text{the areal density} \quad \rho^\nu &= \int_{B_2} f_\nu(\mathbf{r}_{||}, \mathbf{k}_{||}, t) d^2\mathbf{k}_{||}, \\
\text{the longitudinal mean velocity} \quad \mathbf{V} &= \frac{1}{\rho^\nu} \int_{B_2} \mathbf{v}_{||} f_\nu(\mathbf{r}_{||}, \mathbf{k}_{||}, t) d^2\mathbf{k}_{||}, \\
\text{the longitudinal mean energy} \quad W^\nu &= \frac{1}{\rho^\nu} \int_{B_2} \varepsilon_{||} f_\nu(\mathbf{r}_{||}, \mathbf{k}_{||}, t) d^2\mathbf{k}_{||}, \\
\text{the longitudinal mean energy-flux} \quad \mathbf{S}^\nu &= \frac{1}{\rho^\nu} \int_{B_2} \varepsilon_{||} \mathbf{v}_{||} f_\nu(\mathbf{r}_{||}, \mathbf{k}_{||}, t) d^2\mathbf{k}_{||}.
\end{aligned}$$

The corresponding moment system reads

$$\begin{aligned}
\frac{\partial \rho^\nu}{\partial t} + \nabla_{\mathbf{r}_{||}} \cdot (\rho^\nu \mathbf{V}^\nu) &= \rho^\nu \sum_\mu C_\rho^{\nu,\mu}, \\
\frac{\partial (\rho^\nu \mathbf{V}^\nu)}{\partial t} + \nabla_{\mathbf{r}_{||}} \cdot (\rho^\nu \mathbf{F}^{(0)\nu}) + \rho^\nu \mathbf{G}^{(0)\nu} \cdot \nabla_{\mathbf{r}_{||}} \varepsilon_\nu &= \rho^\nu \sum_\mu C_{\mathbf{V}}^{\nu,\mu}, \\
\frac{\partial \rho^\nu W^\nu}{\partial t} + \nabla_{\mathbf{r}_{||}} \cdot (\rho^\nu \mathbf{S}^\nu) + \rho^\nu \nabla_{\mathbf{r}_{||}} \varepsilon_\nu \cdot \mathbf{V}^\nu &= \rho^\nu \sum_\mu C_W^{\nu,\mu}, \\
\frac{\partial (\rho^\nu \mathbf{S}^\nu)}{\partial t} + \nabla_{\mathbf{r}_{||}} \cdot (\rho^\nu \mathbf{F}^{(1)\nu}) + \rho^\nu \mathbf{G}^{(1)\nu} \cdot \nabla_{\mathbf{r}_{||}} \varepsilon_\nu &= \rho^\nu \sum_\mu C_{\mathbf{S}}^{\nu,\mu},
\end{aligned}$$

where

$$\begin{aligned}
\begin{pmatrix} \mathbf{F}^{(0)\nu} \\ \mathbf{F}^{(1)\nu} \end{pmatrix} &= \frac{1}{\rho^\nu} \int_{B_2} \begin{pmatrix} 1 \\ \varepsilon_{||} \end{pmatrix} \mathbf{v}_{||} \otimes \mathbf{v}_{||} f_\nu(\mathbf{r}_{||}, \mathbf{k}_{||}, t)\, d^2\mathbf{k}_{||}, \\
\begin{pmatrix} \mathbf{G}^{(0)\nu} \\ \mathbf{G}^{(1)\nu} \end{pmatrix} &= \frac{1}{\rho^\nu} \int_{B_2} \begin{pmatrix} \frac{1}{\hbar} \nabla_{\mathbf{k}_{||}} \mathbf{v}_{||} \\ \frac{1}{\hbar} \nabla_{\mathbf{k}_{||}} \left(\varepsilon_{||} \mathbf{v}_{||} \right) \end{pmatrix} f_\nu(\mathbf{r}_{||}, \mathbf{k}_{||}, t)\, d^2\mathbf{k}_{||}, \\
\begin{pmatrix} C_\rho^{\nu,\mu} \\ C_W^{\nu,\mu} \end{pmatrix} &= \frac{1}{\rho^\nu} \int_{B_2} \begin{pmatrix} 1 \\ \varepsilon_{||} \end{pmatrix} \left[S_{\mu\nu}(\mathbf{k}'_{||}, \mathbf{k}_{||})\, f'_\mu - S_{\nu\mu}(\mathbf{k}_{||}, \mathbf{k}'_{||})\, f_\nu \right] d^2\mathbf{k}'_{||}\, d^2\mathbf{k}_{||}, \\
\begin{pmatrix} C_{\mathbf{V}}^{\nu,\mu} \\ C_{\mathbf{S}}^{\nu,\mu} \end{pmatrix} &= \frac{1}{\rho^\nu} \int_{B_2} \begin{pmatrix} \mathbf{v}_{||} \\ \varepsilon_{||} \mathbf{v}_{||} \end{pmatrix} \left[S_{\mu\nu}(\mathbf{k}'_{||}, \mathbf{k}_{||})\, f'_\mu - S_{\nu\mu}(\mathbf{k}_{||}, \mathbf{k}'_{||})\, f_\nu \right] d^2\mathbf{k}'_{||}\, d^2\mathbf{k}_{||}.
\end{aligned}$$

The above-written moment system is not closed because there are more unknowns than equations. Therefore constitutive relations in terms of the fundamental variables are needed for the extra-fluxes and the productions terms. The maximum entropy principle leads to a systematic way for obtaining constitutive relations on the basis of information theory [21, 50], and has been widely used for semiconductor modeling [24, 41, 51, 52]. According to MEP, if a given number of moments $M_{a_A}^\nu$, $A = 1, \ldots, N$, are known, the distribution functions f_ν can be estimated by the extremal $f^{MEP} = \left(f_1^{MEP}, f_2^{MEP}, \cdots\right)$ of the entropy functional under the constraints

$$\int a_A f_\nu^{MEP} d\mathbf{k}_{||} = M_{a_A}^\nu, \quad A = 1, \ldots, N. \tag{3.4}$$

Actually, in a semiconductor electrons interact with phonons, which describe the thermal vibrations of the ions placed at the points of the crystal lattice. However, if one considers the phonon gas as a thermal bath, one has to extremize only the electron component of the entropy. Moreover, since we are considering the electron gas as sufficiently dilute, one can take in each subband the expression of the entropy obtained as semiclassical

limit of that arising from the Fermi statistics. We define the entropy of the system as

$$\mathcal{S} = -k_B \sum_{\nu=1}^{+\infty} |\varphi_\nu(z,t)|^2 \int_{B_2} \left(f_\nu \log \frac{f_\nu}{y} - f_\nu \right) d^2\mathbf{k}_{||}, \quad y = \frac{2}{(2\pi)^2},$$

and therefore, according to MEP, the f_ν's are estimated with the distributions f_ν^{MEP}'s that solve the problem

$$\text{extremize } \mathcal{S} \quad \text{under the constraints} \quad M_{a_A}^\nu = \int_{B_2} a_A(\mathbf{k}_{||}) f_\nu^{MEP} d^2\,\mathbf{k}_{||},$$

where $M_{a_A}^\nu$ are the basic moments we have previously considered.

The proposed expression of the entropy combines quantum effects and semiclassical transport along the longitudinal direction, weighting the contribution of each f_ν with the square modulus of the $\varphi_\nu(z,t)$'s arising from the Schrödinger-Poisson block. With the above choice of the functions $a_A(\mathbf{k}_{||}) = (1, \mathbf{v}_{||}, \varepsilon_{||}, \varepsilon_{||}\mathbf{v}_{||})$, the resulting maximum entropy distribution functions read (the factors k_B and y have been included into the multipliers)

$$f_\nu^{MEP} = \exp\left[-\left(\lambda^\nu + \lambda_{\mathbf{V}}^\nu \cdot \mathbf{v}_{||} + \left(\lambda_W^\nu + \lambda_{\mathbf{S}}^\nu \cdot \mathbf{v}_{||} \right) \varepsilon_{||} \right) \right].$$

In order to complete the procedure one has to insert the f_ν^{MEP}'s into the constraint relations (3.4) and express the Lagrangian multipliers as functions of the basic moments ρ^ν, $\mathbf{V}^\nu$, W^ν, $\mathbf{S}^\nu$. However such a procedure requires a numerical inversion, which is not practical for numerical simulations of electron devices, since it must be performed at each time or iteration step (see [25] for the semiclassical case). Following the same approach as in [51, 52, 55], we assume a small anisotropy of the distribution functions and expand them up to first order

$$f_\nu^{MEP} \approx \exp\left[-\lambda^\nu - \lambda_W^\nu \varepsilon_{||} \right] \left[1 - \left(\lambda_{\mathbf{V}}^\nu \cdot \mathbf{v}_{||} + \lambda_{\mathbf{S}}^\nu \cdot \mathbf{v}_{||} \varepsilon_{||} \right) \right]. \tag{3.5}$$

The explicit expressions of the constitutive relations are reported in the Appendix A. By a direct calculation the following property can be proved.

The moment system of the subbands augmented with the MEP closure relations forms a quasilinear hyperbolic system in the time direction, provided $W^\nu > 0$(the demonstration will be furnished for the more general case of the Kane dispersion relation law) .

3.4 Energy-transport model

The production terms of the velocities and the energy fluxes read for each subband in the compact form (see the Appendix A)

$$\begin{pmatrix} C^\nu_{\mathbf{V}} \\ C^\nu_{\mathbf{S}} \end{pmatrix} = \begin{pmatrix} c^\nu_{11}(W^\nu) & c^\nu_{12}(W^\nu) \\ c^\nu_{21}(W^\nu) & c^\nu_{22}(W^\nu) \end{pmatrix} \begin{pmatrix} \mathbf{V}^\nu \\ \mathbf{S}^\nu \end{pmatrix}.$$

The coupling among the subbands in the productions of the velocities and the energy-fluxes is therefore only through the differences of the subband bottom energies. Under the diffusion scaling [56, 59, 60] $t = \mathcal{O}\left(\frac{1}{\delta^2}\right)$, $\mathbf{r}_{||} = \mathcal{O}\left(\frac{1}{\delta}\right)$, $\mathbf{V} = \mathcal{O}(\delta)$, $\mathbf{S} = \mathcal{O}(\delta)$, the following *energy transport model* is obtained from the moment system

$$\frac{\partial \rho^\nu}{\partial t} + \nabla_{\mathbf{r}_{||}} \cdot (\rho^\nu \mathbf{V}^\nu) = \rho^\nu C^\nu_\rho(\mathbf{W}), \tag{3.6}$$

$$\frac{\partial \rho^\nu W^\nu}{\partial t} + \nabla_{\mathbf{r}_{||}} \cdot (\rho^\nu \mathbf{S}^\nu) + \rho^\nu \nabla_{\mathbf{r}_{||}} \varepsilon_\nu \cdot \mathbf{V}^\nu = \rho^\nu C^\nu_W(\mathbf{W}), \tag{3.7}$$

where the index ν runs over the considered subbands, $\mathbf{W} = (W^1, W^2, \dots)$ and

$$\mathbf{V}^\nu = D^\nu_{11}(\mathbf{W}) \nabla_{\mathbf{r}_{||}} \log \rho^\nu + D^\nu_{12}(\mathbf{W}) \nabla_{\mathbf{r}_{||}} W^\nu - D^\nu_{13}(\mathbf{W}) \nabla_{\mathbf{r}_{||}} \varepsilon_\nu,$$
$$\mathbf{S}^\nu = D^\nu_{21}(\mathbf{W}) \nabla_{\mathbf{r}_{||}} \log \rho^\nu + D^\nu_{22}(\mathbf{W}) \nabla_{\mathbf{r}_{||}} W^\nu - D^\nu_{23}(\mathbf{W}) \nabla_{\mathbf{r}_{||}} \varepsilon_\nu,$$

The coefficients D^ν_{ij} are given by

$$D^\nu_{11} = \frac{c^\nu_{22} F^{(0)\nu} - c^\nu_{12} F^{(1)\nu}}{c^\nu}, \quad D^\nu_{12} = \frac{c^\nu_{22} (F^{(0)\nu})' - c^\nu_{12} (F^{(1)\nu})'}{c^\nu}, \quad D^\nu_{13} = \frac{c^\nu_{12} G^{(1)\nu} - c^\nu_{22} G^{(0)\nu}}{m^* c^\nu},$$
$$D^\nu_{21} = \frac{c^\nu_{11} F^{(1)\nu} - c_{21} F^{(0)\nu}}{c^\nu}, \quad D^\nu_{22} = \frac{c_{11} (F^{(1)\nu})' - c_{21} (F^{(0)\nu})'}{c^\nu}, \quad D^\nu_{23} = \frac{c^\nu_{21} G^{(0)\nu} - c^\nu_{11} G^{(1)\nu}}{m^* c^\nu},$$

with $c^\nu = c^\nu_{11} c^\nu_{22} - c^\nu_{12} c^\nu_{21}$ and $F^{(r)\nu}$, $G^{(r)\nu}$ longitudinal components of $\mathbf{F}^{(r)\nu}$, $\mathbf{G}^{(r)\nu}$, $r = 0, 1$. The system (3.37)-(3.38) must be coupled with the Schrödinger-Poisson block.

3.5 Boundary conditions and initial data

Regarding the boundary conditions and the initial data, we discuss separately the Schrödinger-Poisson (SP) block and the energy-transport (ET) equations.

3.5.1 Boundary conditions and initial data for the SP-block

Dirichlet boundary conditions are taken at the gates, that is $V = V_{gu}$ at the upper gate and $V = V_{gl}$ at the lower gate, with V_{gu} and V_{gl} prescribed voltages. Homogeneous

Neumann boundary conditions are assumed at the oxide external boundaries

$$\frac{\partial V}{\partial \nu} = 0,$$

with ν unit outward normal.

More involved are the boundary conditions at source and drain contacts. In the semi-classical case Dirichlet conditions are imposed, but they are no longer valid in a quantum context due to the confinement. In [15] Neumann conditions are used in order to allow the electrostatic potential to float and guarantee the charge neutrality. In [35] a different approach has been proposed. First a one dimensional Schrödinger-Poisson problem is solved at the boundaries representing the drain/source contacts and its solution is used as boundary condition for the 2D problem at thermal equilibrium. Then the boundary conditions at source and drain for arbitrary bias voltage are fixed adding V_b to the result obtained at equilibrium. Here we employ a different approach using both the previous ideas.

We first look for the thermal equilibrium solution, which is obtained setting $V_S = V_D = V_{gu} = V_{gl} = 0$. In order to get the boundary condition as in [35] we proceed solving first the SP equation at x=0. For symmetry reason, the same result holds at the contact at $x = L_x$. Since the potential is defined up to an additive constant, we impose $V(0, t_{ox}) = 0$. Moreover we require that the normal derivative is zero at the oxide /silicon interface $\dfrac{\partial V(0, t_{ox})}{\partial z} = 0$. On account of the symmetry of the device, the same conditions hold at $z = t_{ox} + L_z$, that is $V(0, t_{ox} + L_z) = 0$ and $\dfrac{\partial V(0, t_{ox} + L_z)}{\partial z} = 0$. The following system is therefore solved

$$\begin{cases} \left[-\dfrac{\hbar^2}{2m^*} \dfrac{d^2}{dz^2} - qV \right] \varphi(z) = \varepsilon \varphi(z), & t_{ox} \le z \le t_{ox} + L_z, \\ \dfrac{\partial}{\partial z} \left(\epsilon \dfrac{\partial V(0,z)}{\partial z} \right) = q(n(0,z) - N_D), & 0 \le z \le L_z + 2\, t_{ox}, \end{cases} \tag{3.8}$$

with the density given by the relationship

$$n(0,z) = \frac{\int_{t_{ox}}^{t_{ox}+L_z} N_D(0,\eta)\, d\,\eta}{\mathcal{Z}(0)} \sum_{\nu=1}^{\infty} \exp\left(-\frac{\varepsilon_\nu(0)}{k_B T_L} \right) |\varphi_\nu(0,z)|^2 \tag{3.9}$$

where $\mathcal{Z}$ is the partition function

$$\mathcal{Z}(x) = \sum_{\nu=1}^{\infty} \exp\left(-\frac{\varepsilon_\nu(x)}{k_B T_L} \right).$$

The formula for $n(0,z)$ is based on the fact that the Fermi potential is constant at thermal equilibrium. For the derivation the interested reader is referred to [35]. Note

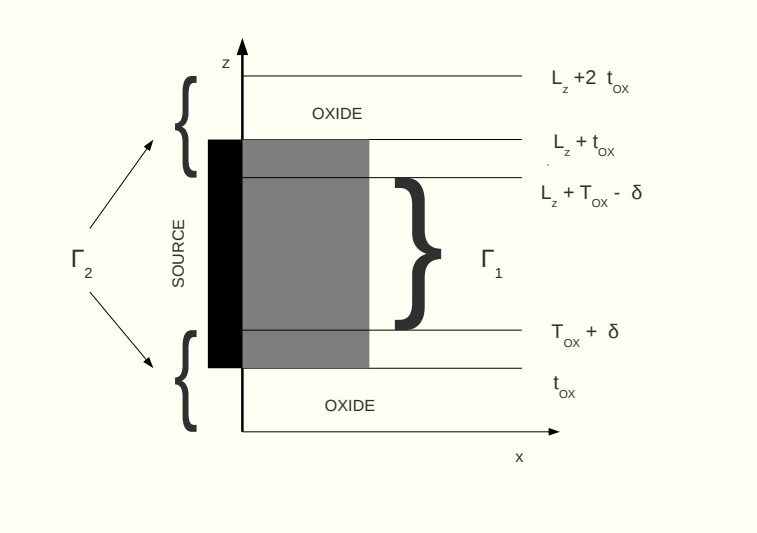

FIGURE 3.2: Boundary condition in the first slice of device.

that the Poisson equation is solved along all the strip $x = 0$.

Once the solution of eq.(3.8) is obtained, we pass to determine the equilibrium solution for the whole device with a procedure where the solution of eq. (3.8) is used to specify the boundary data at $x = 0$ and $x = L_x$ as follows (the details are given only for $x = 0$, since the same considerations hold for $x = L$). The boundary part representing the source contact (fig. 3.2) $\Gamma = \{(x, z) \in \mathbb{R}^2 : x = 0,\ 0 \le z \le L_z + 2\,t_{ox}\}$ is dived into two disjoint parts (fig.3.2) Γ_1 and Γ_2, where $\Gamma_1 = \{(x, z) \in \mathbb{R}^2 : x = 0, t_{ox} + \delta \le z \le L_z + t_{ox} - \delta\}$ and $\Gamma_2 = \{(x, z) \in \mathbb{R}^2 : x = 0, 0 \le z < t_{ox} + \delta\} \cup \{(x, z) \in \mathbb{R}^2 : x = 0,\ L_z + t_{ox} - \delta < z \le L_z + 2t_{ox}\}$, with δ a positive constant less than $L_z/2$. We take homogeneous Neumann conditions $\dfrac{\partial V}{\partial \nu} = 0$ along Γ_2 and $V(0, z) = V(0, z)_{1d}$ along Γ_1, with $V(0, z)_{1d}$ the potential arising from the solution of eq.(3.8). The natural boundary conditions, with homogeneous Neumann conditions on the oxide and Dirichlet conditions on the contact, is recovered setting $\delta = 0$. However, when $\delta = 0$, due to the loss of regularity where the boundary conditions change type, we have a boundary layer. In order to regularize the solution, we have extended the Neumann part also inside the contact.

With the above boundary conditions, the thermodynamical equilibrium without transport is obtained by solving the SP block with the density given by

$$n(x, z) = \frac{\int_{t_{ox}}^{t_{ox}+L_z} N_D(0, \eta)\, d\,\eta}{\mathcal{Z}(0)} \sum_{\nu=1}^{\infty} \exp\left(-\frac{\varepsilon_\nu(x)}{k_B T_L}\right) |\varphi_\nu(x, z)|^2. \tag{3.10}$$

At the end in order to include the transport, we couple the SP block with the ET one, taking Dirichlet boundary conditions for the electrostatic potential

$$V(0, z) = V(0, z)_{(eq)}, \quad V(L, z) = V(0, z)_{(eq)} + V_b, \tag{3.11}$$

where $V(0,z)_{(eq)}$ is the equilibrium potential obtained solving the SP block alone and V_b the applied bias voltage.

3.5.2 Boundary conditions and initial data for the ET-block

At variance with the standard approach in the literature, we do not impose Dirichlet conditions on the areal density and the longitudinal mean energy at source and drain, but

$$\frac{\partial}{\partial x}\rho^\nu(x,t) = \frac{\partial}{\partial x}W^\nu(x,t) = 0, \quad x = 0, L_x, \quad t > 0, \quad \nu = 1,2,\dots$$

which are more flexible from a numerical point of view. Fixing Dirichlet boundary conditions for the energy at source and drain, although common in the literature, leads to an inconsistency with MC simulations in the semiclassical case [17].

By using Boltzmann statistics, the following initial data

$$\rho^\nu(x,0) = \frac{e^{-\varepsilon_\nu/k_BT_L}}{\sum_\mu e^{-\varepsilon_\mu/k_BT_L}}\,\overline{N}_D(x), \quad W^\nu(x,0) = k_BT_L, \quad \nu = 1,2,\dots$$

are taken, where T_L is the lattice temperature and

$$\overline{N}_D(x) = \int_{t_{ox}}^{L_z+t_{ox}} N_D(x,z)\,dz$$

is the integrated doping with respect to the transversal coordinate.

3.6 Numerical method

The main aim now is to simulate the DG-MOSFET of Fig. 3.1 with the model presented above, which consists of the Schrödinger-Poisson block (3.1), (3.2) coupled to the energy-transport equations (3.37), (3.38). The numerical method we propose advances in time by an explicit discretization of (3.37), (3.38) with the energy subband bottoms ε_ν frozen at the previous time step. This allows to split the numerical scheme into two parts: the discretization of the Schrödinger-Poisson (SP) block and the discretization of the energy-transport (ET) equations

Along the x direction let us introduce the grid points x_i, $i = i_a,\dots,i_b$, with $x_{i+1}-x_i = h$ = constant, and the middle points $x_{i\pm1/2} = x_i \pm h/2$. Along the z direction let us introduce the grid points z_j, $j = j_a,\dots,j_b$, with $z_{j+1}-z_j = k$ = constant. Moreover let us take a uniform time step Δt and set $u_{ij}^n = u(x_i,z_j,n\,\Delta t)$, for a generic function u. It is straightforward to extend the scheme to a non uniform grid and time step.

3.6.1 Discretization of the Schrödinger-Poisson equations

The discretization of the Schrödinger-Poisson equations has been performed following standard approaches. Let suppose that time is fixed at level n, which will be omitted for the sake of clarity in the notation. In order to couple eq.(1) with the Poisson equation, an iterative scheme based on the Gummel method has been adopted. For each subband let us denote with $\varphi^{(l)}_{\nu_{ij}}$ the value of $\varphi_{\nu_{ij}}$ at the l-iterate. The Schrödinger equation is discretized in each slice $x = x_i$ with central differencing

$$-\frac{\hbar^2}{2m^*}\frac{\varphi^{(l)}_{i,j+1} - 2\varphi^{(l)}_{i,j} + \varphi^{(l)}_{i,j-1}}{k^2} - qV_{i,j}\varphi^{(l)}_{i,j} = \varepsilon_i\,\varphi^{(l)}_{i,j}, \quad j = j_a + 1, \cdots, j_b - 1, \tag{3.12}$$

$$\varphi_{i,j_a} = 0, \quad \varphi_{i,j_b} = 0, \tag{3.13}$$

where $z_{j_a} = t_{ox}$ and $z_{j_b} = t_{ox} + L_z$. Known $\varphi^{(l)}_{\nu_{i,j}}$, we reconstruct an approximation of $n(x_i, z_j, n\Delta t)$ as

$$n^{(l)}_{i,j} = \sum_{\nu} \rho_{\nu_i}(x_i)|\varphi^{(l)}_{\nu_{i,j}}|^2, \tag{3.14}$$

and this latter is inserted into the discretization of a modified Poisson equation

$$\begin{aligned}
&\frac{1}{h^2}\left[\frac{\epsilon_{i+1,j} + \epsilon_{i,j}}{2}\left(V^{(l+1)}_{i+1,j} - V^{(l+1)}_{i,j}\right) - \frac{\epsilon_{i,j} + \epsilon_{i-1,j}}{2}\left(V^{(l+1)}_{i,j} - V^{(l+1)}_{i-1,j}\right)\right] \\
&+\frac{1}{k^2}\left[\frac{\epsilon_{i,j+1} + \epsilon_{i,j}}{2}\left(V^{(l+1)}_{i,j+1} - V^{(l+1)}_{i,j}\right) - \frac{\epsilon_{i,j} + \epsilon_{i,j-1}}{2}\left(V^{(l+1)}_{i,j} - V^{(l+1)}_{i,j-1}\right)\right] \\
&+Q^{(l)}_{i,j} = \frac{q^2\, n^{(l)}_{i,j}}{k_B T_L}\left(V^{(l+1)}_{i,j} - V^{(l)}_{i,j}\right), \; i = i_a + 1, \cdots, i_b - 1, \quad j = j_a + 1, \cdots, j_b - 1, \quad \text{plus (3.16)}
\end{aligned}$$

where

$$Q^{(l)}_{i,j} = \begin{cases} q(N_{D_{i,j}} - n^{(l)}_{i,j}), & \text{if} \quad i = i_a \cdots i_b, \quad j = j_a \cdots j_b, \quad \text{(silicon body)}, \\ 0, & \text{otherwise}, \qquad\qquad\qquad\quad \text{(oxide layers)}, \end{cases}$$

and the dielectric constant is a piecewise constant function

$$\epsilon = \begin{cases} \epsilon_{Si} & \text{in silicon}, \\ \epsilon_{ox} & \text{in the oxide}. \end{cases}$$

The r.h.s. of the previous equation gives the nonlinear coupling of the Gummel method. As $V^{(l)}_{i,j}$ converges to the exact solution, the r.h.s. vanishes and one has the solution of the original Poisson equation. A simple coupling with zero r.h.s. is possible but the convergence is very slow, and therefore not practical for realistic simulations. Instead the Gummel method assures a rather fast convergence. In the literature other approaches have been tried, e.g. the Newton-Raphson one (the interested reader can see [35]). The

iteration is continued until the stopping criterium

$$\frac{||n_{i,j}^{(l+1)} - n_{i,j}^{(l)}||_\infty}{||n_{i,j}^{(l+1)}||_\infty} < \text{tollerance}, \quad \frac{||V_{i,j}^{(l+1)} - V_{i,j}^{(l)}||_\infty}{||V_{i,j}^{(l+1)}||_\infty} < \text{tollerance}$$

is fulfilled. In the numerical simulation we set the tollerance equal to 10^{-6} and take as initial guess $\varphi_{i,j}^{(0)}$ the result of the previous time step. In particular for the first time step we take as initial guess the solution of (3.12) with $V_{i,j}^{(0)} = 0$. At each iteration (3.12) leads to $i_b - i_a + 1$ independent eigenvalues problems, that are solved with the subroutine DSTEVX of the LAPACK library. The linear system arising from (3.15), after ordering the nodes by columns, is solved with the subroutine DGESV of the LAPACK library, without preconditioner.

Remark. As discussed in section 3.5, when we integrate the SP block to get the thermodynamical equilibrium, homogeneous Newman boundary conditions are imposed on Γ_2 and Dirichlet conditions on Γ_1 in order to regularize the solution. This allows the solution to float, but can create a spurious difference of potential between the gate and the edges of the source and drain contacts. To avoid such a drawback, we need to iterate the solution as follows. At each iterate, the difference of potential between the edges of the contact (source or drain) and the gate is evaluated $\Delta V = V(0, z_c) - V_g$, $z_c = t_{ox}, L_z + t_{ox}$ and then we impose in the 1D SP block $V(0, z_c) = -\Delta V$. After few iterations ΔV becomes negligible. As stopping criterium $|\Delta V| < 10^{-5}$ has been adopted. Of course, such further iterations are not necessary for non equilibrium solutions.

3.6.2 Discretization of the energy-transport equations

The key point for the formulation of the numerical scheme is the following proposition which can be proved by a direct calculation The following relations hold

$$G^{(0)\nu} = \lambda_W^\nu F^{(0)\nu}, \tag{3.16}$$

$$G^{(1)\nu} = \lambda_W^\nu F^{(1)\nu}. \tag{3.17}$$

Thanks to the above proposition in each subband the current density $\mathbf{J} = \rho\mathbf{V}$ and the energy-flux density $\mathbf{Z} = \rho\,\mathbf{S}$ can be rewritten as (the subband index is omitted)

$$\mathbf{J} = \mathbf{J}^{(1)} - \mathbf{J}^{(2)}, \quad \mathbf{Z} = \mathbf{Z}^{(1)} - \mathbf{Z}^{(2)}, \tag{3.18}$$

where each term is in a *drift-diffusion form*

$$\mathbf{J}^{(1)} = \frac{c_{22}}{c}\left[\nabla_{\mathbf{r}_{||}}(\rho F^{(0)}) + \rho\lambda_W F^{(0)}\nabla_{\mathbf{r}_{||}}\varepsilon\right], \quad \mathbf{J}^{(2)} = \frac{c_{12}}{c}\left[\nabla_{\mathbf{r}_{||}}(\rho F^{(1)}) + \rho\lambda_W F^{(1)}\nabla_{\mathbf{r}_{||}}\varepsilon\right], \tag{3.19}$$

$$\mathbf{Z}^{(1)} = \frac{c_{11}}{c}\left[\nabla_{\mathbf{r}_{||}}(\rho F^{(1)}) + \rho\lambda_W F^{(1)}\nabla_{\mathbf{r}_{||}}\varepsilon\right], \quad \mathbf{Z}^{(2)} = \frac{c_{21}}{c}\left[\nabla_{\mathbf{r}_{||}}(\rho F^{(0)}) + \rho\lambda_W F^{(0)}\nabla_{\mathbf{r}_{||}}\varepsilon\right], \tag{3.20}$$

The drift-diffusion form is evident if one identifies $\frac{c_{ij}}{c}F^{(r)}$, $r = 0, 1$, as generalized mobilities and $q\lambda_W$ as the inverse of a sort of thermal potential. This fact is even more evident in the parabolic case, which we are considering here, where $\lambda_W = 1/W$, which at thermal equilibrium reads $\lambda_W = 1/k_B T_L$.

The previous consideration allows us to formulate a numerical method for the transport part by a suitable extension of that proposed in [17] for the semiclassical MEP energy-transport model.

We discretize the balance equations (3.37) and (3.38) in the one dimensional case as

$$\frac{\rho_i^{n+1} - \rho_i^n}{\Delta t} + \frac{(J)_{i+1/2}^n - (J)_{i-1/2}^n}{h} - \rho_i^n C_{\rho_i}^n + O(h^2, \Delta t) = 0, \tag{3.21}$$

$$\frac{(\rho W)_i^{n+1} - (\rho W)_i^n}{\Delta t} + \frac{Z_{i+1/2}^n - Z_{i-1/2}^n}{h} + \frac{J_{i+1/2}^n + J_{i-1/2}^n}{2}\frac{\varepsilon_{i+1}^n - \varepsilon_{i-1}^n}{2h} - \rho_i^n C_{W_i}^n + O(h^2, \Delta t) = 0 \tag{3.22}$$

In order to evaluate the components of the currents in the middle points, let us consider the cells $I_{i+1/2} = [x_i, x_{i+1}]$, and expand $J^{(r)}$, r= 0,1, in Taylor's series in $I_{i+1/2}$ (hereafter the variables with no temporal index have to be evaluated at the time step $t = n\Delta t$)

$$J^{(r)}(x) = (J^{(r)})_{i+1/2} + (x - x_{i+1/2})\left(\frac{\partial J^{(r)}}{\partial x}\right)_{i+1/2} + o(h).$$

Moreover, we introduce $U_T = \frac{1}{q\lambda_W}$, which, as said, plays a role analogous to the thermal potential in the drift-diffusion model (see [17] for more details), and indicate by $\overline{U}_T$ its piecewise constant approximation $\overline{U}_T = \frac{1}{2}\left[\frac{1}{\lambda_W(W_{i+1})} + \frac{1}{\lambda_W(W_i)}\right]$ in the cell $I_{i+1/2}$. Then we define the *local* mobilities

$$g_{11} = \frac{\overline{c}_{22}}{\overline{c}}\rho F^{(0)}, \quad g_{12} = \frac{\overline{c}_{12}}{\overline{c}}\rho F^{(1)}, \tag{3.23}$$

$$g_{21} = \frac{\overline{c}_{11}}{\overline{c}}\rho F^{(1)}, \quad g_{22} = \frac{\overline{c}_{21}}{\overline{c}}\rho F^{(0)}, \tag{3.24}$$

where $\overline{c}_{pq}$ is a piecewise constant approximation of c_{pq}, $p, q = 1, 2$, given by $\overline{c}_{pq} = \frac{c_{pq}(W_i) + c_{pq}(W_{i+1})}{2}$ in the cell $I_{i+1/2}$, $\overline{c} = \overline{c}_{11}\overline{c}_{22} - \overline{c}_{12}\overline{c}_{21}$, and, as in [32], the *local* Slotboom variables

$$s_{kr} = \exp\left(\varepsilon/q\,\overline{U}_T\right) g_{kr} \quad k, r = 1, 2.$$

Since in each cell

$$J^{(1)} \approx \frac{\partial}{\partial x}\left(\frac{\overline{c}_{22}}{\overline{c}}\rho F^{(0)}\right) + \frac{\overline{c}_{22}}{\overline{c}}\frac{\rho F^{(0)}}{\overline{U}_T}\frac{\partial \varepsilon}{\partial x}, \quad J^{(2)} \approx \frac{\partial}{\partial x}\left(\frac{\overline{c}_{12}}{\overline{c}}\rho F^{(1)}\right) + \frac{\overline{c}_{22}}{\overline{c}}\frac{\rho F^{(1)}}{\overline{U}_T}\frac{\partial \varepsilon}{\partial x},$$
$$Z^{(1)} \approx \frac{\partial}{\partial x}\left(\frac{\overline{c}_{11}}{\overline{c}}\rho F^{(1)}\right) + \frac{\overline{c}_{11}}{\overline{c}}\frac{\rho F^{(1)}}{\overline{U}_T}\frac{\partial \varepsilon}{\partial x}, \quad Z^{(2)} \approx \frac{\partial}{\partial x}\left(\frac{\overline{c}_{21}}{\overline{c}}\rho F^{(0)}\right) + \frac{\overline{c}_{21}}{\overline{c}}\frac{\rho F^{(0)}}{\overline{U}_T}\frac{\partial \varepsilon}{\partial x},$$

the *local* Slotboom variables satisfy

$$\frac{\partial s_{1r}(x)}{\partial x} \simeq \exp\left(\varepsilon/q\,\overline{U}_T\right) J^{(r)}(x) = \exp\left(\varepsilon/q\,\overline{U}_T\right)\left\{(J^{(r)})_{i+1/2} + (x - x_{i+1/2})\left(\frac{\partial J^{(r)}}{\partial x}\right)_{i+1/2} + o(h)\right\} \quad (3.25)$$

At each time step ε is approximated in $I_{i+1/2}$ by a piece-wise linear function

$$\varepsilon(x, n\Delta t) = \varepsilon_i^n + \frac{x - x_i}{x_{i+1} - x_i}\left(\varepsilon_{i+1}^n - \varepsilon_i^n\right).$$

Integrating (3.25) over $I_{i+1/2}$, one has

$$(s_{1r})_{i+1} - (s_{1r})_i = \int_{x_i}^{x_{i+1}} \exp\left(\frac{\varepsilon(x)}{q\,\overline{U}_T}\right) J_{i+1/2}^{(r)}\, dx + O(h^2)$$
$$= J_{i+1/2}^{(r)} \frac{h\,q\,\overline{U}_T}{\varepsilon_{i+1}^n - \varepsilon_i^n}\left(\exp\left(\frac{\varepsilon_{i+1}}{q\,\overline{U}_T}\right) - \exp\left(\frac{\varepsilon_i}{q\,\overline{U}_T}\right)\right) + O(h^2),$$

which, with some algebra, gives

$$(J^{(r)})_{i+1/2} = \sigma_{i+1/2}\coth\sigma_{i+1/2}\,\frac{(g_{1r})_{i+1} - (g_{1r})_i}{h} + \sigma_{i+1/2}\frac{(g_{1r})_{i+1} + (g_{1r})_i}{h}, \quad r = 1, 2 \quad (3.26)$$

where $\sigma_{i+1/2} = \frac{\varepsilon_{i+1} - \varepsilon_i}{2\,q\,\overline{U}_T}$.

With the same procedure the following discrete expressions for the two parts of the energy flux are obtained

$$(Z^{(r)})_{i+1/2} = \sigma_{i+1/2}\coth\sigma_{i+1/2}\,\frac{(g_{2r})_{i+1} - (g_{2r})_i}{h} + \sigma_{i+1/2}\frac{(g_{2r})_{i+1} + (g_{2r})_i}{h}, \quad r = 1, 2 \quad (3.27)$$

The spatial error in formulas (3.26),(3.27) is $O(h^2)$.

3.7 Numerical results

A spatial grid of 65×37 points has been adopted. By using as units picoseconds for time, microns for length and electron volts for energy, it is not necessary to adimensionalize the variables. The physical parameters are reported in tables A.1, A.2 of the Appendix A The numerical experiments indicate that it is sufficient to take into account only the

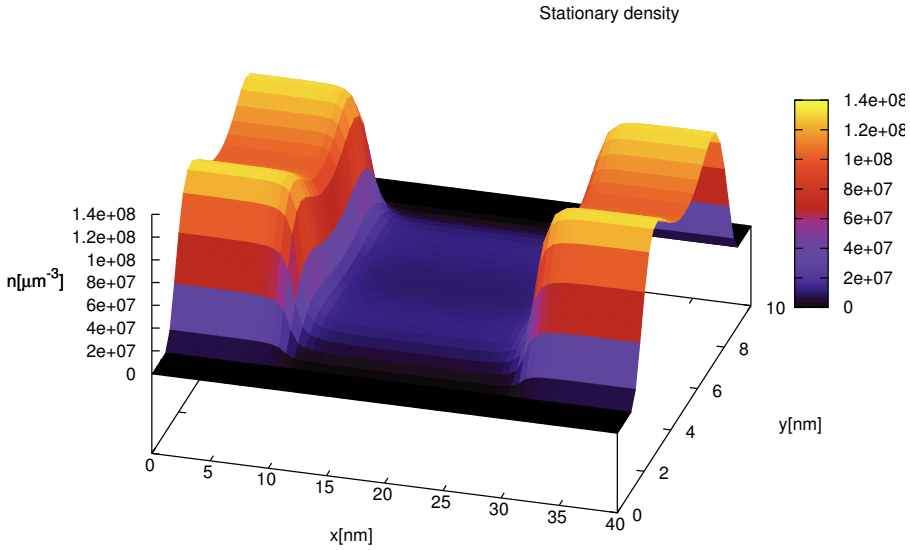

FIGURE 3.3: Stationary density in the case $V_D = 0.2$ V and $V_{gl} = V_{gu} = 0$ V

first three subbands since the other ones are very scarcely populated. The steady state is reached after about 5 picoseconds.

The preliminary numerical simulation is the thermal equilibrium which represents also the initial data for the other simulations. The 1D SP has required 288 iterations, the adopted CFL condition has been $\Delta t = h/20$. As first case we consider the following applied voltages: $V_D = 0.2$ V and $V_{gl} = V_{gu} = 0$ V. For this and the simulations below, the CFL condition $\Delta t = h/50$ has been adopted. In Fig.s 3.3, 3.4 we plot the steady state density and the potential. The solution does not present any spurious oscillations or boundary layer and reflects the symmetry of the problem. It is evident that the boundary conditions at source and drain are completely different from the semiclassical ones that are simply $n = N_D$. In Fig. 3.5 the first three subband bottoms are shown. We have a good qualitative agreement with the other numerical simulations known in the literature.

Areal densities, macroscopic velocities and energies measured from the subband bottom, and currents in the first three subbands are shown in Fig.s 3.6-3.9. The surface density in the third subband is about 2 % of the total surface density as a confirmation that the inclusion of further subbands has a negligible effect even far from equilibrium. It is worth mentioning that the energy has an evidently different value between source and drain as happens in the semiclassical case. The use of Dirichlet conditions for the energy at the contacts misses such an effect. Observe that we have a very accurate current conservation, proving the robustness of the numerical method.

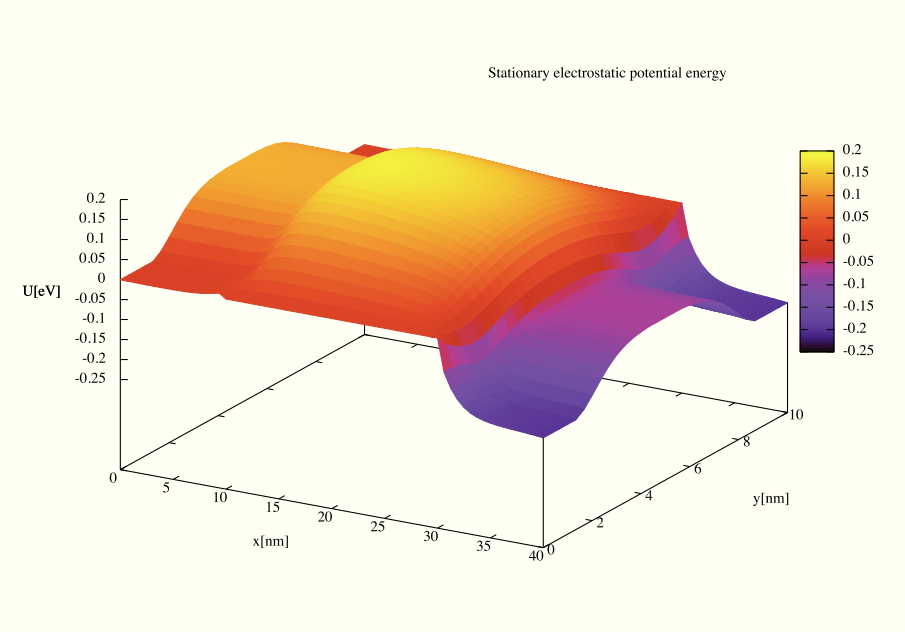

FIGURE 3.4: Stationary electrostatic potential energy in the case $V_D = 0.2$ V and $V_{gl} = V_{gu} = 0$ V

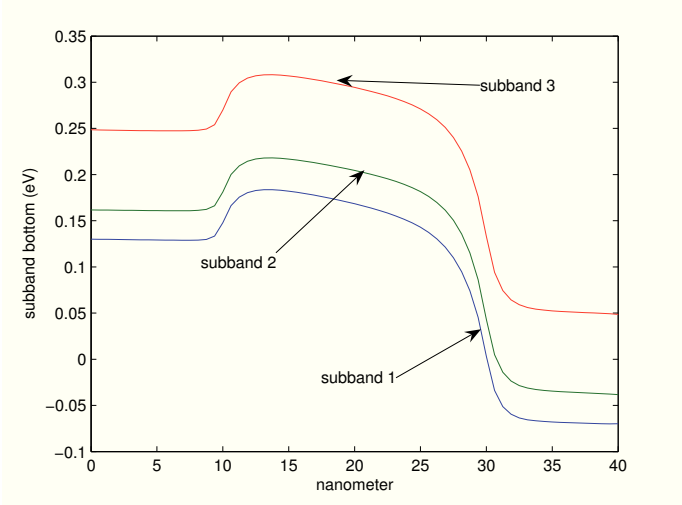

FIGURE 3.5: First three subbands at the steady state in the case $V_D = 0.2$ V and $V_{gl} = V_{gu} = 0$ V

The mean velocity, evaluated according to the formula

$$\mathbf{V} = \frac{\sum_\nu \rho^\nu \mathbf{V}^\nu}{\sum_\mu \rho^\mu}, \tag{3.28}$$

is shown along with the mean energy, evaluated taking as reference value the bottom of the first subband

$$W = \frac{\sum_\nu \rho^\nu \left(W^\nu + \varepsilon_\nu - \varepsilon_1\right)}{\sum_\mu \rho^\mu} \tag{3.29}$$

It is possible to observe that the maximum velocity in the channel is more than two

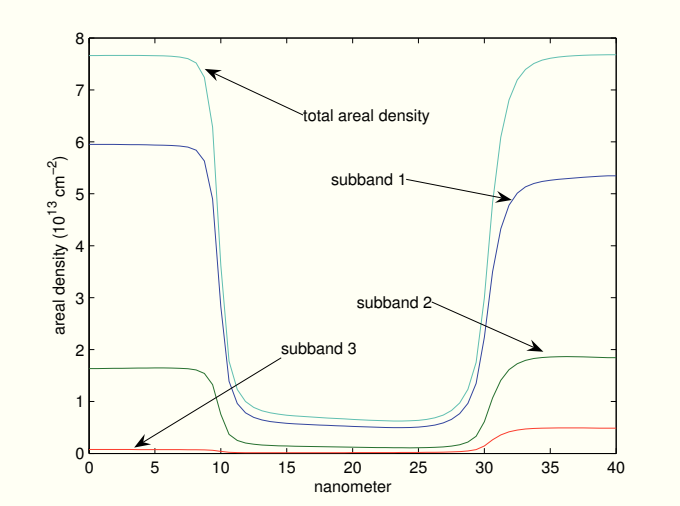

FIGURE 3.6: Surface densities in the first three subbands in the case $V_D = 0.2$ V and $V_{gl} = V_{gu} = 0$ V

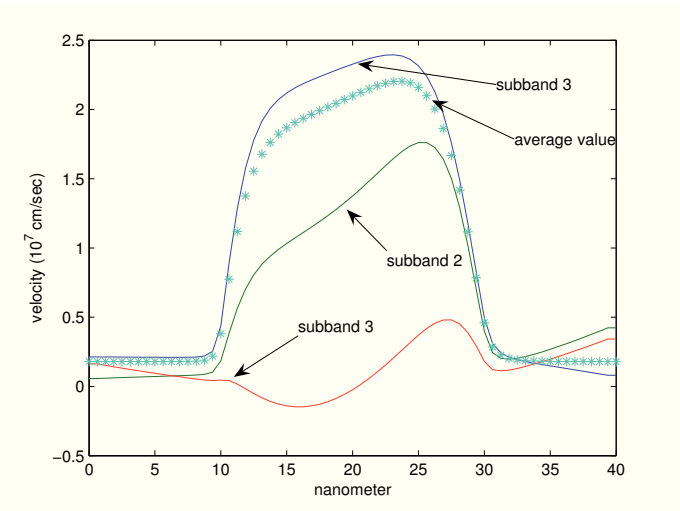

FIGURE 3.7: Average velocities in the first three subbands and global mean velocity in the case $V_D = 0.2$ V and $V_{gl} = V_{gu} = 0$ V

times the saturation velocity. In order to see the influence of the gate voltage on the currents, we have also simulated the case with $V_D = 0.2$ V and $V_{gl} = V_{gu} = 0.1$ V. From a qualitative point of view we have stationary results similar to those obtained in the previously considered case. The most relevant differences are in the electrostatic potential, which is plotted in Fig. 3.10, and, as expected, in the currents which are shown in Fig. 3.11. The gate voltages open the channel and as a consequence the current increases, as required in the switching operation typical of the DG-MOSFET.

At last we have also considered a case with negative gate voltages: $V_D = 0.2$ V and $V_{gl} = V_{gu} = -0.2$. The electrostatic potential is plotted in Fig. 3.12 where it is evident the influence of the boundary data. Now, as expected, the negative gate voltages close

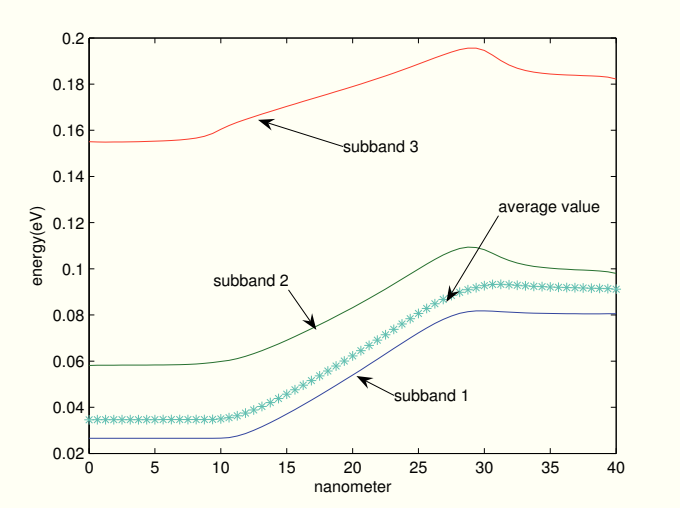

FIGURE 3.8: Average energies in the first three subbands and global mean energy in the case $V_D = 0.2$ V and $V_{gl} = V_{gu} = 0$ V

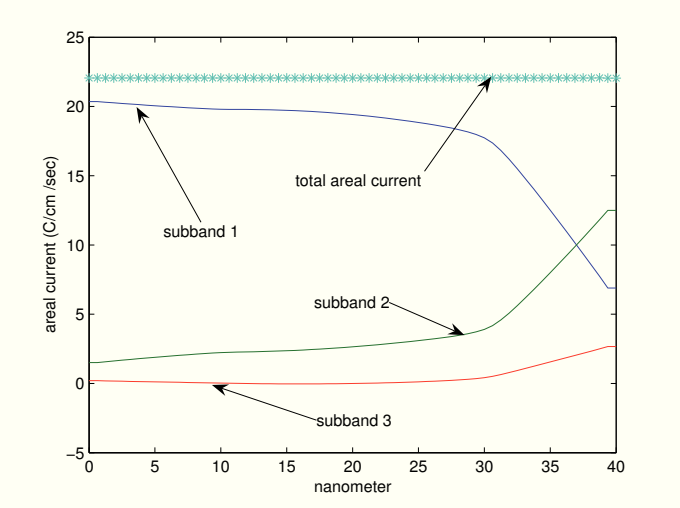

FIGURE 3.9: Average areal currents in the first three subbands and global areal current in the case $V_D = 0.2$ V and $V_{gl} = V_{gu} = 0$ V

the channel and as a result the current flowing in the device is much lower than that in the previous case (see Fig. 3.13).

3.8 The Kane dispersion relation case

Now, let us improve the model by substituting the parabolic energy dispersion relation by the Kane one

$$E_\nu(\mathbf{r}_{||}, \mathbf{k}_{||}) = \varepsilon_\nu(\mathbf{r}_{||}) + \frac{1}{2\alpha}\left(\sqrt{1 + 4\alpha\frac{\hbar^2}{2m^*}\left(k_x^2 + k_y^2\right)} - 1\right) \equiv \varepsilon_\nu(\mathbf{r}_{||}) + \varepsilon_{||}(\mathbf{k}_{||}),$$

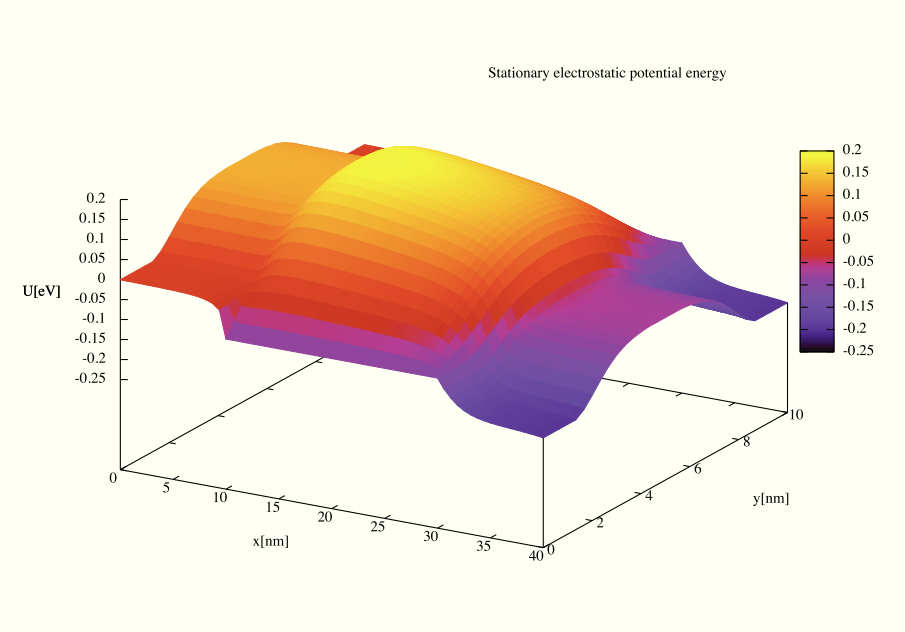

FIGURE 3.10: Stationary electrostatic potential energy in the case $V_D = 0.2$ V and $V_{gl} = V_{gu} = 0.1$ V

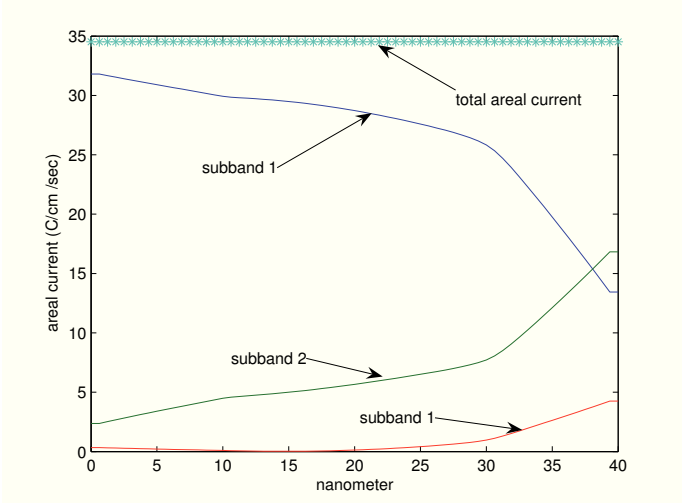

FIGURE 3.11: Average areal current in the first three subbands and global areal current in the case $V_D = 0.2$ V and $V_{gl} = V_{gu} = 0.1$ V

where α is the non-parabolicity parameter. Consequently the longitudinal electron velocity is

$$\mathbf{v}_{||} = \frac{1}{\hbar}\nabla_{\mathbf{k}_{||}}\varepsilon_{||} = \frac{\hbar\mathbf{k}_{||}}{m^*\left(1+2\alpha\varepsilon_{||}\right)}. \tag{3.30}$$

Using again the above definitions for the moments and the same procedure of the parabolic case (see Appendix B for the details), one finds the following expressions

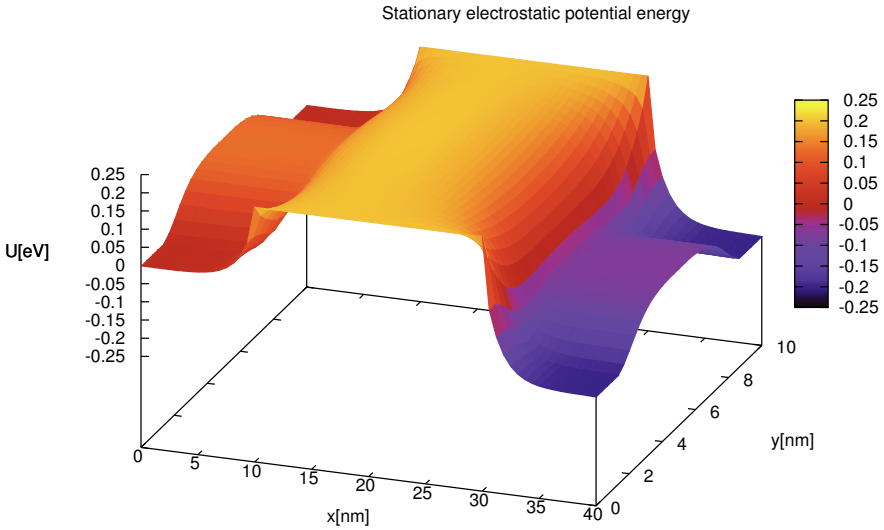

FIGURE 3.12: Stationary electrostatic potential energy in the case $V_D = 0.2$ V and $V_{gl} = V_{gu} = -0.2$ V

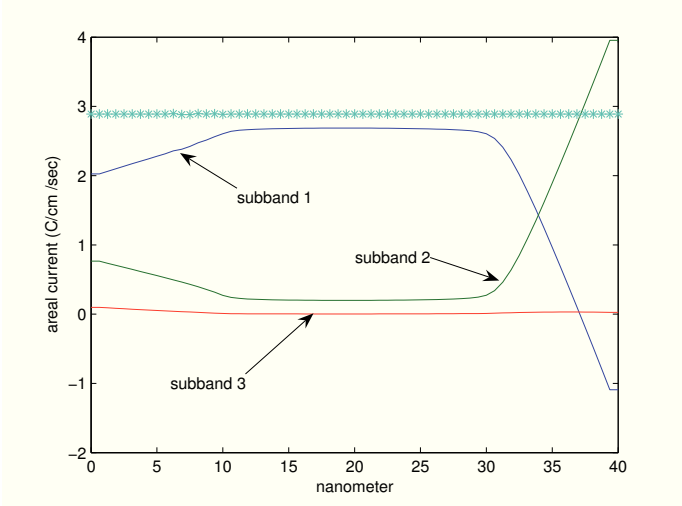

FIGURE 3.13: Average areal current in the first three subbands and global areal current in the case $V_D = 0.2$ V and $V_{gl} = V_{gu} = -0.2$ V

for the densities and the energies in polar coordinates [1]

$$\rho = \frac{m^*}{\hbar^2} \int_0^{2\pi} \int_0^{+\infty} \exp\left(-\lambda - \lambda_W \varepsilon_{||}\right) \left(1 + 2\alpha\varepsilon_{||}\right) \, d\varepsilon_{||} \, d\theta,$$

$$\rho W = \frac{2\pi m^*}{\hbar^2} \exp\left(-\lambda\right) \int_0^{+\infty} \varepsilon_{||} \exp\left(-\lambda_W \varepsilon_{||}\right) \left(1 + 2\alpha\varepsilon_{||}\right) \, d\varepsilon_{||},$$

[1] Here and whenever possible we omit the subband index , for simplicity

wherefrom

$$\lambda_W = \frac{1 - 2\alpha W + \sqrt{(1-2\alpha W)^2 + 16\alpha W}}{2W}, \quad \lambda = -\ln\left(\frac{\hbar^2}{2\pi m^*}\rho\, g(W)\right), \tag{3.31}$$

with

$$g(W) = \left(\frac{1}{\lambda_W} + \frac{2\alpha}{(\lambda_W)^2}\right)^{-1}.$$

Similarly, substituting (3.5) into the remaining constraints for the velocities and the energy-fluxes and inverting, one has

$$\lambda_{\mathbf{V}} = b_{11}(W)\,\mathbf{V} + b_{12}(W)\,\mathbf{S}, \quad \lambda_{\mathbf{S}} = b_{21}(W)\,\mathbf{V} + b_{22}(W)\,\mathbf{S}, \tag{3.32}$$

where

$$b_{ij}(W) = \frac{(-1)^{i+j-1} m^*}{b(W)\, g(W)} \left[\gamma_{(5-i-j)}(W,0) + \alpha\, \gamma_{(6-i-j)}(W,0)\right],$$
$$b(W) = \left[\gamma_1(W,0) + \alpha\,\gamma_2(W,0)\right]\left[\gamma_3(W,0) + \alpha\,\gamma_4(W,0)\right] - \left[\gamma_2(W,0) + \alpha\,\gamma_3(W,0)\right]^2.$$

Note the symmetry of the coefficients, $b_{12} = b_{21}$, which reminds us of the Onsager reciprocity conditions [64]. The γ's are reported in the Appendix B.

By using the explicit expressions of the f_ν^{MEP}'s, the needed constitutive relations are obtained. They are reported in the Appendix A. By a direct calculation now we prove the following property.

The moment system of the subbands augmented with the MEP closure relations forms a quasilinear hyperbolic system in the time direction in the physically relevant range of W^ν.

Proof

Since the differential part of each subband is decoupled in the moment system, we can limit our analysis to the study of a single subband. Let us consider the quasilinear system of PDEs

$$\frac{\partial}{\partial t}\mathcal{F}^{(0)}(\mathbf{U}) + \sum_{i=1}^{2} \frac{\partial}{\partial x^i}\mathcal{F}^{(i)}(\mathbf{U}) = \mathcal{B}(\mathbf{U}, \mathbf{x}, t), \tag{3.33}$$

with $\mathbf{U}(\mathbf{x}, t)$ vector field belonging to a connected open set $\Omega \subset \mathbb{R}^m$, $\forall\, t > 0$ and $\forall\, \mathbf{x} = (x_1, x_2)$ belonging to a domain $D \subseteq \mathbb{R}^2$, and

$$\mathcal{F}^{(\beta)} : \Omega \mapsto \mathbb{R}^m, \quad \beta = 0, 1, 2$$

sufficiently smooth functions. Defining the Jacobian matrices

$$\mathcal{A}^{(\beta)} = \nabla_{\mathbf{U}} \mathcal{F}^{(\beta)}, \quad \beta = 0, 1, 2,$$

the system (4.48) is said to be *hyperbolic in the t-direction* if $\det\left(\mathcal{A}^{(0)}(\mathbf{U})\right) \neq 0$ and the eigenvalue problem

$$\det\left(\sum_{i=1}^{2} n_i \mathcal{A}^{(i)}(\mathbf{U}) - \lambda \mathcal{A}^{(0)}(\mathbf{U})\right) = 0 \tag{3.34}$$

has real eigenvalues and the eigenvectors span $\mathbb{R}^m$ for all unit vectors $\mathbf{n} = (n_1, n_2)$.

In the case under consideration, by omitting the subband index, we have

$$\mathbf{U} = \begin{pmatrix} \rho \\ V^1 \\ V^2 \\ W \\ S^1 \\ S^2 \end{pmatrix}, \quad \mathcal{F}^{(0)} = \rho \begin{pmatrix} 1 \\ V^1 \\ V^2 \\ W \\ S^1 \\ S^2 \end{pmatrix}, \quad \mathcal{F}^{(1)} = \rho \begin{pmatrix} V^1 \\ F^{(0)} \\ 0 \\ S^1 \\ F^{(1)} \\ 0 \end{pmatrix}, \quad \mathcal{F}^{(2)} = \rho \begin{pmatrix} V^2 \\ 0 \\ F^{(0)} \\ S^2 \\ 0 \\ F^{(1)} \end{pmatrix},$$

and the Jacobian matrices are given by

$$\mathcal{A}^{(0)} = \begin{pmatrix} 1 & 0 & 0 & 0 & 0 & 0 \\ V^1 & \rho & 0 & 0 & 0 & 0 \\ V^2 & 0 & \rho & 0 & 0 & 0 \\ W & 0 & 0 & \rho & 0 & 0 \\ S^1 & 0 & 0 & 0 & \rho & 0 \\ S^2 & 0 & 0 & 0 & 0 & \rho \end{pmatrix}, \; \mathcal{A}^{(n)} = \sum_{i=1}^{2} n_i \mathcal{A}^{(i)} = \begin{pmatrix} \mathbf{n}\cdot\mathbf{V} & n_1\rho & n_2\rho & 0 & 0 & 0 \\ n_1 F^{(0)} & 0 & 0 & n_1\rho (F^{(0)})' & 0 & 0 \\ n_2 F^{(0)} & 0 & 0 & n_2\rho (F^{(0)})' & 0 & 0 \\ \mathbf{n}\cdot\mathbf{S} & 0 & 0 & 0 & n_1\rho & n_2\rho \\ n_1 F^{(1)} & 0 & 0 & n_1\rho (F^{(1)})' & 0 & 0 \\ n_2 F^{(1)} & 0 & 0 & n_2\rho (F^{(1)})' & 0 & 0 \end{pmatrix},$$

where the prime denotes partial derivation with respect to W.

The equation

$$\det\left(\mathcal{A}^{(n)} - \lambda \mathcal{A}^{(0)}\right) = 0$$

gives the eigenvalues

$$\lambda_{1,2} = 0, \quad \text{with multiplicity } 2 \tag{3.35}$$

$$\lambda_{3,4,5,6} = \pm\sqrt{\frac{a(W) \pm \sqrt{a(W)^2 - 4b(W)}}{2}} \tag{3.36}$$

where

$$a(W) = F^{(0)} + (F^{(1)})' - W(F^{(0)})', \quad b(W) = F^{(0)}(F^{(1)})' - (F^{(0)})' F^{(1)}.$$

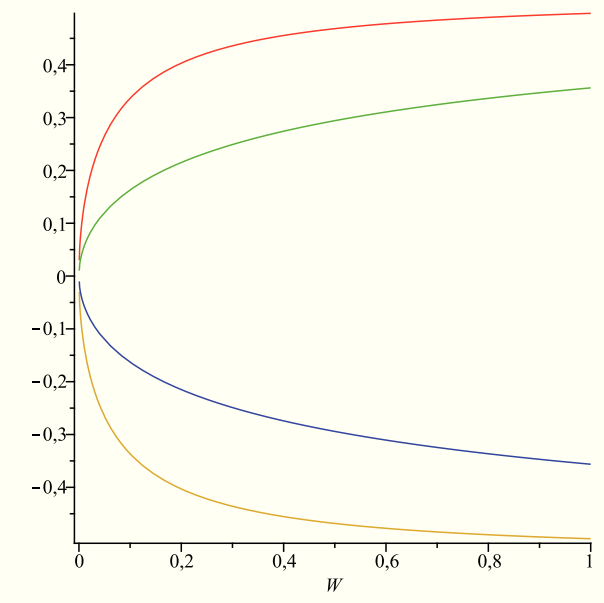

FIGURE 3.14: The eigenvalues $\lambda_{3,4,5,6}$ (10^8cm/s) versus the mean longitudinal energy W ranging from 0 eV to 1 eV

In Fig. 3.14 the eigenvalues $\lambda_{3,4,5,6}$ are plotted in the range 0 eV $\div$ 1 eV which covers at room temperature of the crystal the physical relevant range of the longitudinal mean energy W. The four eigenvalues $\lambda_{3,4,5,6}$ are real and distinct. Therefore each of them has a corresponding eigenspace of dimension one. Concerning the eigenvalue $\lambda = 0$, we observe that whatever $\mathbf{n}$ we take, the first and fourth rows of $\mathcal{A}^{(n)}$ are linearly independent, the second and third rows are proportional and similarly the last two rows since $\rho > 0$ and n_1 and n_2 cannot be both zero. We observe that

$$\det \begin{pmatrix} F^{(0)} & \rho(F^{(0)})' \\ F^{(1)} & \rho(F^{(1)})' \end{pmatrix} = \rho\, b(W).$$

The fact that the eigenvalues $\lambda_{3,4,5,6}$ are real implies that $b(W) > 0$ and it is straightforward to see that the rank of $\mathcal{A}^{(n)}$ is four. This implies that the eigenspace associated to $\lambda = 0$ has dimension two and completes the proof of the hyperbolicity of the system (4.48).

In the one dimensional case one has only the eigenvalues $\lambda_{3,4,5,6}$ and again by similar computations hyperbolicity is recovered.

In the particular case of parabolic energy subbands ($\alpha = 0$) we explicitly have

$$\lambda_{3,4,5,6} = \pm\sqrt{\left(2 \pm \sqrt{2}\right) \frac{W}{m^*}}$$

which are real and distinct provided $W > 0$. □

3.9 Energy-transport model

The method to obtain the energy transport model is the same described in the parabolic case, so we have again

$$\frac{\partial \rho^\nu}{\partial t} + \nabla_{\mathbf{r}_{||}} \cdot (\rho^\nu \mathbf{V}^\nu) = \rho^\nu C_\rho^\nu(\mathbf{W}), \tag{3.37}$$

$$\frac{\partial \rho^\nu W^\nu}{\partial t} + \nabla_{\mathbf{r}_{||}} \cdot (\rho^\nu \mathbf{S}^\nu) + \rho^\nu \nabla_{\mathbf{r}_{||}} \varepsilon_\nu \cdot \mathbf{V}^\nu = \rho^\nu C_W^\nu(\mathbf{W}), \tag{3.38}$$

where the index ν runs over the considered subbands, $\mathbf{W} = (W^1, W^2, \dots)$ and

$$\mathbf{V}^\nu = D_{11}^\nu(\mathbf{W}) \nabla_{\mathbf{r}_{||}} \log \rho^\nu + D_{12}^\nu(\mathbf{W}) \nabla_{\mathbf{r}_{||}} W^\nu - D_{13}^\nu(\mathbf{W}) \nabla_{\mathbf{r}_{||}} \varepsilon_\nu,$$
$$\mathbf{S}^\nu = D_{21}^\nu(\mathbf{W}) \nabla_{\mathbf{r}_{||}} \log \rho^\nu + D_{22}^\nu(\mathbf{W}) \nabla_{\mathbf{r}_{||}} W^\nu - D_{23}^\nu(\mathbf{W}) \nabla_{\mathbf{r}_{||}} \varepsilon_\nu.$$

The coefficients D_{ij}^ν are given by

$$D_{11}^\nu = \frac{c_{22}^\nu F^{(0)\nu} - c_{12}^\nu F^{(1)\nu}}{c^\nu}, \quad D_{12}^\nu = \frac{c_{22}^\nu (F^{(0)\nu})' - c_{12}^\nu (F^{(1)\nu})'}{c^\nu}, \quad D_{13}^\nu = \frac{c_{12}^\nu G^{(1)\nu} - c_{22}^\nu G^{(0)\nu}}{m^* c^\nu},$$
$$D_{21}^\nu = \frac{c_{11}^\nu F^{(1)\nu} - c_{21} F^{(0)\nu}}{c^\nu}, \quad D_{22}^\nu = \frac{c_{11} (F^{(1)\nu})' - c_{21} (F^{(0)\nu})'}{c^\nu}, \quad D_{23}^\nu = \frac{c_{21}^\nu G^{(0)\nu} - c_{11}^\nu G^{(1)\nu}}{m^* c^\nu},$$

with $c^\nu = c_{11}^\nu c_{22}^\nu - c_{12}^\nu c_{21}^\nu$ and $F^{(r)\nu}$, $G^{(r)\nu}$ longitudinal components of $\mathbf{F}^{(r)\nu}$, $\mathbf{G}^{(r)\nu}$, $r = 0, 1$. The system (3.37)-(3.38) must be coupled with the Schrödinger-Poisson block.

In order to classify the ET equations, let us rewrite the system (3.37)-(3.38) as

$$\frac{\partial}{\partial t} \begin{pmatrix} \rho^\nu \\ \rho^\nu W^\nu \end{pmatrix} + \operatorname{div} \begin{pmatrix} (D_{11}^\nu - W^\nu D_{12}^\nu) \nabla \rho^\nu + D_{12}^\nu \nabla (\rho^\nu W^\nu) \\ (D_{21}^\nu - W^\nu D_{22}^\nu) \nabla \rho^\nu + D_{22}^\nu \nabla (\rho^\nu W^\nu) \end{pmatrix} + \text{r.t.} = \begin{pmatrix} 0 \\ 0 \end{pmatrix}$$

where r.t. stands for the remaining lower order derivative terms. We would like to show that the diffusion matrix

$$\hat{D}^\nu = \begin{pmatrix} D_{11}^\nu - W^\nu D_{12}^\nu & D_{12}^\nu \\ D_{21}^\nu - W^\nu D_{22}^\nu & D_{22}^\nu \end{pmatrix} \tag{3.39}$$

in the relevant physical cases is negative definite, that is $\xi \cdot \hat{D}^\nu \xi < 0, \quad \forall \xi \in \mathbb{R}^2, \xi \neq (0,0)^T$. The elements of $\hat{D}^\nu$ indeed depend on the bottom of the subbands ε_ν and envelope functions $\varphi_\nu(z)$, $\nu = 1, 2, 3, \dots$ that can be evaluated only numerically in a DG-MOSFET. However, if we consider the case of an infinite potential barrier, one has

the explicit formulas

$$\varepsilon_\nu = \frac{\nu^2\pi^2\hbar^2}{2L_z^2 m^*}, \quad \varphi_\nu(z) = \sqrt{\frac{2}{L_z}}\sin\frac{\nu\pi}{L_z}(z - t_{ox}), \quad z \in [t_{ox}, t_{ox} + L_z], \quad \nu = 1, 2, \dots$$

By evaluating the eigenvalues of $\hat{D}^\nu$ with the previous expressions of the bottom energy of the first three subbands, one finds the results plotted in Fig. 3.15. No additional subbands are considered because as will be shown in the last section, the inclusion of more than three subbands is practically irrelevant. For the relevant range of energy W^ν we have two distinct and real negative eigenvalues in each subband. Therefore *at least in the case of an infinite potential barrier, employing the first three subbands, the ET model is represented by two parabolic equations for each band coupled to the Poisson equation.*

The reader interested in analytical questions about general ET models is referred to [14, 47]. A recent result of existence for the semiclassical ET MEP model has been obtained in [16].

3.10 Numerical simulations for the Kane case

Also these simulations have been performed on a Workstation with a 8 GB RAM and a 2.67GHz Intel(R) Xeon(R) X3450 CPU. The code has been compiled using the GNU gfortran compiler and every simulation has taken an average of 4-6 hours, depending on the applied voltages. The numerical experiments indicate that it is sufficient to take into account only the first three subbands. The steady state is reached after about 5 picoseconds. By using as units picoseconds for time, microns for length and electron volts for energy, it is not necessary to adimensionalize the variables. The physical parameters are reported in tables A.1, A.2 of the Appendix A. In order to fix the number of grid points, some preliminary numerical simulations of the thermal equilibrium, which represents also the initial data for the other simulations, suggest to take about $30 \div 40$ nodes in the transversal direction. So we take 37 points along the z-axis, but we consider along the longitudinal direction grids with 16, 32 and 64 cells (17, 33 and 65 grid points respectively), in the case $V_D = 0.5$ V and $V_{gl} = V_{gu} = 0$ V, with V_D voltage applied at the drain with respect to that at the source, and V_{gl} and V_{gu} voltages respectively applied at the lower and the upper gate. The results relative to the areal density and the longitudinal average energy are plotted for each subband in Fig.s 3.16. At variance with the simplified cases considered in [20], the behaviour of the error is not uniform due to the coupling with the Schrödinger-Poisson block. In the drain one has a degradation of the convergence rate c_R which is worse in the third subband than in the first subband.

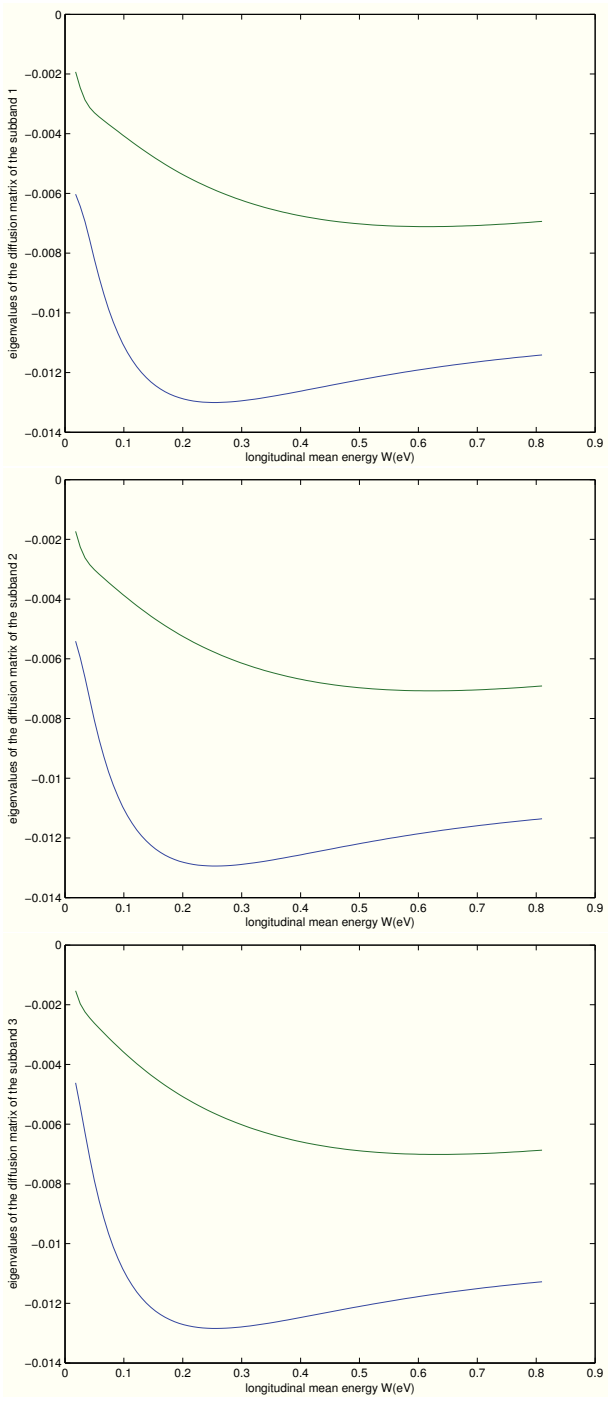

FIGURE 3.15: Eigenvalues of the matrix $\hat{D}^{\nu}$ for $\nu = 1, 2, 3$ versus the mean longitudinal energy.

TABLE 3.1: Mean convergence rate by comparing meshes with 17, 33, 65 grid points in the case $V_D = 0.5$ V and $V_{gl} = V_{gu} = 0$ V

	ρ^1	ρ^2	ρ^3	W^1	W^2	W^3
c_R	1.1066	0.7701	0.7302	1.4020	1.4849	1.4430

If we denote by $u_{(k)}$ the generic variable of the solution with k cells, at each grid point of the coarser grid, c_R can be estimated as

$$c_{Ri} = \log_2 \left| \frac{u_{(16)i} - u_{(32)i}}{u_{(32)i} - u_{(64)i}} \right|, \quad i = 1, 2, \ldots, 17, \tag{3.40}$$

while a global estimate is given by the average

$$c_R = \frac{1}{17} \sum_{i=1}^{17} c_{Ri}. \tag{3.41}$$

In table 3.1 the mean convergence rates are reported. The longitudinal energies present a converge of high order than the areal densities. On the base of the previous considerations in the following simulations a grid with 65×37 grid points is used.

As first case we consider a symmetric situation: $V_D = 0.5$ V and $V_{gl} = V_{gu} = -3$ V. In Fig.s 3.17 and 3.18 we plot the steady state density and the potential. The solution does not present any spurious oscillation or boundary layer and reflects the symmetry of the problem. It is evident that the boundary conditions at source and drain are completely different from the semiclassical ones that are simply $n = N_D$. In Fig. 3.21 the first three subband bottoms are shown. We have a good qualitative agreement with the other numerical simulations known in the literature [34, 35].

As second case we take $V_D = 0.5$ V, $V_{gl} = -3$ V and $V_{gu} = 3$ V. In Fig.s 3.19 and 3.20 we plot the density and the potential respectively, while in Fig. 3.21_2 the first three subband bottoms are shown. One can note the depletion region beneath the upper gate.

From Fig.s 3.22 it is evident a very accurate current conservation, proving the robustness of the numerical method. In the second case the current is reduced by one half due to the gate voltage in agreement with the behaviour of the density.

Areal density, average velocity and energy measured from the subband bottom and current in the first three subbands are shown in Fig.s 3.23-3.25. The areal density is not symmetric between source and drain within each subband but the total areal density is so.

The drift (mean) velocity has been evaluated according again to the formula 3.28 Similarly the global longitudinal mean energy has been evaluated taking as reference value

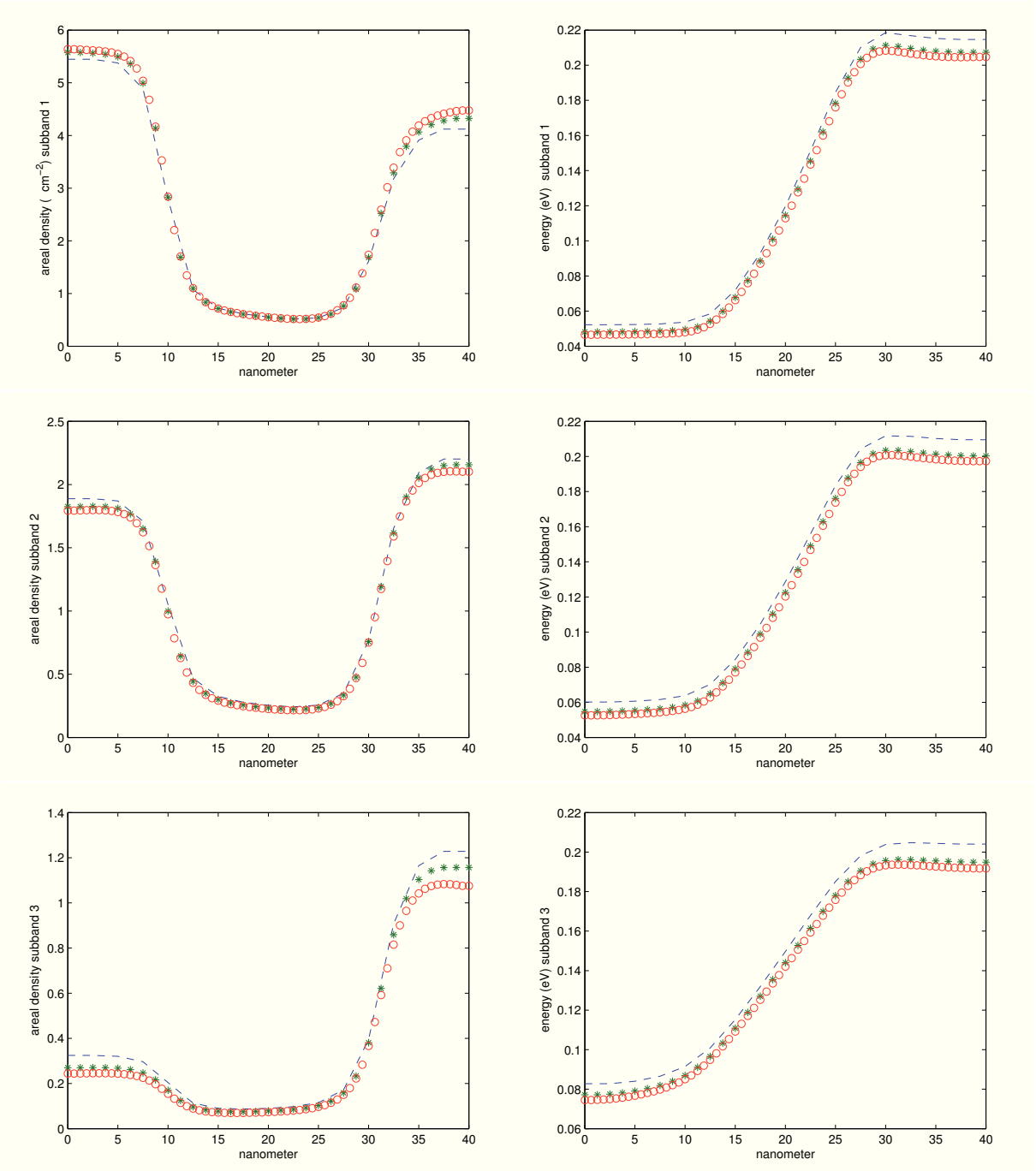

FIGURE 3.16: Comparison of the results for the areal density and the average longitudinal energy in the case $V_D = 0.5$ V and $V_{gl} = V_{gu} = 0$ V by using 17(–), 33 (*), 65 (o) grid points

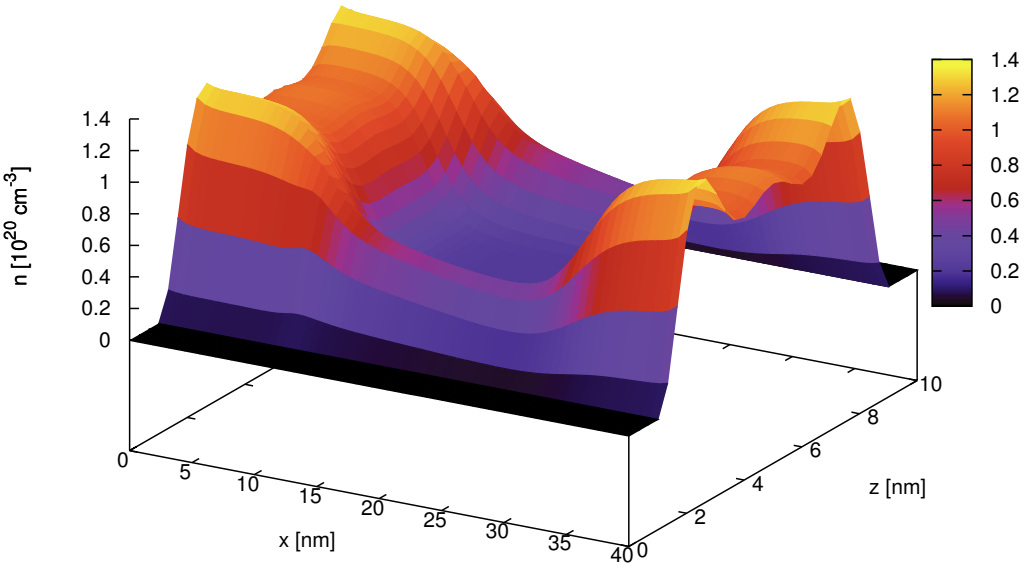

FIGURE 3.17: Stationary density in the case $V_D = 0.5$ V and $V_{gl} = V_{gu} = -3$ V

the bottom of the first subband according to the formula 3.29 The maximum drift velocity in the channel is one and half times the saturation velocity when $V_{gl} = V_{gu} = -3$ V, while it is about two times the saturation velocity when $V_{gl} = -3$ V and $V_{gu} = 3$ V. Moreover in the first case the velocity in the first subband is lower than that in the first subband in the second case. Instead the velocity in the second and third subbands is higher in the first case, but with a resulting lower total longitudinal current.

The energy has an evidently different value between source and drain as happens in the semiclassical case. The use of Dirichlet conditions for the energy at the contacts misses such an effect.

At last the characteristic curves have been calculated and shown in Fig. 3.26 by fixing $V_{gl} = -3$ V and varying V_{gu} from - 3 V to 3 V. With increasing V_{gu} the average longitudinal current increases as consequence of the controlling effect of the gate voltage on the electric characteristics of the device.

The comparison with the parabolic band case regarding the current is reported in table 3.2. For moderate values of V_D the currents differ of about 10 %, but at higher fields ($\approx$0.35 V) the difference becomes of about 25%, clearly showing the influence of the band structure and the fact, already known in the semiclassical case, that the currents are lower when the non-parabolicity effects are included.

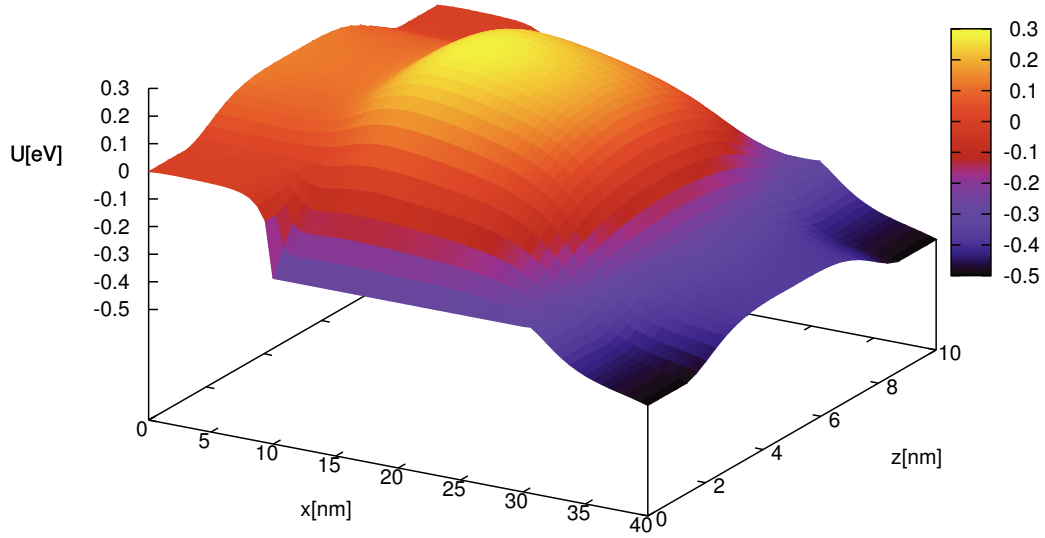

FIGURE 3.18: Stationary electrostatic potential energy in the case $V_D = 0.5$ V and $V_{gl} = V_{gu} = -3$ V

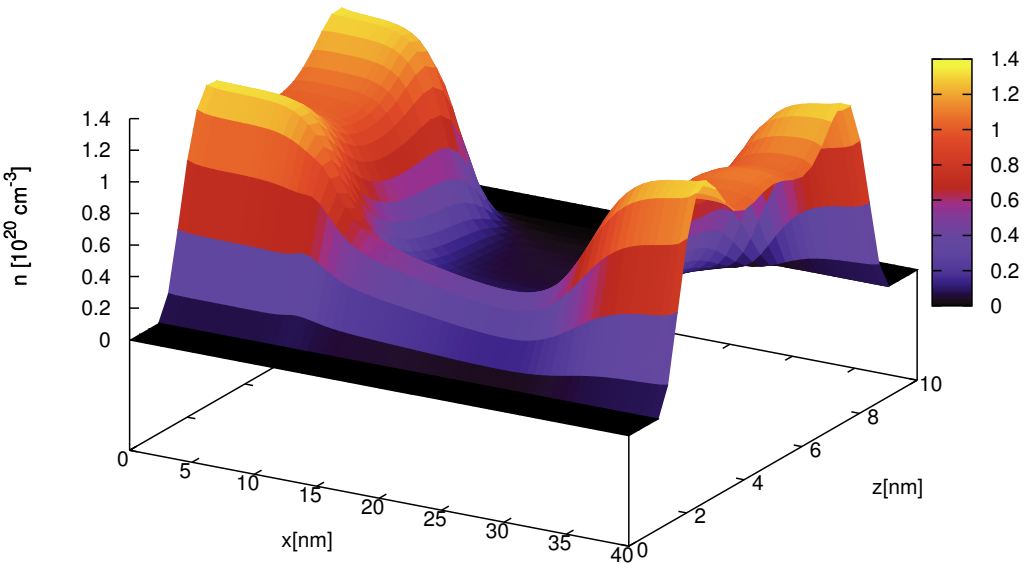

FIGURE 3.19: Stationary density in the case $V_D = 0.5$ V and $V_{gl} = -3$ V, $V_{gu} = 3$ V

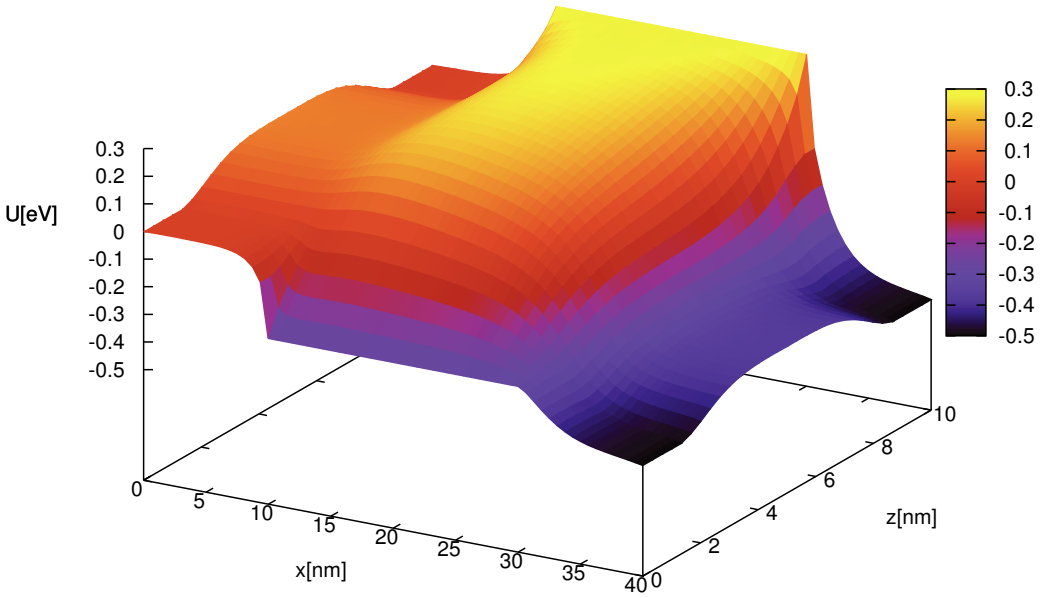

FIGURE 3.20: Stationary electrostatic potential energy in the case $V_D = 0.5$ V and $V_{gl} = -3$ V, $V_{gu} = 3$ V

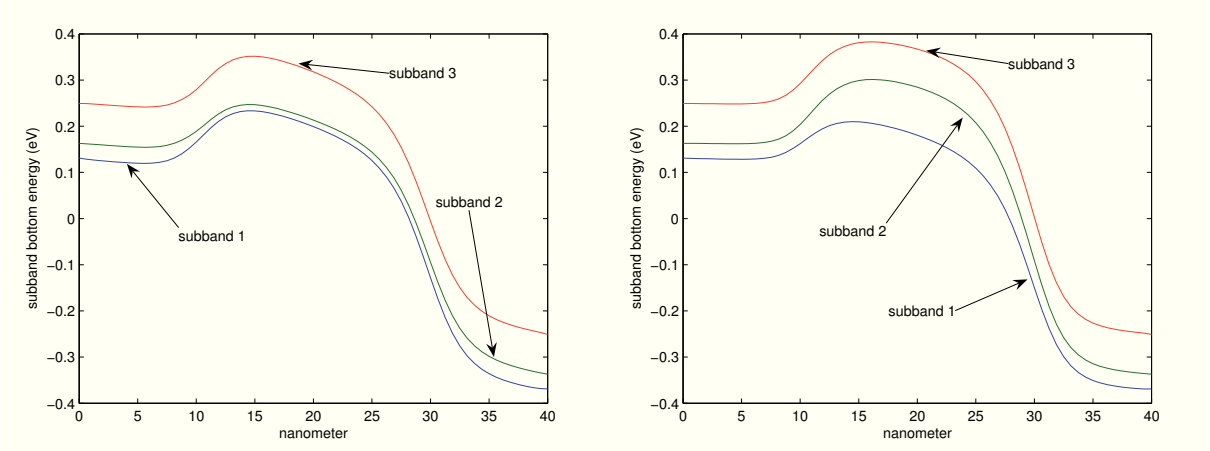

FIGURE 3.21: First three subbands at the steady state in the case $V_D = 0.5$ V and $V_{gl} = V_{gu} = -3$ V (left), $V_D = 0.5$ V and $V_{gl} = -3$ V, $V_{gu} = 3$ V (right).

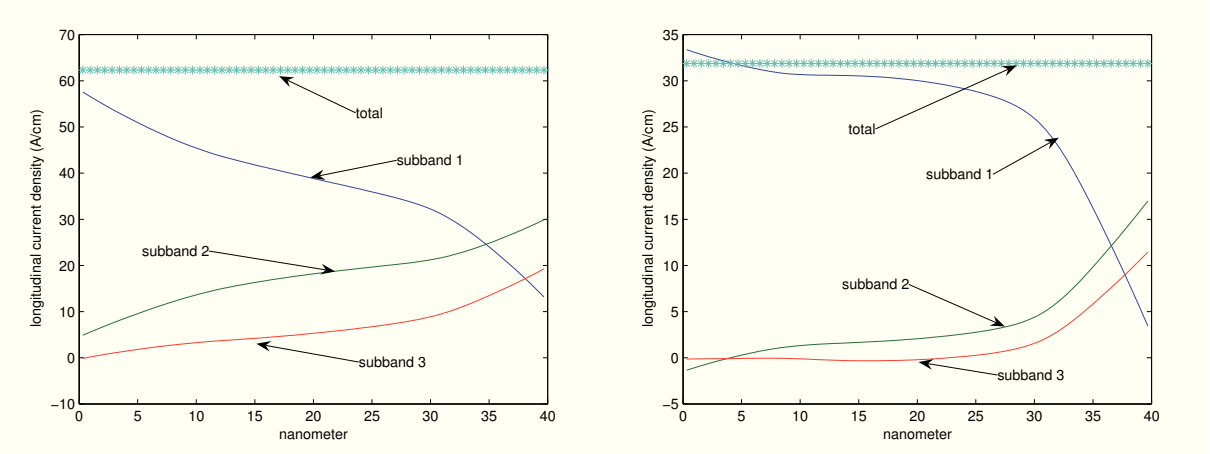

FIGURE 3.22: Average areal current in the first three subbands and global areal current in the case $V_D = 0.5$ V and $V_{gl} = V_{gu} = -3$ V (left), $V_D = 0.5$ V and $V_{gl} = -3$ V, $V_{gu} = 3$ V (right).

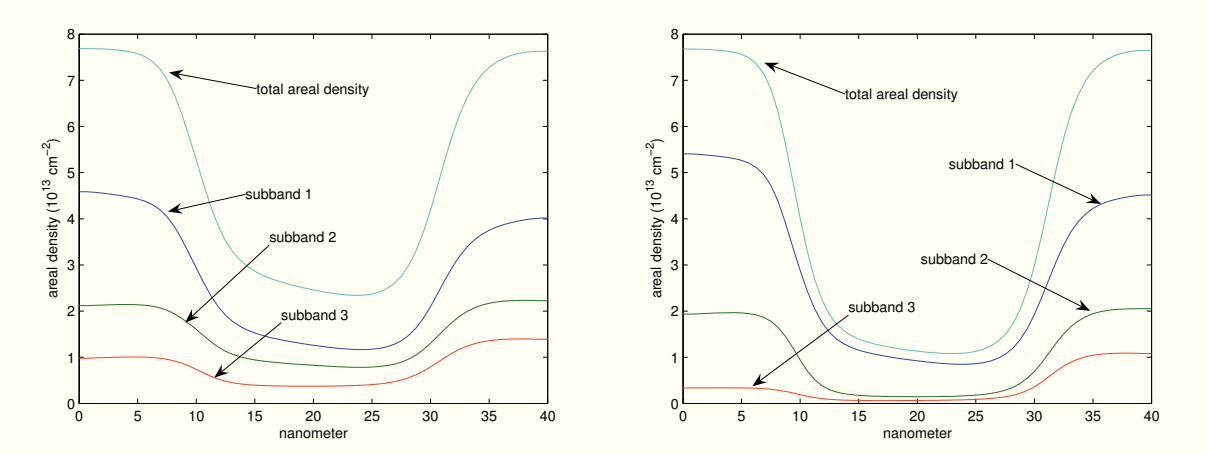

FIGURE 3.23: Areal density in the first three subbands in the case $V_D = 0.5$ V and $V_{gl} = V_{gu} = -3$ V (left), $V_D = 0.5$ V and $V_{gl} = -3$ V, $V_{gu} = 3$ V (right).

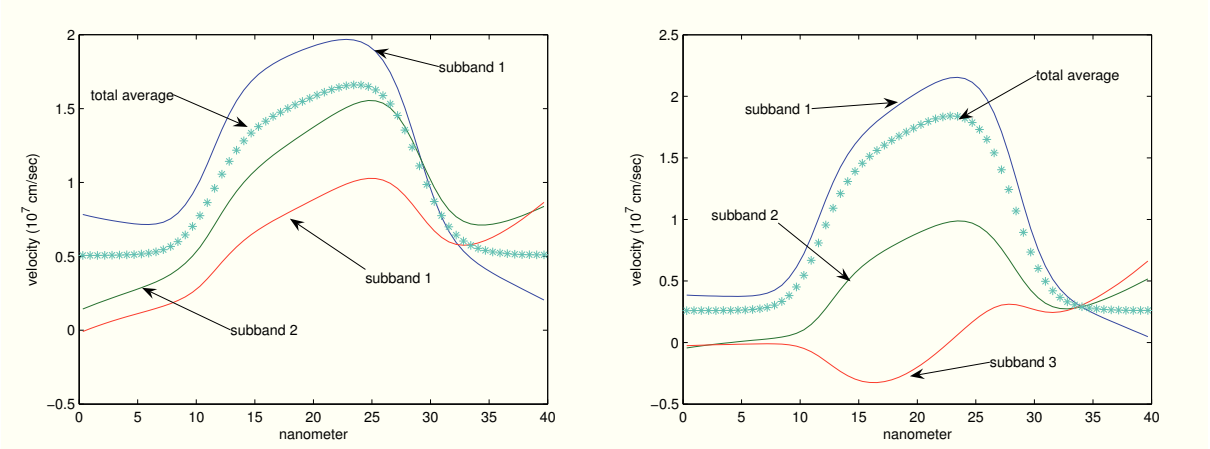

FIGURE 3.24: Average velocity in the first three subbands and global mean velocity in the case $V_D = 0.5$ V and $V_{gl} = V_{gu} = -3$ V (left), $V_D = 0.5$ V and $V_{gl} = -3$ V, $V_{gu} = 3$ V (right).

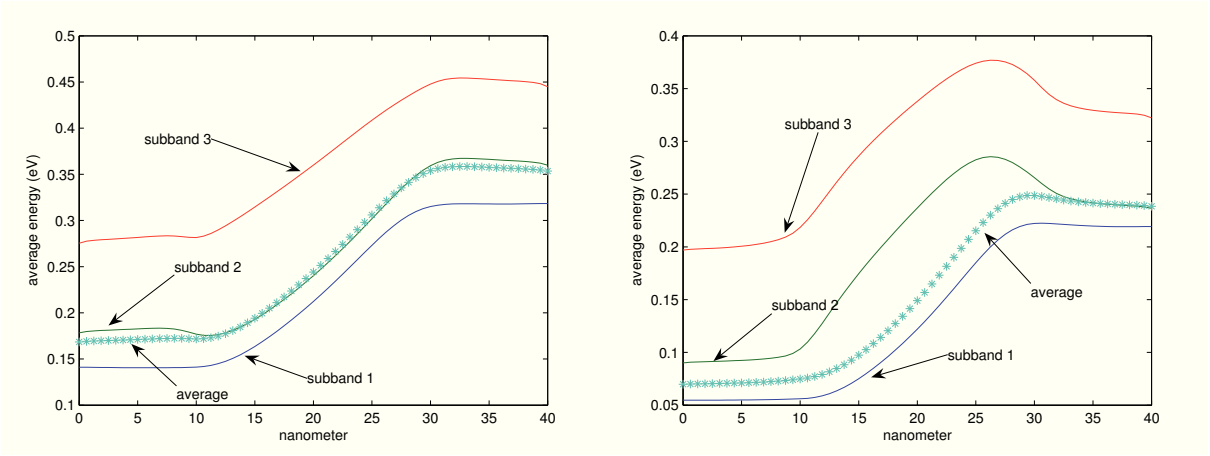

FIGURE 3.25: Average total energy measured from the bottom of the first subband $W^{\nu} + \varepsilon_{\nu} - \varepsilon_1$ in the first three subbands and global mean energy in the case $V_D = 0.5$ V and $V_{gl} = V_{gu} = -3$ V (left), $V_D = 0.5$ V and $V_{gl} = -3$ V, $V_{gu} = 3$ V (right).

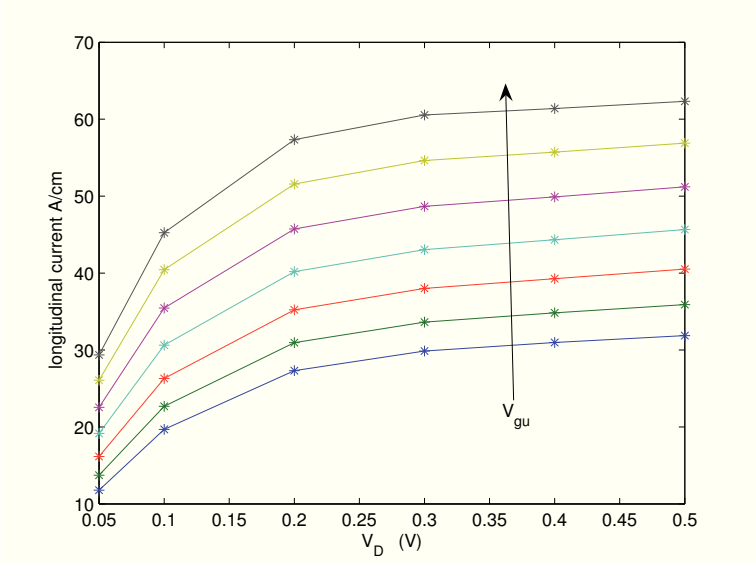

FIGURE 3.26: Longitudinal mean current (A/cm) versus the source- drain voltage V_D with $V_{gl} = -3$ V and V_{gu} ranging from - 3 V to +3 V according to the arrow

TABLE 3.2: Total longitudinal currents (A/cm) versus V_D (V), for $V_{gl} = V_{gu} = 0$ V in the parabolic and non-parabolic case

V_D (V)	0.15	0.2	0.25	0.3	0.35
longitudinal current: parabolic case	23.065	25.256	27.436	29.113	32.790
longitudinal current: non-parabolic case	21.026	23.289	24.597	25.391	25.939

Chapter 4

2DEG-3DEG charge transport model for MOSFET

After the exposition of the transport model for the DG-MOSFET, in this last chapter a charge transport model for the MOSFET will be developed taking into account the coexistence of 2D and 3D electron gas.
The model here exposed has been extracted by the preprint

- Camiola, V.D., Romano, V.: 2DEG-3DEG charge transport model for mosfet based on the Maximum Entropy Principle, (submitted)

4.1 Confinement effects in nanoscale MOSFET

In a MOSFET (fig.4.1), in the proximity of the Si/SiO_2 interface a two dimensional electron gas (2DEG) is created with a discrete energy spectrum along the z-direction (fig.4.2). Above a fixed energy level, the energy spectrum is continuous and a three dimensional electron gas (3DEG) coexists with the 2DEG. To describe the whole system, we define a spatial quantum region $\mathcal{R}_Q$ where the 2DEG is confined, associated with an energy quantum region $\mathcal{R}_E$ in the wave-vector space. Outside $\mathcal{R}_Q$ electrons are only belonging to the 3DEG.

In the quasi-static approximation, the 2D-charges in $\mathcal{R}_Q$ are described by the steady wave function

$$\psi_\nu(\mathbf{k},\mathbf{r}) = \psi_\nu(k_x,k_y,k_z,x,y,z) = \frac{1}{\sqrt{\mathcal{A}}}\phi_\nu(\mathbf{r}_{||},z)e^{i\mathbf{k}_{||}\cdot\mathbf{r}_{||}}$$

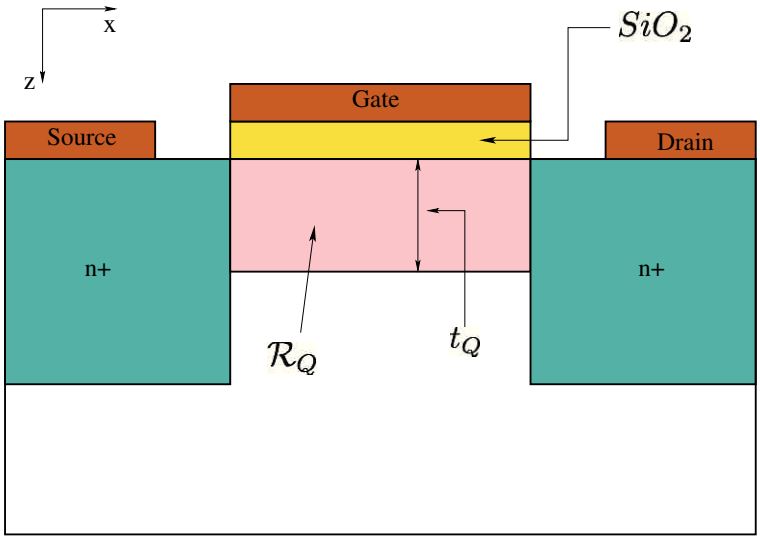

FIGURE 4.1: Simulated MOSFET.

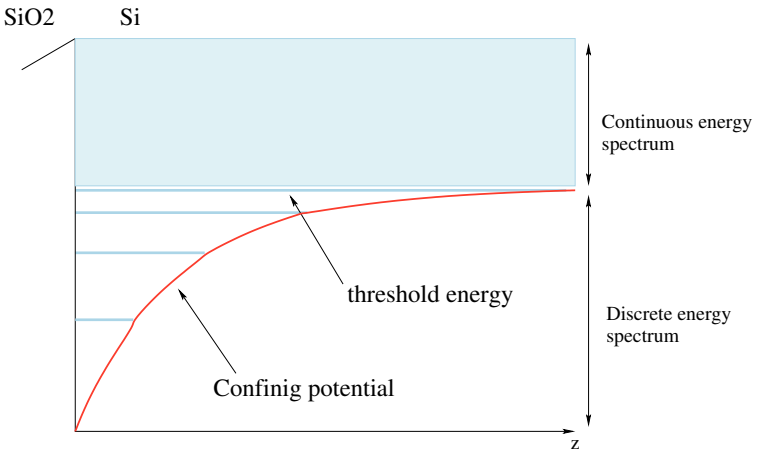

FIGURE 4.2: Energy spectrum.

with $\mathbf{k}_{||} = (k_x, k_y)$ and $\mathbf{r}_{||} = (x, y)$ denoting the longitudinal components of the wave-vector $\mathbf{k}$ and the position vector $\mathbf{r}$, respectively, and $\mathcal{A}$ symbolizing the area of the xy cross-section of $\mathcal{R}_Q$.

$\phi_\nu(\mathbf{r}_{||}, z)$ is called envelope function and, under the scaling where the ratio between transversal and longitudinal characteristic lengths is small [31], it is solution of the following Schrödinger equation in the effective mass approximation

$$\left[-\frac{\hbar^2}{2m^*}\frac{d^2}{dz^2} - q(V_C + V)\right]\phi_\nu(\mathbf{r}_{||}, z) = \varepsilon_\nu \phi_\nu(\mathbf{r}_{||}, z) \tag{4.1}$$

where $\hbar$ is the reduced Planck constant, m^* is the effective electron mass, V_C is the confining potential and V is the self-consistent electrostatic potential which solves the Poisson equation. Note that in (4.1) $\mathbf{r}_{||}$ enters as a parameters.

Under the assumption that the confining potential gives rise to an infinite barrier at the oxide/silicon interface (z=0) and that a fictitious boundary is posed at $z = t_Q$, we solve eq.(4.1) only inside the $\mathcal{R}_Q$ region by setting $\phi = 0$ at $z = 0$ and $z = t_Q$, the boundary of $\mathcal{R}_Q$. Equation (4.1) with the previous boundary is a self-adjoint problem posed on a limited domain. So one finds a countable set of normalized eigen-pairs (subbands) $(\phi_\nu, \varepsilon_\nu)$.

In each subband the energy E_ν is the sum of a transversal contribution $\varepsilon_\nu(\mathbf{r}_{||})$ and a longitudinal (kinetic) contribution $\varepsilon_{||} = \frac{\hbar^2}{2m^*}(k_x^2 + k_y^2)$, that is

$$E_\nu(\mathbf{r}_{||}, \mathbf{k}_{||}) = \varepsilon_\nu(\mathbf{r}_{||}) + \varepsilon_{||}(\mathbf{k}_{||}). \tag{4.2}$$

The corresponding longitudinal velocity is

$$\mathbf{v}_{||} = \frac{1}{\hbar}\nabla_{\mathbf{k}_{||}}\varepsilon_{||} = \frac{\hbar\mathbf{k}_{||}}{m^*}. \tag{4.3}$$

We assume that above a threshold energy E_T electrons are 3D and therefore only the subbands with $E_\nu < E_T$ are retained. We will denote by ν_T the threshold subband index. Formally let us define

$$\mathcal{R}_E(x) = \left\{\varepsilon_\nu(\mathbf{r}_{||}, z) : E_\nu < E_T\right\}. \tag{4.4}$$

Then $\mathbf{k}_{||} = (k_x, k_y) \in B_2^\nu$, where

$$B_2^\nu = \left\{(k_x, k_y) \in \mathbb{R}^2 : 0 \leq \frac{\hbar^2}{2m^*}(k_x^2 + k_y^2) \leq E_T - \varepsilon_\nu, \varepsilon_\nu \in \mathcal{R}_E\right\}$$

is the selected Brillouin zone for 2D electrons in the ν-th subband.

The Brillouin zone for the 3D electrons is

$$B_3^* = \left\{(k_x, k_y, k_z) \in \mathbb{R}^3 : \mathcal{E}(\mathbf{k}) \geq E_T\right\}$$

where we are assuming a Kane dispersion relation in order to take into account the effetcs of nonparabolicity at high energies

$$\mathcal{E}(\mathbf{k})\left[1 + \alpha\mathcal{E}(\mathbf{k})\right] = \frac{\hbar^2 k^2}{2m^*}.$$

Under the assumption that the channel length is no shorter than few tents of nanometers, the transport of the carriers is assumed to be well described by semiclassical Boltzmann equations. 2D electrons in each subband are considered as different populations and for each subband it is introduced a distribution function $f_\nu(\mathbf{x}_{||}, \mathbf{k}_{||}, t)$ obeying the Boltzmann

equation

$$\frac{\partial f_\nu(\mathbf{x}_{||},\mathbf{k}_{||},t)}{\partial t}+\mathbf{v}_{||}\cdot\nabla_{\mathbf{r}}f_\nu(\mathbf{x}_{||},\mathbf{k}_{||},t)-\frac{q}{\hbar}\mathbf{E}_\nu^{eff}\cdot\nabla_{\mathbf{k}}f_\nu(\mathbf{x}_{||},\mathbf{k}_{||},t)=C_\nu^{2D},\quad \mathbf{k}\in B_2^\nu \tag{4.5}$$

where $\mathbf{E}_\nu^{eff}=\frac{1}{q}\nabla_{\mathbf{r}}\varepsilon(\mathbf{r}_{||})$ and C_ν^{2D} describes the scattering with phonons, including the mechanisms pushing 2D electrons into the 3DEG (see later for more details).

The 3DEG in the region $\mathcal{R}_Q$ is described by the Boltzmann equation

$$\frac{\partial f(\mathbf{x},\mathbf{k},t)}{\partial t}+\mathbf{v}\cdot\nabla_{\mathbf{r}}f(\mathbf{x},\mathbf{k},t)-\frac{q}{\hbar}\mathbf{E}\cdot\nabla_{\mathbf{k}}f(\mathbf{x},\mathbf{k},t)=C^{3D},\quad \mathbf{k}\in B_3^* \tag{4.6}$$

where $\mathbf{v}=\frac{1}{\hbar}\nabla_{\mathbf{k}}\mathcal{E}$ is the electron group velocity

$$\mathbf{v}=\frac{1}{m^*}\frac{\hbar\mathbf{k}}{1+2\alpha\mathcal{E}}. \tag{4.7}$$

C^{3D} represents the scattering of 3D electrons with phonons, including the mechanisms pushing 3D electrons into the 2DEG (see later for more details). $\mathbf{E}=-\nabla_{\mathbf{r}}V$ is the self-consistent electric field which is related to the electron distributions function through Poisson's equation

$$\nabla\left(\epsilon\nabla V\right)=-q\left(n_d(\mathbf{r})-n_T(\mathbf{r})\right) \tag{4.8}$$

with ϵ the relative permittivity, $n_d(\mathbf{r})$ the doping concentration and $n_T(\mathbf{r})$ the total charge density given by

$$n_T(\mathbf{r},t)=n(\mathbf{r},t)+\sum_{\nu=1}^{\nu_T}\rho_\nu(x,y,t)|\phi_\nu(z,t)|^2 \tag{4.9}$$

with

$$n(\mathbf{r},t)=\int_{B_3^*}f(\mathbf{x},\mathbf{k},t)d^3\mathbf{k} \tag{4.10}$$

the density of the bulk electrons, and

$$\rho^\nu\left(\mathbf{r}_{||},t\right)=\int_{B_2^\nu}f_\nu(\mathbf{r}_{||},\mathbf{k}_{||},t)d^2\mathbf{k}_{||} \tag{4.11}$$

the areal density of electrons in the ν-th subband.

Now, let us examine in more detail the collisional terms. The main scattering processes considered in this paper are due to acoustic phonons and non polar optical phonons. The first ones are considered in the elastic approximation so, after the scattering, a 2D electron in the ν-subband can remain in the same subband or scatter in another subband. In any case it remains belonging to the 2DEG because the total energy (4.2)

is conserved. The same consideration holds for the 3D electrons that remains belonging to the 3DEG as well.

Instead the electron scattering due to non polar optical phonons is an inelastic process, so a 2D electrons can absorb a phonon and occupy a quantum state with a total energy greater than E_T, becoming a 3D electron, while an electron of the 3DEG can be scattered into the 2DEG after the emission of a phonon. To describe these processes, let us define the following sets:

$$B_2^{*\nu} = \left\{ (k_x, k_y) \in \mathbb{R}^2 : \frac{\hbar^2}{2m^*}(k_x^2 + k_y^2) \geq E_T - \hbar\omega \right\}$$

$$B_3^{**} = \left\{ (k_x, k_y, k_z) \in \mathbb{R}^3 : \mathcal{E}(\mathbf{k}) \leq E_T + \hbar\omega \right\}$$

where $\hbar\omega$ is the phonon energy. Of course these sets depend on the specific non polar optical phonon scattering we are dealing with.

The collisional terms of (4.5) and (4.6) can be written in the following manner

$$C_\nu^{2D} = \sum_{\mu=1}^{\nu_T} C_{\nu\mu}^{(ac)}(\mathbf{k}) + \sum_{\mu=1}^{\nu_T} C_{\mu\nu}^{(no)}(\mathbf{k}) + C_\nu^{(no),3D}(\mathbf{k}) \tag{4.12}$$

$$C_{3D} = C_{3D}^{(ac)}(\mathbf{k}) + C_{3D}^{(no)}(\mathbf{k}) + C^{(no),2D}(\mathbf{k}) \tag{4.13}$$

The terms $C_{\nu\mu}^{(ac)}$ and $C_{3D}^{(ac)}$ describe the scattering due to acoustical phonons; $C_{\mu\nu}^{(no)}$ and $C_{3D}^{(no)}$ describe the scattering with non polar optical phonons, respectively in 2DEG and 3DEG; $C_\nu^{(no),3D}(\mathbf{k})$ and $C^{(no),2D}(\mathbf{k})$ describe the scattering with non polar optical phonons from the ν-subband to the 3DEG and vice versa. Note that when $\mu = \nu$ one has an intra-subband scattering, otherwise an inter-subband scattering.

The general expression for acoustic collision terms are the following

$$C_{\nu\mu}^{(ac)} = \int_{B_2^\nu} [S_{\mu\nu}(\mathbf{k}'_{||}, \mathbf{k}_{||}) f_\mu(\mathbf{k}') - S_{\nu\mu}(\mathbf{k}_{||}, \mathbf{k}'_{||}) f_\nu(\mathbf{k})] d^3\mathbf{k} \tag{4.14}$$

$$C_{3D}^{(ac)} = \int_{B_3^*} \left[P(\mathbf{k}', \mathbf{k}) f(\mathbf{k}') - P(\mathbf{k}, \mathbf{k}') f(\mathbf{k}) \right] d^3\mathbf{k} \tag{4.15}$$

Regarding the non polar optical phonons, figure (4.3) shows the energy ranges of the scattering for each term.

The non polar phonon scattering intra the 2DEG and intra the 3DEG are given by

$$C_\nu^{(no)} = \int_{B_2^\nu} [S_{\mu\nu}(\mathbf{k}'_{||}, \mathbf{k}_{||}) f_\mu(\mathbf{k}') - S_{\nu\mu}(\mathbf{k}_{||}, \mathbf{k}'_{||}) f_\nu(\mathbf{k})] d^3\mathbf{k} \tag{4.16}$$

$$C^{(no)} = \int_{B_3^*} \left[P(\mathbf{k}', \mathbf{k}) f(\mathbf{k}') - P(\mathbf{k}, \mathbf{k}') f(\mathbf{k}) \right] d^3\mathbf{k} \tag{4.17}$$

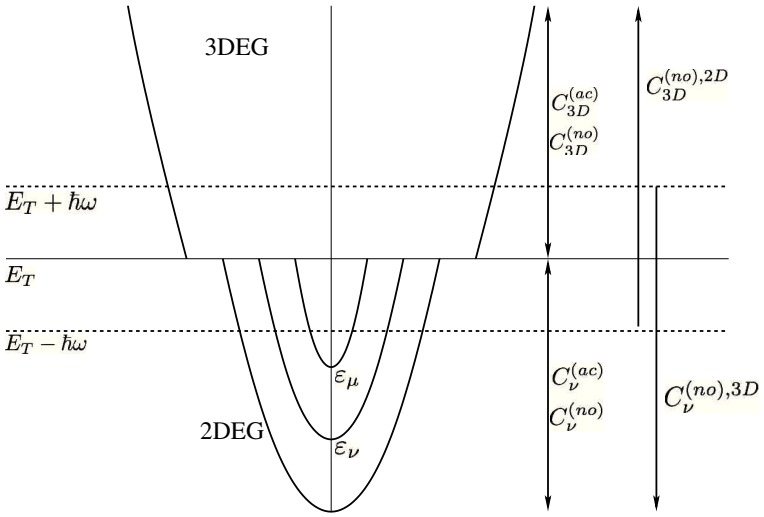

FIGURE 4.3: Schematics representation of scattering between 2DEG and 3DEG

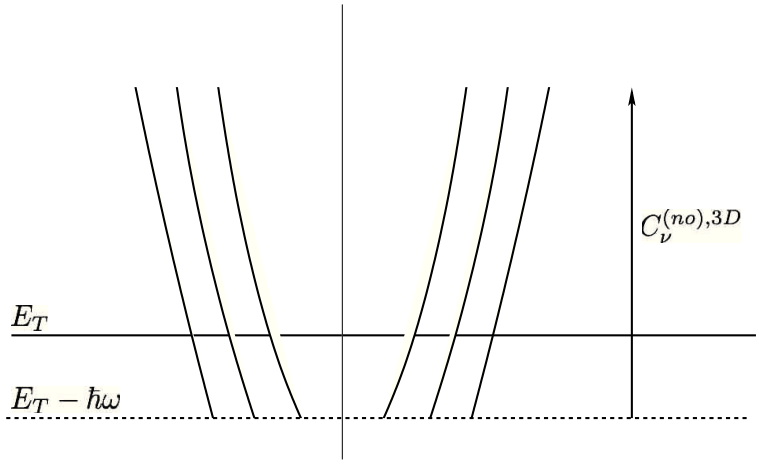

FIGURE 4.4: Schematic representation of $B_2^{*\nu}$ which is the energy region above $E_T - \hbar\omega$

Now, let us note that 2D-electrons in the energy interval $(E_T - \hbar\omega, E_T)$ can absorb a non polar optical phonon and go into the 3DEG. This process is described by the term

$$C_\nu^{(no),3D} = \int_{B_2^{*\nu}} [S_{\mu\nu}(\mathbf{k}'_{||}, \mathbf{k}_{||}) f_\mu(\mathbf{k}') - S_{\nu\mu}(\mathbf{k}_{||}, \mathbf{k}'_{||}) f_\nu(\mathbf{k})] d^3\mathbf{k} \tag{4.18}$$

where the integral is calculated on $B_2^{*\nu}$, that can be viewed as an extension of the 2D zone (fig. 4.4).

At the same time, a 3D electron in the energy interval $(E_T, E_T + \hbar\omega)$ can loose energy by the emission of a phonon and became a 2D charge. In this case the process is described by

$$C^{(no),2D} = \int_{B_3^{**}} \left[P(\mathbf{k}', \mathbf{k}) f(\mathbf{k}') - P(\mathbf{k}, \mathbf{k}') f(\mathbf{k})\right] d^3\mathbf{k} \tag{4.19}$$

where the integration is performed on B_3^{**} (see fig.4.5).

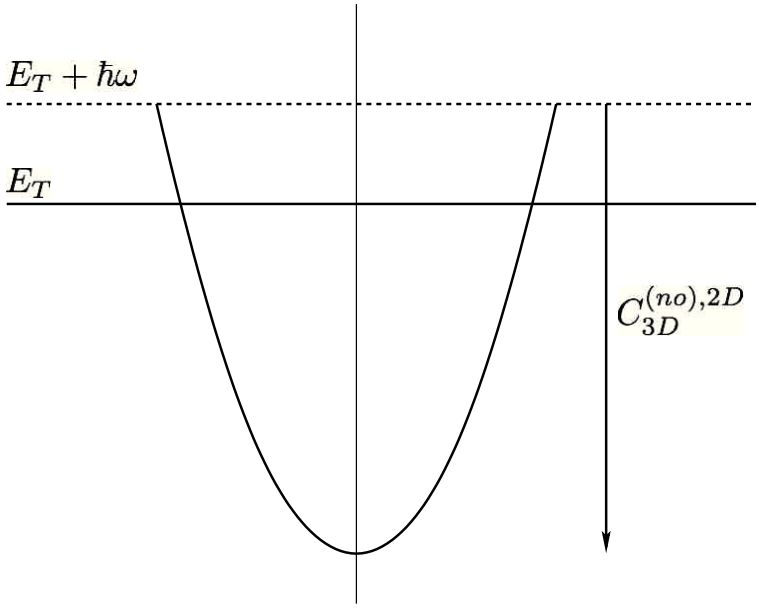

FIGURE 4.5: Schematic representation of B_3^{**} which is the energy region below $E_T + \hbar\omega$

For the electron-acoustic phonon scattering in the elastic approximation, the transition rate is given by

$$S_{\mu\nu}^{(ac)}(\mathbf{k}_{||}, \mathbf{k}'_{||}) = \frac{k_B T_L \Xi_d^2}{4\pi^2 \hbar \rho v_S^2} G_{\nu\mu} \delta(E_\mu(\mathbf{k}'_{||}) - E_\nu(\mathbf{k}_{||})). \tag{4.20}$$

where k_B is the Boltzmann constant, T_L the lattice temperature, which will be kept constant in this paper, ρ the silicon density, Ξ_d the acoustic phonon deformation potential, and v_S the longitudinal sound speed. Their values are the same reported in the Table **??**. The $G_{\mu\nu}$'s are the interaction integrals

$$G_{\mu\nu} = \int_{-\infty}^{+\infty} |\mathbf{I}_{\nu\mu}(q_z)|^2 dq_z, \quad \mathbf{I}_{\mu\nu}(q_z) = \int_0^{t_Q} \overline{\phi}_\nu(z) \phi_\mu(z) e^{iq_z z} dz \tag{4.21}$$

with $\mathbf{q}$ denoting the 3D-phonon wave vector, and bar indicating complex conjugation. Let us note that $G_{\mu\nu} = G_{\nu\mu}$ holds.

Similarly for non-polar optical phonon scattering one has

$$S_{\mu\nu}^{(no)}(\mathbf{k}_{||}, \mathbf{k}'_{||}) = Z_f \frac{(D_t K)^2}{8\pi^2 \rho \omega} \left(N_q + \frac{1}{2} \mp \frac{1}{2} \right) \delta(E_\mu(\mathbf{k}'_{||}) - E_\nu(\mathbf{k}_{||}) \mp \hbar\omega) \tag{4.22}$$

N_q is the Bose-Einstein distribution of phonons, $D_t K$ is the non polar optical phonon deformation potential and Z_f is the degeneracy of the final valley. Their values are reported again in the Tables **??**. Note that there are six types of non polar optical phonon. The total scattering is the sum of the contribution of each type.

In the same manner for the 3DEG

$$P^{(ac)}(\mathbf{k},\mathbf{k}') = \frac{k_B T_L \Xi_d^2}{4\pi^2\hbar\rho v_S^2}\delta(E(\mathbf{k}) - E(\mathbf{k}')) \tag{4.23}$$

$$P^{(no)}(\mathbf{k},\mathbf{k}') = Z_f \frac{(D_t K)^2}{8\pi^2\rho\omega}\left(N_q + \frac{1}{2} \mp \frac{1}{2}\right)\delta(E(\mathbf{k}') - E(\mathbf{k}) \mp \hbar\omega) \tag{4.24}$$

4.2 The moment system and its closure by the MEP

The system (4.1),(4.5),(4.6),(4.8) furnishes a complete mathematical model for the simulation of the carrier transport in the channel of a MOSFET and we use them to develop a macroscopic model as in the previous chapter.
The generic moment associated with electrons in the subband ν with respect to a weight function $a(\mathbf{k}_{||})$ is defined as

$$M_a\left(\mathbf{r}_{||},t)\right) = \int a(\mathbf{k}_{||}) f(\mathbf{r},\mathbf{k}_{||},t) d^2\mathbf{k}_{||}.$$

In particular we take as basic moments for the 2DEG the following ones

$$\text{areal density} \quad \rho^\nu\left(\mathbf{r}_{||},t)\right) = \int_{B_2^\nu} f_\nu(\mathbf{r}_{||},\mathbf{k}_{||},t) d^2\mathbf{k}_{||}$$

$$\text{longitudinal mean velocity} \quad \mathbf{V}^\nu\left(\mathbf{r}_{||},t)\right) = \frac{1}{\rho^\nu\left(\mathbf{r}_{||},t\right)}\int_{B_2^\nu} \mathbf{v}_{||} f_\nu(\mathbf{r}_{||},\mathbf{k}_{||},t) d^2\mathbf{k}_{||}$$

$$\text{longitudinal mean energy} \quad W^\nu\left(\mathbf{r}_{||},t)\right) = \frac{1}{\rho^\nu\left(\mathbf{r}_{||},t\right)}\int_{B_2^\nu} \varepsilon_{||} f_\nu(\mathbf{r}_{||},\mathbf{k}_{||},t) d^2\mathbf{k}_{||}$$

$$\text{longitudinal mean energy flux} \quad \mathbf{S}^\nu\left(\mathbf{r}_{||},t)\right) = \frac{1}{\rho^\nu\left(\mathbf{r}_{||},t\right)}\int_{B_2^\nu} \varepsilon_{||}\mathbf{v}_{||} f_\nu(\mathbf{r}_{||},\mathbf{k}_{||},t) d^2\mathbf{k}_{||}$$

The corresponding moment system is obtained by multiplying the Boltzmann equation (4.5) by the weight functions entering into the definition of the fundamental moments and by integrating with respect to $d^2\mathbf{k}_{||}$. Explicitly we get

$$\frac{\partial\rho^\nu}{\partial t} + \nabla_{\mathbf{r}_{||}}\cdot(\rho^\nu\mathbf{V}_\nu) + \rho^\nu L_0^\nu = \rho^\nu C_{\rho_\nu}^{(ac)} + \rho^\nu C_{\rho_\nu}^{(no)} + \rho^\nu C_{\rho_\nu}^{(no),3D} \tag{4.25}$$

$$\frac{\partial}{\partial t}(\rho^\nu\mathbf{V}^\nu) + \nabla_{\mathbf{r}_{||}}\cdot(\rho^\nu\mathbf{F}^{(0)\nu}) + (\rho^\nu\mathbf{G}^{(0)\nu})\cdot\nabla_{\mathbf{r}_{||}}\varepsilon_\nu = \rho^\nu C_{\mathbf{V}^\nu}^{(ac)} + \rho^\nu C_{\mathbf{V}^\nu}^{(no)} + \rho^\nu C_{\mathbf{V}^\nu}^{(no),3D} \tag{4.26}$$

$$\frac{\partial}{\partial t}(\rho^\nu W^\nu) + \nabla_{\mathbf{r}_{||}}\cdot(\rho^\nu\mathbf{S}^\nu) + (\rho^\nu\mathbf{V}^\nu)\cdot\nabla_{\mathbf{r}_{||}}\varepsilon_\nu + \rho^\nu L_1^\nu = \rho^\nu C_W^{(ac)} + \rho^\nu C_W^{(no)} + \rho^\nu C_W^{(no),3D} \tag{4.27}$$

$$\frac{\partial}{\partial t}(\rho^\nu\mathbf{S}^\nu) + \nabla_{\mathbf{r}_{||}}\cdot(\rho_\nu\mathbf{F}^{(1)\nu}) + (\rho_\nu\mathbf{G}^{(1)\nu})\cdot\nabla_{\mathbf{r}_{||}}\epsilon_\nu = \rho_\nu C_{\mathbf{S}^\nu}^{(ac)} + \rho_\nu C_{\mathbf{S}^\nu}^{(no)} + \rho_\nu C_{\mathbf{S}^\nu}^{(no),3D} \tag{4.28}$$

where

$$
\begin{aligned}
\begin{pmatrix} \mathbf{F}^{(0)\nu} \\ \mathbf{F}^{(1)\nu} \end{pmatrix} &= \frac{1}{\rho^\nu} \int_{B_2^\nu} \begin{pmatrix} 1 \\ \varepsilon_{||} \end{pmatrix} \mathbf{v}_{||} \otimes \mathbf{v}_{||}\, f_\nu(\mathbf{r}_{||}, \mathbf{k}_{||}, t)\, d^2\mathbf{k}_{||}, \\
\begin{pmatrix} \mathbf{G}^{(0)\nu} \\ \mathbf{G}^{(1)\nu} \end{pmatrix} &= -\frac{1}{\rho^\nu} \int_{B_2^\nu} \begin{pmatrix} \frac{1}{\hbar}\mathbf{v}_{||}\nabla_{\mathbf{k}_{||}} \\ \frac{1}{\hbar}\varepsilon_{||}\mathbf{v}_{||}\nabla_{\mathbf{k}_{||}} \end{pmatrix} f_\nu(\mathbf{r}_{||}, \mathbf{k}_{||}, t)\, d^2\mathbf{k}_{||}, \\
\begin{pmatrix} C_{\rho_\nu} \\ C_{W_\nu} \end{pmatrix} &= \frac{1}{\rho^\nu} \int_{B_2^\nu} \begin{pmatrix} 1 \\ \varepsilon_{||} \end{pmatrix} \left[S_{\mu\nu}(\mathbf{k}'_{||}, \mathbf{k}_{||})\, f'_\mu - S_{\nu\mu}(\mathbf{k}_{||}, \mathbf{k}'_{||})\, f_\nu \right] d^2\mathbf{k}'_{||}\, d^2\mathbf{k}_{||}, \\
\begin{pmatrix} C_{\mathbf{V}_\nu} \\ C_{\mathbf{S}_\nu} \end{pmatrix} &= \frac{1}{\rho^\nu} \int_{B_2^\nu} \begin{pmatrix} \mathbf{v}_{||} \\ \varepsilon_{||}\mathbf{v}_{||} \end{pmatrix} \left[S_{\mu\nu}(\mathbf{k}'_{||}, \mathbf{k}_{||})\, f'_\mu - S_{\nu\mu}(\mathbf{k}_{||}, \mathbf{k}'_{||})\, f_\nu \right] d^2\mathbf{k}'_{||}\, d^2\mathbf{k}_{||} \\
& L_0^\nu = -\frac{1}{\hbar\rho^\nu} \nabla_{\mathbf{r}_{||}} \varepsilon_\nu \int_{B_2^\nu} \nabla_{\mathbf{k}_{||}} f_\nu d^2\mathbf{k}_{||} \\
& L_1^\nu = -\frac{1}{\hbar\rho^\nu} \nabla_{\mathbf{r}_{||}} \varepsilon_\nu \int_{B_2^\nu} \nabla_{\mathbf{k}_{||}} (\varepsilon_{||} f_\nu) d^2\mathbf{k}_{||}.
\end{aligned}
$$

It is worth to underline here that the two last drift terms (L_0^ν and L_1^ν) are due to the anisotropy of the distribution function. Usually they do not appear in the constitutive equations of the carriers transport because the boundary of the first Brillouin zone is moved to infinity or the distribution function is symmetric on this boundary.

For the 3DEG the expression of the moment associated to a weight function $b(\mathbf{k})$ is

$$M_b(\mathbf{r}, \mathbf{t}) = \int_{B_3^*} b(\mathbf{k})\, f(\mathbf{r}, \mathbf{k}, t) d^3\mathbf{k}$$

The basic moments we take for 3D electrons are the following ones

$$
\begin{aligned}
&\text{density} \quad n(\mathbf{r}, t) = \int_{B_3^*} f(\mathbf{r}, \mathbf{k}, t) d^3\mathbf{k} \\
&\text{mean velocity} \quad \mathbf{V}(\mathbf{r}, t) = \frac{1}{n(\mathbf{r}, t)} \int_{B_3^*} \mathbf{v}(\mathbf{k}) f(\mathbf{r}, \mathbf{k}, t) d^3\mathbf{k} \\
&\text{mean energy} \quad W(\mathbf{r}, t) = \frac{1}{n(\mathbf{r}, t)} \int_{B_3^*} \varepsilon(\mathbf{k}) f(\mathbf{r}, \mathbf{k}, t) d^3\mathbf{k} \\
&\text{mean energy flux} \quad \mathbf{S}(\mathbf{r}, t) = \frac{1}{n(\mathbf{r}, t)} \int_{B_3^*} \varepsilon(\mathbf{k})\, \mathbf{v}(\mathbf{k}) f(\mathbf{r}, \mathbf{k}, t) d^3\mathbf{k}.
\end{aligned}
$$

and the corrisponding moments system reads

$$\frac{\partial n}{\partial t} + \nabla_{\mathbf{r}}\Big(n(\mathbf{r},t)\mathbf{v}(\mathbf{n},t)\Big) = nC_n^{(ac)} + nC_n^{(no)} + nC_n^{(no),2D} \tag{4.29}$$

$$\frac{\partial}{\partial t}(n\mathbf{v}) + \nabla_{\mathbf{r}}\Big(n\mathbf{F}^{(0)}\Big) + q\mathbf{E}\Big(n\mathbf{G}^{(0)}\Big) = nC_{\mathbf{V}}^{(ac)} + nC_{\mathbf{V}}^{(no)} + nC_{\mathbf{V}}^{(no),2D} \tag{4.30}$$

$$\frac{\partial}{\partial t}(nW) + \nabla_{\mathbf{r}}\Big(n\mathbf{S}\Big) + q\mathbf{E}\Big(n\mathbf{V}\Big) = nC_W^{(ac)} + nC_W^{(no)} + nC_W^{(no),2D} \tag{4.31}$$

$$\frac{\partial}{\partial t}(n\mathbf{S}) + \nabla_{\mathbf{r}}(n\mathbf{F}^{(1)}) + q\mathbf{E}(n\mathbf{G}^{(1)}) = nC_{\mathbf{S}}^{(ac)} + nC_{\mathbf{S}}^{(no)} + nC_{\mathbf{S}}^{(no),2D} \tag{4.32}$$

with

$$\begin{aligned}
\begin{pmatrix} \mathbf{F}^{(0)} \\ \mathbf{F}^{(1)} \end{pmatrix} &= \frac{1}{n}\int_{B_3^*} \begin{pmatrix} 1 \\ \varepsilon \end{pmatrix} \mathbf{v}\otimes\mathbf{v}\, f(\mathbf{r},\mathbf{k},t)\, d^2\mathbf{k}, \\
\begin{pmatrix} \mathbf{G}^{(0)} \\ \mathbf{G}^{(1)} \end{pmatrix} &= -\frac{1}{n}\int_{B_3^*} \begin{pmatrix} \frac{1}{\hbar}\mathbf{v}\cdot\nabla_{\mathbf{k}} \\ \frac{1}{\hbar}\varepsilon\mathbf{v}\cdot\nabla_{\mathbf{k}} \end{pmatrix} f(\mathbf{r},\mathbf{k},t)\, d^2\mathbf{k}, \\
\begin{pmatrix} C_n \\ C_W \end{pmatrix} &= \frac{1}{n}\int_{B_3^*} \begin{pmatrix} 1 \\ \varepsilon \end{pmatrix} \left[S(\mathbf{k}',\mathbf{k})\, f' - S(\mathbf{k},\mathbf{k}')\, f\right]\, d^2\mathbf{k}'\, d^2\mathbf{k}, \\
\begin{pmatrix} C_{\mathbf{V}} \\ C_{\mathbf{S}} \end{pmatrix} &= \frac{1}{n}\int_{B_3^*} \begin{pmatrix} \mathbf{v} \\ \varepsilon\mathbf{v}_{||} \end{pmatrix} \left[S(\mathbf{k}',\mathbf{k})\, f' - S(\mathbf{k},\mathbf{k}')\, f\right]\, d^2\mathbf{k}'\, d^2\mathbf{k}.
\end{aligned}$$

Let us observe that $n_T(\mathbf{r},t)$ must be conserved so

$$\frac{dn_T(\mathbf{r},t)}{dt} = 0$$

and from (4.9) we has

$$\frac{dn(\mathbf{r},t)}{dt} + \sum_{\nu=1}^{\nu_T}\frac{d\rho_\nu}{dt}|\phi_\nu|^2 + \sum_{\nu=1}^{\nu_T}\rho_\nu\frac{d}{dt}|\phi_\nu|^2 = 0 \tag{4.33}$$

Now we use again the MEP to close the above written moment system.
According to the MEP, if a given number of moments of f_ν

$$M_{a_A}^{\nu}\left(\mathbf{r}_{||},\mathbf{k}_{||},t)\right), \quad A = 1,.....,N_\nu \quad \text{and} \quad \nu = 1,2\ldots$$

are known along with a given number of moments of f

$$M_{b_B}\left(\mathbf{r},\mathbf{k},\mathbf{t}\right) \quad B = 1,2,\ldots N$$

the distribution functions $f(\mathbf{r},\mathbf{k},\mathbf{t})$, $f_\nu\left(\mathbf{r}_{||},\mathbf{k}_{||},t\right)\big)$, $\nu=1,2\ldots$, can be estimated by the extremal $(f^{MEP}, f_1^{MEP}, f_2^{MEP}, ...)$ of the entropy functional under the constrains

$$\int_{B_2^\nu} a_A(\mathbf{k}_{||}) f_\nu^{MEP}\left(\mathbf{r}_{||},\mathbf{k}_{||},t\right)\big)\, d\mathbf{k} = M_{a_A}^\nu\left(\mathbf{r}_{||},t\right)\big) \quad A=1,...,N_\nu, \quad \nu=1,2,\ldots$$
$$\int_{B_3^*} b_B(\mathbf{k})\, f^{MEP}(\mathbf{r},\mathbf{k},t) d^3\mathbf{k} = M_{b_B}(\mathbf{r},\mathbf{t}) \quad B=1,2,\ldots N.$$

Also in this case, the phonons gas is considered as a thermal bath.
We define the entropies of the two subsystems, 2DEG and 3DEG, as

$$\mathcal{S}_{2D} = -k_B \sum_{\nu=1}^{+\infty} |\phi_\nu(z,t)|^2 \int_{B_2^\nu} \left(f_\nu \log \frac{f_\nu}{y} - f_\nu \right) d^2\mathbf{k}_{||}, \quad y = \frac{2}{(2\pi)^2},$$
$$\mathcal{S}_{3D} = -k_B \int_{B_3^*} f(\mathbf{k}) \left[\log f(\mathbf{k}) - 1\right] d^3\mathbf{k}$$

The total entropy is of course

$$\mathcal{S} = \mathcal{S}_{2D} + \mathcal{S}_{3D}.$$

The proposed expression of the entropy of the 2DEG combines quantum effects and semiclassical transport along the longitudinal direction, weighting the contribution of each f_ν with the squared modulus of the $\phi_\nu(z,t)$'s arising from the Schrödinger-Poisson block. Therefore, according to MEP and our choice of the basic moments in the case we are dealing with, f and the f_ν's are estimated with the distributions f^{MEP} and f_ν^{MEP}'s that solve the problem:

maximize $\mathcal{S}$ under the constraints

$$\int_{B_3^*} f^{MEP}(\mathbf{r},\mathbf{k},t) d^3\mathbf{k} = n(\mathbf{r},t), \int_{B_3^*} \mathbf{v}(\mathbf{k}) f^{MEP}(\mathbf{r},\mathbf{k},t) d^3\mathbf{k} = n(\mathbf{r},t)\mathbf{V}(\mathbf{r},t) \tag{4.34}$$
$$\int_{B_3^*} \varepsilon(\mathbf{k}) f^{MEP}(\mathbf{r},\mathbf{k},t) d^3\mathbf{k} = n(\mathbf{r},t)\, W(\mathbf{r},t), \int_{B_3^*} \varepsilon\mathbf{v} f^{MEP}(\mathbf{r},\mathbf{k},t) d^3\mathbf{k} = n(\mathbf{r},t)\, \mathbf{S}(\mathbf{r},t) \tag{4.35}$$

and for $\nu=1,2,\ldots$

$$\int_{B_2^\nu} f_\nu(\mathbf{r}_{||},\mathbf{k}_{||},t) d^2\mathbf{k}_{||} = \rho^\nu\left(\mathbf{r}_{||},t\right), \int_{B_2^\nu} \mathbf{v}_{||} f_\nu(\mathbf{r}_{||},\mathbf{k}_{||},t) d^2\mathbf{k}_{||} = \rho^\nu\left(\mathbf{r}_{||},t\right)\mathbf{V}^\nu\left(\mathbf{r}_{||},t\right)\big) \tag{4.36}$$
$$\int_{B_2^\nu} \varepsilon_{||} f_\nu(\mathbf{r}_{||},\mathbf{k}_{||},t) d^2\mathbf{k}_{||} = \rho^\nu\left(\mathbf{r}_{||},t\right) W^\nu\left(\mathbf{r}_{||},t\right), \int_{B_2^\nu} \varepsilon_{||}\mathbf{v}_{||} f_\nu(\mathbf{r}_{||},\mathbf{k}_{||},t) d^2\mathbf{k}_{||} = \rho^\nu\left(\mathbf{r}_{||},t\right)\mathbf{S}^\nu\left(\mathbf{r}_{||},t\right)\big) \tag{4.37}$$

In order to solve the above problem, we introduce the Legendre transform

$$\mathcal{S}' = \mathcal{S}_{2D} + \sum_{\nu=1}^{\infty}\sum_{A=1}^{4} \lambda^{\nu}_{a_A} |\varphi_\nu(z,t)|^2 \left[M^{\nu}_{a_A} - \int_{B_2^\nu} a_A f_\nu^{MEP} d^2\mathbf{k}_{||} \right] + \mathcal{S}_{3D} + \sum_{B=1}^{4} \lambda_{b_B} \left[M_{b_B} - \int_{B_3^*} b_B f^{MEB} d^3\mathbf{k} \right]$$

where λ_{b_B}, $B = 1, 2, \ldots, 4$, and $\lambda^{\nu}_{a_A}$, $A = 1, 2, \ldots, 4$, and $\nu = 1, 2, \ldots$ are the lagrangian multipliers associated to the constraints (4.34)-(4.37) while $(b_B(\mathbf{k})) = (1, \mathbf{v}, \varepsilon, \varepsilon\mathbf{v})$ and $(a^{\nu}_A(\mathbf{k}_{||})) = (1, \mathbf{v}_{||}, \varepsilon_{||}, \varepsilon_{||}\mathbf{v}_{||})$ for each ν.

Requiring that the first variations must be zero, $\delta\mathcal{S}' = 0$, one has

$$f_\nu^{MEP} = \exp\left[- \left(\lambda^\nu + \lambda^\nu_{\mathbf{V}} \cdot \mathbf{v}_{||} + \left(\lambda^\nu_W + \lambda^\nu_{\mathbf{S}} \cdot \mathbf{v}_{||} \right) \varepsilon_{||} \right) \right] \quad \nu = 1, 2, \ldots \tag{4.38}$$

and

$$f^{MEP} = \exp\left[-(\lambda + \lambda_{\mathbf{V}} \cdot \mathbf{v} + (\lambda_W + \lambda_{\mathbf{S}} \cdot \mathbf{v})\varepsilon) \right] \tag{4.39}$$

To complete the procedure one has to insert the f_ν^{MEP}'s into the constraint relations (4.36)-(4.37) and express the lagrangian multipliers $\lambda^{\nu}_{a_A}$'s as functions of the basic moments ρ^ν, $\mathbf{V}^\nu$, W^ν, $\mathbf{S}^\nu$. Similarly, by inserting f^{MEP} into the constraints (4.34)-(4.35) one can write the lagrangian multipliers λ_{b_B}'s in terms of the basic moments $n, \mathbf{V}, W, \mathbf{S}$. Following the same previous approach, we assume a small anisotropy of the distribution functions and expand them up to first order with respect to the lagrangian multipliers relative to velocity and energy-flux

$$f_\nu^{MEP} \approx \exp\left(-\lambda^\nu - \lambda^\nu_W \varepsilon_{||} \right) \left[1 - \left(\lambda^\nu_{\mathbf{V}} \cdot \mathbf{v}_{||} + \lambda^\nu_{\mathbf{S}} \cdot \mathbf{v}_{||}\varepsilon_{||} \right) \right], \tag{4.40}$$

$$f^{MEP} \approx \exp(-\lambda^B - \lambda^B_W \varepsilon)[1 - (\lambda^B_{\mathbf{V}} \cdot \mathbf{v} + \lambda^B_{\mathbf{S}} \cdot \mathbf{v}\varepsilon)] \tag{4.41}$$

Inserting the above-written expansions into the constraints (4.34)-(4.37), it is possible to get analytical explicit expressions of the lagrangian multipliers and in turn to get the closure relations for the moment system.

4.3 Closure relations for the 2DEG

Inserting (4.40) into (4.36) and (4.37) one finds the following relations for Lagrange's multipliers of the subbands into the 2DEG

$$\rho^\nu = \frac{2\pi m^*}{\hbar^2} e^{-\lambda^\nu} I_0^\nu \tag{4.42}$$

$$W^\nu = \frac{1}{\lambda_W^\nu}\left[1 + \frac{\lambda_W^\nu (E_T - \varepsilon_\nu)}{1 - e^{\lambda_W^\nu (E_T - \varepsilon_\nu)}}\right], \tag{4.43}$$

$$\lambda_{\mathbf{V}}^\nu = b_{11}(W^\nu)\mathbf{V}^\nu + b_{12}(W^\nu)\mathbf{S}^\nu, \quad \lambda_{\mathbf{S}} = b_{21}(W^\nu)\mathbf{V}^\nu + b_{22}(W^\nu)\mathbf{S}^\nu \tag{4.44}$$

where

$$b_{11} = -\frac{m^*\mathcal{I}_0^\nu}{\Delta_\nu}\mathcal{I}_3^\nu, \quad b_{12} = b_{21} = \frac{m^*\mathcal{I}_0^\nu}{\Delta_\nu}\mathcal{I}_2^\nu$$
$$b_{22} = -\frac{m^*\mathcal{I}_0^\nu}{\Delta_\nu}\mathcal{I}_1^\nu, \quad \Delta_\nu = \mathcal{I}_1^\nu\mathcal{I}_3^\nu - (\mathcal{I}_2^\nu)^2$$

with

$$\mathcal{I}_0^\nu = \frac{1 - e^{-\lambda_W^\nu (E_T - \varepsilon_\nu)}}{\lambda_W^\nu}$$
$$\mathcal{I}_n^\nu = (-1)^n \frac{d^n}{d(\lambda_W^\nu)^n}\mathcal{I}_0^\nu, \quad n = 0, 1, 2, ...$$

We remark that letting $E_T \to +\infty$ in (4.43), one obtains $W^\nu = \dfrac{1}{\lambda_W^\nu}$ as in the parabolic case. In general (4.43) must be solved numerically. However it must be done once and for all and for computational purposes, a numerical table λ_W^ν versus W^ν can be easily evaluated. In a numerical code, the actual values can be recovered by interpolation. In Fig. 4.6 λ_W^ν is plotted versus the energy W^ν for several values of $E_T - \varepsilon_\nu$. By increasing $E_T - \varepsilon_\nu$, λ_W^ν tends to the case $E_T - \varepsilon_\nu \to \infty$ (dashed line in the figure) where only the 2DEG is present in the parabolic band approximation as in [26]. Note that for each $E_T - \varepsilon_\nu$ there exists a threshold energy W_c^ν such that λ_W^ν vanishes, which, according to the definition of W^ν, is given by

$$W_c^\nu = \lim_{\lambda_W^\nu \mapsto 0^+} \frac{\int_0^{E_T - \varepsilon_\nu} \varepsilon \exp\left(-\lambda_W^\nu \varepsilon\right) d\varepsilon}{\int_0^{E_T - \varepsilon_\nu} \exp\left(-\lambda_W^\nu \varepsilon\right) d\varepsilon} = \frac{E_T - \varepsilon_\nu}{2}.$$

This implies that the region of realizability [61] is characterized by $k_B T_L < W^\nu < W_c^\nu$ with T_L lattice temperature, kept constant in this paper.

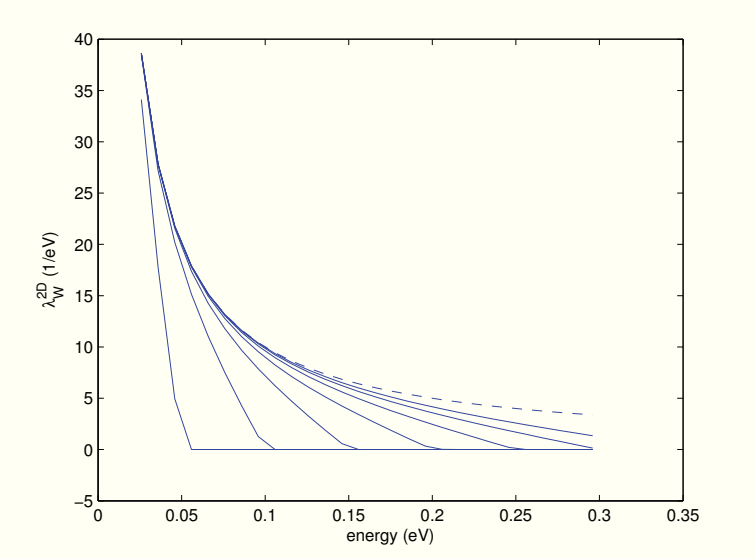

FIGURE 4.6: Plot of λ_W^ν versus the energy W^ν for the 2DEG for $E_T - \varepsilon_\nu = 0.1$, 0.2, 0.3, 0.4, 0.5, 0.6, 0.7 eV. The dashed line represents the case $E_T - \varepsilon_\nu \to \infty$ where only the 2DEG is present.

Once the lagrangian multipliers have been obtained, we can calculate the extra fluxes and the drift and production terms. For the fluxes one gets

$$\begin{aligned}
\mathbf{F}^{(0)\nu} &= \frac{\mathcal{I}_1^\nu}{m^* \mathcal{I}_0^\nu}\mathbf{I} \\
\mathbf{F}^{(1)\nu} &= \frac{\mathcal{I}_2^\nu}{m^* \mathcal{I}_0^\nu}\mathbf{I} \\
\mathbf{G}^{(0)\nu} &= -\frac{E_T - \varepsilon_\nu}{m^* \mathcal{I}_0^\nu} e^{-\lambda_W^\nu (E_T - \varepsilon_\nu)}\mathbf{I} + \frac{1}{m^*}\mathbf{I} \\
\mathbf{G}^{(1)\nu} &= -\frac{(E_T - \varepsilon_\nu)^2}{m^* \mathcal{I}_0^\nu} e^{-\lambda_W^\nu (E_T - \varepsilon_\nu)}\mathbf{I} + \mathbf{F}^{(0)\nu} + \frac{W^\nu}{m^*}\mathbf{I}
\end{aligned}$$

where $\mathbf{I}$ is the identity tensor.

The expression of the tensors present in the drift terms are

$$\begin{aligned}
L_0^\nu &= \frac{1}{m^* I_0^\nu}(\varepsilon_T - \varepsilon_\nu) e^{-\lambda_W^\nu (\varepsilon_T - \varepsilon_\nu)} \{[b_{11} + (\varepsilon_T - \varepsilon_\nu) b_{21}]\mathbf{V}^\nu + [b_{12} + (\varepsilon_T - \varepsilon_\nu) b_{22}]\mathbf{S}^\nu\} \nabla_{\mathbf{r}_{||}} \varepsilon_\nu \\
L_1^\nu &= \frac{1}{m^* I_0^\nu}(\varepsilon_T - \varepsilon_\nu)^2 e^{-\lambda_W^\nu (\varepsilon_T - \varepsilon_\nu)} \{[b_{11} + (\varepsilon_T - \varepsilon_\nu) b_{21}]\mathbf{V}^\nu + [b_{12} + (\varepsilon_T - \varepsilon_\nu) b_{22}]\mathbf{S}^\nu\} \nabla_{\mathbf{r}_{||}} \varepsilon_\nu
\end{aligned}$$

Concerning the production terms, for the acoustic phonons scattering one has

$$\begin{aligned}
C^{(ac)}_{\rho_\nu} &= \frac{2\pi m^*}{\hbar^2}\sum_\mu C_{\nu\mu}\left\{\frac{\rho_\mu}{\rho_\nu}\frac{1}{\lambda^\mu_W\mathcal{I}^\mu_0}e^{-\lambda^\mu_W\Delta_{\nu\mu}}\left[e^{-\lambda^\mu_W a_{\nu\mu}}-e^{-\lambda^\mu_W(E_T-\varepsilon_\mu)}\right]\right.\\
&\quad\left.-\frac{1}{\lambda^\nu_W\mathcal{I}^\nu_0}\left[e^{-\lambda^\nu_W a_{\nu\mu}}-e^{-\lambda^\nu_W(E_T-\varepsilon_\nu)}\right]\right\}\\
C^{(ac)}_{W_\nu} &= \frac{2\pi m^*}{\hbar^2}\sum_\mu C_{\nu\mu}\left[\frac{\rho^\mu}{\rho^\nu\mathcal{I}^\mu_0}e^{-\lambda^\mu_W\Delta_{\nu\mu}}B^{(1)}(a_{\nu\mu},E_T-\varepsilon_\nu,\lambda^\mu_W)-\frac{1}{\mathcal{I}^\mu_0}B^{(1)}(a_{\nu\mu},E_T-\varepsilon_\nu,\lambda^\nu_W)\right]\\
C^{(ac)}_{\mathbf{V}_\nu} &= \frac{2\pi}{\hbar^2\mathcal{I}^\nu_0}\sum_\mu C_{\nu\mu}\Big[(b_{11}B^{(1)}(a_{\nu\mu},E_T-\varepsilon_\nu,\lambda^\mu_W)+b_{12}B^{(2)}(a_{\nu\mu},E_T-\varepsilon_\nu,\lambda^\mu_W))\mathbf{V}^\nu+\\
&\quad b_{12}B^{(1)}(a_{\nu\mu},E_T-\varepsilon_\nu,\lambda^\mu_W)+b_{22}B^{(2)}(a_{\nu\mu},E_T-\varepsilon_\nu,\lambda^\mu_W))\mathbf{S}^\nu\Big]\\
C^{(ac)}_{\mathbf{S}_\nu} &= \frac{2\pi}{\hbar^2\mathcal{I}^\nu_0}\sum_\mu C_{\nu\mu}\Big[(b_{11}B^{(2)}(a_{\nu\mu},E_T-\varepsilon_\nu,\lambda^\mu_W)+b_{21}B^{(3)}(a_{\nu\mu},E_T-\varepsilon_\nu,\lambda^\mu_W))\mathbf{V}^\nu+\\
&\quad (b_{12}B^{(2)}(a_{\nu\mu},E_T-\varepsilon_\nu,\lambda^\mu_W)+b_{22}B^{(3)}(a_{\nu\mu},E_T-\varepsilon_\nu,\lambda^\mu_W))\mathbf{S}^\nu\Big]
\end{aligned}$$

with

$$B^{(n)}(x,y,\alpha)=\int_x^y\varepsilon^n e^{-\alpha\varepsilon}d\varepsilon\quad n=0,1,2,...$$

and

$$\Delta_{\nu\mu}=\varepsilon_\nu-\varepsilon_\mu,\quad a_{\nu\varepsilon_\nu}=\max\{0,\varepsilon_\mu-\varepsilon_\nu\}.$$

The coupling constants are given by $C_{\nu\mu}=\dfrac{k_BT_L\Xi_d^2}{4\pi^2\hbar\rho v_S^2}\,G_{\nu\mu}=A^{(ac)}\,G_{\nu\mu}$.

For non polar optical phonon scattering intra the 2DEG we find

$$\begin{aligned}
\begin{pmatrix}C^{(no)}_{\rho_\nu}\\ C^{(no)}_{W_\nu}\end{pmatrix} &= \frac{2\pi m^*}{\hbar^2}\left(N_q+\frac{1}{2}\mp\frac{1}{2}\right)\sum_\mu D_{\nu\mu}\left\{\frac{\rho^\mu}{\rho^\nu\mathcal{I}^\mu_0}e^{-\lambda^\mu_W(\Delta_{\mu\nu}\pm\hbar\omega)\pm\frac{\hbar\omega}{K_BT}}\cdot\begin{pmatrix}B^{(0)}(a^\mp_{\nu\mu},E^\mp_\nu,\lambda^\mu_W)\\ B^{(1)}(a^\mp_{\nu\mu},E^\mp_\nu,\lambda^\mu_W)\end{pmatrix}-\right.\\
&\quad\left.\frac{1}{\mathcal{I}^\nu_0}\cdot\begin{pmatrix}B^{(0)}(a^\mp_{\nu\mu},E^\mp_\nu,\lambda^\mu_W)\\ B^{(1)}(a^\mp_{\nu\mu},E^\mp_\nu,\lambda^\mu_W)\end{pmatrix}\right\}\\
\begin{pmatrix}C^{(no)}_{\mathbf{V}_\nu}\\ C^{(no)}_{\mathbf{S}_\nu}\end{pmatrix} &= \frac{2\pi}{\hbar^2}\left(N_q+\frac{1}{2}\mp\frac{1}{2}\right)\frac{1}{\mathcal{I}^\nu_0}\sum_\mu D_{\nu\mu}\left\{\left[b_{11}\begin{pmatrix}B^{(1)}(a^\mp_{\nu\mu},E^\mp_\nu,\lambda^\mu_W)\\ B^{(2)}(a^\mp_{\nu\mu},E^\mp_\nu,\lambda^\mu_W)\end{pmatrix}\right.\right.\\
&\quad\left.+b_{21}\begin{pmatrix}B^{(2)}(a^\mp_{\nu\mu},E^\mp_\nu,\lambda^\mu_W)\\ B^{(3)}(a^\mp_{\nu\mu},E^\mp_\nu,\lambda^\mu_W)\end{pmatrix}\right]\mathbf{V}^\nu+\\
&\quad\left.\left[b_{12}\begin{pmatrix}B^{(1)}(a^\mp_{\nu\mu},E^\mp_\nu,\lambda^\mu_W)\\ B^{(2)}(a^\mp_{\nu\mu},E^\mp_\nu,\lambda^\mu_W)\end{pmatrix}+b_{22}\begin{pmatrix}B^{(2)}(a^\mp_{\nu\mu},E^\mp_\nu,\lambda^\mu_W)\\ B^{(3)}(a^\mp_{\nu\mu},E^\mp_\nu,\lambda^\mu_W)\end{pmatrix}\right]\mathbf{S}^\nu\right\}
\end{aligned}$$

with

$$a^\mp_{\nu\mu}=\max\{0,\varepsilon_\mu-\varepsilon_\nu\mp\hbar\omega\},\quad E^\mp_\nu=\min\{E_T-\varepsilon_\nu\mp\hbar\omega,E_T-\varepsilon_\nu\}.$$

The coupling constants for each type of non polar phonon are given by $D_{\nu\mu} = Z_f \frac{(D_t K)^2}{8\pi^2 \rho\omega} G_{\nu\mu} = A^{(no)} G_{\nu\mu}$.

Analogously, the production terms which arise from scattering due to absorption process and push the 2DEG into the 3DEG, are given by

$$\begin{aligned}
\begin{pmatrix} C^{(no),3D}_{\rho_\nu} \\ C^{(no),3D}_{W_\nu} \end{pmatrix} &= \frac{2\pi m^*}{\hbar^2} N_q \sum_\mu D_{\nu\mu} \Bigg[e^{\frac{\hbar\omega}{K_B T} - \lambda^\mu_W (\Delta_{\nu\mu} + \hbar\omega)} \frac{\rho^\mu}{\rho^\nu \mathcal{I}^\mu_0} \cdot \begin{pmatrix} B^{(0)}(E_T - \varepsilon_\nu - \hbar\omega, E_T - \varepsilon_\nu, \lambda^\mu_W) \\ B^{(1)}(E_T - \varepsilon_\nu - \hbar\omega, E_T - \varepsilon_\nu, \lambda^\mu_W) \end{pmatrix} - \\
&\quad \frac{1}{\mathcal{I}^\nu_0} \begin{pmatrix} B^{(0)}(E_T - \varepsilon_\nu - \hbar\omega, E_T - \varepsilon_\nu, \lambda^\mu_W) \\ B^{(1)}(E_T - \varepsilon_\nu - \hbar\omega, E_T - \varepsilon_\nu, \lambda^\mu_W) \end{pmatrix} \Bigg] \\
\begin{pmatrix} C^{(no),3D}_{\mathbf{V}_\nu} \\ C^{(no),3D}_{\mathbf{S}_\nu} \end{pmatrix} &= \frac{2\pi}{\hbar^2} N_q \frac{1}{\mathcal{I}^\nu_0} \sum_\mu D_{\nu\mu} \Bigg\{ \Big[b_{11} \begin{pmatrix} B^{(1)}(E_T - \varepsilon_\nu - \hbar\omega, E_T - \varepsilon_\nu, \lambda^\nu_W) \\ B^{(2)}(E_T - \varepsilon_\nu - \hbar\omega, E_T - \varepsilon_\nu, \lambda^\nu_W) \end{pmatrix} + \\
&\quad b_{21} \begin{pmatrix} B^{(2)}(E_T - \varepsilon_\nu - \hbar\omega, E_T - \varepsilon_\nu, \lambda^\nu_W) \\ B^{(3)}(E_T - \varepsilon_\nu - \hbar\omega, E_T - \varepsilon_\nu, \lambda^\nu_W) \end{pmatrix} \Big] \mathbf{V}^\nu + \\
&\quad \Big[b_{12} \begin{pmatrix} B^{(1)}(E_T - \varepsilon_\nu - \hbar\omega, E_T - \varepsilon_\nu, \lambda^\nu_W) \\ B^{(2)}(E_T - \varepsilon_\nu - \hbar\omega, E_T - \varepsilon_\nu, \lambda^\nu_W) \end{pmatrix} + b_{22} \begin{pmatrix} B^{(2)}(E_T - \varepsilon_\nu - \hbar\omega, E_T - \varepsilon_\nu, \lambda^\nu_W) \\ B^{(3)}(E_T - \varepsilon_\nu - \hbar\omega, E_T - \varepsilon_\nu, \lambda^\nu_W) \end{pmatrix} \Big] \mathbf{S}
\end{aligned}$$

4.4 Closure relations for the 3DEG

In the same manner as for the 2DEG, explicit formulas for the closure relations of the 3DEG part of the moment system are obtained. The lagrangian multipliers are given by the following relationships

$$n = \frac{4\pi m^* \sqrt{2m^*}}{\hbar^3} e^{-\lambda^B} \mathcal{I}(E_T, \lambda^B_W) \tag{4.45}$$

$$W = -\frac{d}{d\lambda^B_W} \ln \mathcal{I}(E_T, \lambda^B_W) \tag{4.46}$$

$$\lambda^B_{\mathbf{V}} = B_{11}\mathbf{V} + B_{12}\mathbf{S}, \quad \lambda^B_{\mathbf{V}} = B_{21}\mathbf{V} + B_{22}\mathbf{S} \tag{4.47}$$

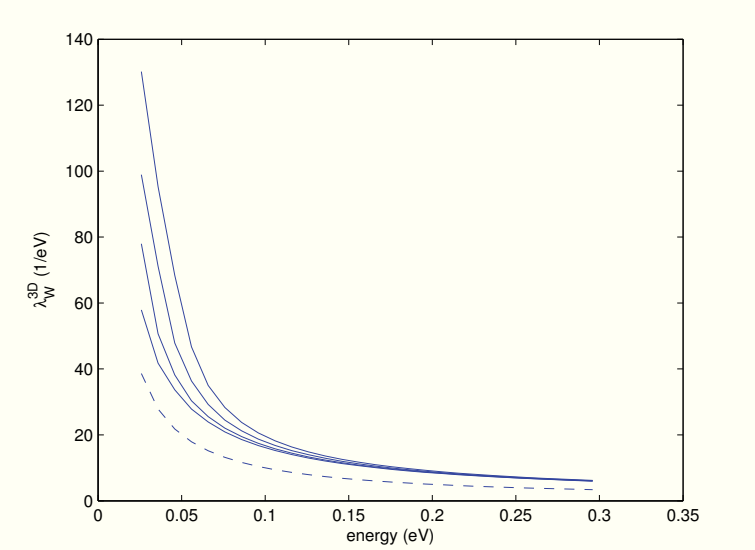

FIGURE 4.7: Plot of λ_W^ν versus the energy W^ν for the 3DEG for $E_T = 0.0$, 0.01, 0.02, 0.03 eV. The dashed line represents the case $E_T = 0$ in the parabolic band approximation where $\lambda_W^\nu = \dfrac{3}{2W}$.

with

$$
\begin{aligned}
B_{11} &= -\frac{3m^*}{2\Delta}\mathcal{I}(E_T,\lambda_W^B)\mathcal{L}^{(2)}(E_T,\lambda_W^B),\\
B_{12} &= B_{21} = \frac{3m^*}{2\Delta}\mathcal{I}(E_T,\lambda_W^B)\mathcal{L}^{(1)}(E_T,\lambda_W^B),\\
B_{22} &= -\frac{3m^*}{2\Delta}\mathcal{I}(E_T,\lambda_W^B)\mathcal{L}^{(0)}(E_T,\lambda_W^B),\\
\Delta &= \mathcal{L}^{(0)}(E_T,\lambda_W^B)\mathcal{L}^{(2)}(E_T,\lambda_W^B) - (\mathcal{L}^{(1)}(E_T,\lambda_W^B))^2\\
\mathcal{I}(x,\beta) &= \int_x^{+\infty}(1+2\alpha\varepsilon)\sqrt{\varepsilon(1+\alpha\varepsilon)}e^{-\beta\varepsilon}d\varepsilon\\
\mathcal{L}^{(0)}(x,\beta) &= \int_x^{+\infty}e^{-\beta\varepsilon}\frac{[\varepsilon(1+\alpha\varepsilon)]^{3/2}}{1+2\alpha\varepsilon}d\varepsilon\\
\mathcal{L}^{(n)}(x,\beta) &= (-1)^n\frac{d^n}{d(\beta)^n}\mathcal{L}^{(0)}(x,\beta)
\end{aligned}
$$

Again (4.46) must be solved numerically. However a numerical table λ_W versus W can be easily evaluated and in a numerical code, the actual values can be recovered by interpolation. In Fig. 4.7 λ_W versus W is plotted for several vaues of E_T. At variance of the 2DEG, no threshold energy arises.

Once λ_W has been obtained, the extra fluxes and production terms can be obtained. The fluxes are given by

$$\begin{aligned}
\mathbf{F}^{(0)} &= \frac{2}{3m^*\mathcal{I}(E_T,\lambda_W^B)}\mathcal{L}^{(0)}(E_T,\lambda_W^B)\\
\mathbf{F}^{(1)} &= \frac{2}{3m^*\mathcal{I}(E_T,\lambda_W^B)}\mathcal{L}^{(1)}(E_T,\lambda_W^B)\\
\mathbf{G}^{(0)} &= \frac{2}{3m^*}\left[\mathcal{I}(E_T,\lambda_W^B)\right]^{-1}\frac{[E_T(1+\alpha E_T)]^{3/2}}{1+2\alpha E_T}e^{-\lambda_W^B\varepsilon}\mathbf{I}+\\
&\quad -\frac{1}{m^*}\left[\mathcal{I}(E_T,\lambda_W^B)\right]^{-1}\left\{\int_{E_T}^{+\infty}e^{-\lambda_W^B\varepsilon}\sqrt{\varepsilon(1+\alpha\varepsilon)}d\varepsilon+\right.\\
&\quad \left.-\frac{4\alpha}{3}\int_{E_T}^{+\infty}\frac{[\varepsilon(1+\alpha\varepsilon)]^{3/2}}{(1+2\alpha\varepsilon)^2}e^{-\lambda_W^B\varepsilon}d\varepsilon\right\}\mathbf{I}\\
\mathbf{G}^{(1)} &= \frac{\hbar^2}{m^{*2}}\left[\mathcal{I}(E_T,\lambda_W^B)\right]^{-1}\frac{E_T^3\sqrt{E_T(1+\alpha E_T)}}{1+2\alpha E_T}e^{\lambda_W^B E_T}\mathbf{I}
\end{aligned}$$

The production terms for acoustic phonons are given by

$$\begin{aligned}
\begin{pmatrix}C_n^{(ac)}\\ C_W^{(ac)}\end{pmatrix} &= \begin{pmatrix}0\\0\end{pmatrix}\\
\begin{pmatrix}C_{\mathbf{V}}^{(ac)}\\ C_{\mathbf{S}}^{(ac)}\end{pmatrix} &= \frac{8\pi\sqrt{2m^*}}{3\hbar^3}\frac{A^{(ac)}}{\mathcal{I}(E_T,\lambda_W^B)}\left\{\left[B_{11}\begin{pmatrix}\mathcal{B}^{(0)}(E_T,\lambda_W^B)\\ \mathcal{B}^{(1)}(E_T,\lambda_W^B)\end{pmatrix}+B_{21}\begin{pmatrix}\mathcal{B}^{(1)}(E_T,\lambda_W^B)\\ \mathcal{B}^{(2)}(E_T,\lambda_W^B)\end{pmatrix}\right]\mathbf{V}+\right.\\
&\quad \left.\left[B_{12}\begin{pmatrix}\mathcal{B}^{(0)}(E_T,\lambda_W^B)\\ \mathcal{B}^{(1)}(E_T,\lambda_W^B)\end{pmatrix}+B_{22}\begin{pmatrix}\mathcal{B}^{(1)}(E_T,\lambda_W^B)\\ \mathcal{B}^{(2)}(E_T,\lambda_W^B)\end{pmatrix}\right]\mathbf{S}\right\}
\end{aligned}$$

with

$$\mathcal{B}^{(n)}(x,\beta)=\int_x^{+\infty}\varepsilon^{n+2}(1+\alpha\varepsilon)^2e^{-\beta\varepsilon}d\varepsilon.$$

For non polar optical phonons intra the 3DEG one gets

$$\begin{aligned}
\begin{pmatrix}C_n^{(no)}\\ C_W^{(no)}\end{pmatrix} &= \frac{4\pi m^*\sqrt{2m^*}}{\hbar^3}\frac{D^{(no)}}{\mathcal{I}(E_T,\lambda_W^B)}\left(N_q+\frac{1}{2}\mp\frac{1}{2}\right)\left[e^{\mp\left(\lambda_W^B-\frac{1}{K_BT}\right)\hbar\omega}-1\right]\begin{pmatrix}\Gamma_{\mp}^{(0)}(b^{\mp},+\infty,\lambda_W^B)\\ \Gamma_{\mp}^{(1)}(b^{\mp},+\infty,\lambda_W^B)\end{pmatrix}\\
\begin{pmatrix}C_{\mathbf{V}}^{(no)}\\ C_{\mathbf{S}}^{(no)}\end{pmatrix} &= \frac{8\pi\sqrt{2m^*}}{3\hbar^3}\frac{D^{(no)}}{\mathcal{I}(E_T,\lambda_W^B)}\left(N_q+\frac{1}{2}\mp\frac{1}{2}\right)\left\{\left[B_{11}\begin{pmatrix}\Lambda^{(0)}(b^{\mp},+\infty,\lambda_W^B)\\ \Lambda^{(1)}(b^{\mp},+\infty,\lambda_W^B)\end{pmatrix}+\right.\right.\\
&\quad \left.B_{21}\begin{pmatrix}\Lambda^{(1)}(b^{\mp},+\infty,\lambda_W^B)\\ \Lambda^{(2)}(b^{\mp},+\infty,\lambda_W^B)\end{pmatrix}\right]\mathbf{V}+\left[B_{12}\begin{pmatrix}\Lambda^{(0)}(b^{\mp},+\infty,\lambda_W^B)\\ \Lambda^{(1)}(b^{\mp},+\infty,\lambda_W^B)\end{pmatrix}+B_{22}\begin{pmatrix}\Lambda^{(1)}(b^{\mp},+\infty,\lambda_W^B)\\ \Lambda^{(2)}(b^{\mp},+\infty,\lambda_W^B)\end{pmatrix}\right]\mathbf{S}\Bigg\}
\end{aligned}$$

with

$$\begin{aligned}
\Lambda^{(n)}(x,y,\beta) &= \int_x^y\varepsilon^n e^{-\beta\varepsilon}\frac{[\varepsilon(1+\alpha\varepsilon)]^{3/2}}{1+2\alpha\varepsilon}[1+2\alpha(\varepsilon\pm\hbar\omega)]\sqrt{(\varepsilon\pm\hbar\omega)[1+\alpha(\varepsilon\pm\hbar\omega)]}d\varepsilon\\
\Gamma_{\mp}^{(n)}(x,y,\beta) &= \int_x^y\varepsilon^n e^{-\beta\varepsilon}[1+2\alpha(\varepsilon\pm\hbar\omega)](1+2\alpha\varepsilon)\sqrt{\varepsilon(1+\alpha\varepsilon)(\varepsilon\pm\hbar\omega)[1+\alpha(\varepsilon\pm\hbar\omega)]}d\varepsilon
\end{aligned}$$

and

$$a^{\mp} = E_T \mp \hbar\omega, \quad b^{\mp} = \max\{a^{\mp}, E_T\}.$$

The coupling constant is given by $D^{(no)} = Z_f \frac{(D_t K)^2}{8\pi^2 \rho \omega}$.

At last the production terms arising from the scattering due to emission processes and pushing 3D electrons into the 2DEG are given by

$$\begin{aligned}
\begin{pmatrix} C_n^{(no),2D} \\ C_W^{(no),2D} \end{pmatrix} &= \frac{4\pi m^* \sqrt{2m^*}}{\hbar^3} \frac{D^{(no)}}{\mathcal{I}(E_T, \lambda_W^B)} (N_q + 1) \left[e^{\left(\lambda_W^B - \frac{1}{K_B T}\right)\hbar\omega} - 1 \right] \begin{pmatrix} \Gamma_+^{(0)}(E_{ext}, E_T + \hbar\omega, \lambda_W^B) \\ \Gamma_+^{(1)}(E_{ext}, E_T + \hbar\omega, \lambda_W^B) \end{pmatrix} \\
\begin{pmatrix} C_{\mathbf{V}}^{(no),2D} \\ C_{\mathbf{S}}^{(no),2D} \end{pmatrix} &= \frac{8\pi \sqrt{2m^*}}{3\hbar^3} \frac{D^{(no)}}{\mathcal{I}(E_T, \lambda_W^B)} (N_q + 1) \left\{ \left[B_{11} \begin{pmatrix} \Lambda_+^{(0)}(E_{ext}, E_T + \hbar\omega, \lambda_W^B) \\ \Lambda_+^{(1)}(E_{ext}, E_T + \hbar\omega, \lambda_W^B) \end{pmatrix} + \right.\right. \\
&\quad \left. + B_{21} \begin{pmatrix} \Lambda_+^{(1)}(E_{ext}, E_T + \hbar\omega, \lambda_W^B) \\ \Lambda_+^{(2)}(E_{ext}, E_T + \hbar\omega, \lambda_W^B) \end{pmatrix} \right] \mathbf{V} + \left[B_{12} \begin{pmatrix} \Lambda_+^{(0)}(E_{ext}, E_T + \hbar\omega, \lambda_W^B) \\ \Lambda_+^{(1)}(E_{ext}, E_T + \hbar\omega, \lambda_W^B) \end{pmatrix} + \right. \\
&\quad \left.\left. + B_{22} \begin{pmatrix} \Lambda_+^{(1)}(E_{ext}, E_T + \hbar\omega, \lambda_W^B) \\ \Lambda_+^{(2)}(E_{ext}, E_T + \hbar\omega, \lambda_W^B) \end{pmatrix} \right] \mathbf{S} \right\}
\end{aligned}$$

with $E_{ext} = \max\{E_T, \hbar\omega\}$.

4.5 Mathematical structure of the moment system closed with MEP

We want to give *a strong numerical evidence that the moment system of the subbands and bulk electrons augmented with the MEP closure relations forms a quasilinear hyperbolic system* in the time direction in the physically relevant range of W^ν.

Since the differential part of each subband and of the 3DEG is decoupled in the moment system, we can limit our analysis to the study of a single subband and the 3DEG. Let us consider the quasilinear system of PDEs

$$\frac{\partial}{\partial t} \mathcal{F}^{(0)}(\mathbf{U}) + \sum_{i=1}^{2} \frac{\partial}{\partial x^i} \mathcal{F}^{(i)}(\mathbf{U}) = \mathcal{P}(\mathbf{U}, \mathbf{x}, t), \tag{4.48}$$

with $\mathbf{U}(\mathbf{x}, t)$ vector field belonging to a connected open set $\Omega \subset \mathbb{R}^m$, $\forall\, t > 0$ and $\forall\, \mathbf{x}$ belonging to a domain $D \subseteq \mathbb{R}^k$ with $k = 2$ for th 2DEG or $k = 3$ for the 3DEG, and

$$\mathcal{F}^{(\beta)} : \Omega \mapsto \mathbb{R}^m, \quad \beta = 0, \ldots, k$$

sufficiently smooth functions. Defining the Jacobian matrices

$$\mathcal{A}^{(\beta)} = \nabla_{\mathbf{U}} \mathcal{F}^{(\beta)}, \quad \beta = 0, \ldots, k,$$

the system (4.48) is said to be *hyperbolic in the t-direction* if $\det\left(\mathcal{A}^{(0)}(\mathbf{U})\right) \neq 0$ and the eigenvalue problem

$$\det\left(\sum_{i=1}^{2} n_i \mathcal{A}^{(i)}(\mathbf{U}) - \lambda \mathcal{A}^{(0)}(\mathbf{U})\right) = 0 \tag{4.49}$$

has real eigenvalues and the eigenvectors span $\mathbb{R}^m$ for all unit vectors $\mathbf{n} = (n_1, \ldots, n_k)$ of $\mathbb{R}^k$. Will first treat the case of a generic subband and then the 3DEG case.

4.5.1 Iperbolicity of the generic subband subsystem

In the case under consideration, by omitting the subband index, we have

$$\mathbf{U} = \begin{pmatrix} \rho \\ V^1 \\ V^2 \\ W \\ S^1 \\ S^2 \end{pmatrix}, \quad \mathcal{F}^{(0)} = \rho \begin{pmatrix} 1 \\ V^1 \\ V^2 \\ W \\ S^1 \\ S^2 \end{pmatrix}, \quad \mathcal{F}^{(1)} = \rho \begin{pmatrix} V^1 \\ F^{(0)} \\ 0 \\ S^1 \\ F^{(1)} \\ 0 \end{pmatrix}, \quad \mathcal{F}^{(2)} = \rho \begin{pmatrix} V^2 \\ 0 \\ F^{(0)} \\ S^2 \\ 0 \\ F^{(1)} \end{pmatrix},$$

and the Jacobian matrices are given by

$$\mathcal{A}^{(0)} = \begin{pmatrix} 1 & 0 & 0 & 0 & 0 & 0 \\ V^1 & \rho & 0 & 0 & 0 & 0 \\ V^2 & 0 & \rho & 0 & 0 & 0 \\ W & 0 & 0 & \rho & 0 & 0 \\ S^1 & 0 & 0 & 0 & \rho & 0 \\ S^2 & 0 & 0 & 0 & 0 & \rho \end{pmatrix}, \; \mathcal{A}^{(n)} = \sum_{i=1}^{2} n_i \mathcal{A}^{(i)} = \begin{pmatrix} \mathbf{n}\cdot\mathbf{V} & n_1\rho & n_2\rho & 0 & 0 & 0 \\ n_1 F^{(0)} & 0 & 0 & n_1\rho(F^{(0)})' & 0 & 0 \\ n_2 F^{(0)} & 0 & 0 & n_2\rho(F^{(0)})' & 0 & 0 \\ \mathbf{n}\cdot\mathbf{S} & 0 & 0 & 0 & n_1\rho & n_2\rho \\ n_1 F^{(1)} & 0 & 0 & n_1\rho(F^{(1)})' & 0 & 0 \\ n_2 F^{(1)} & 0 & 0 & n_2\rho(F^{(1)})' & 0 & 0 \end{pmatrix},$$

where the prime denotes partial derivation with respect to W.

The equation

$$\det\left(\mathcal{A}^{(n)} - \lambda \mathcal{A}^{(0)}\right) = 0$$

gives the eigenvalues

$$\lambda_{1,2} = 0, \quad \text{with multiplicity } 2 \tag{4.50}$$

$$\lambda_{3,4,5,6} = \pm\sqrt{\frac{a(W) \pm \sqrt{a(W)^2 - 4b(W)}}{2}} \tag{4.51}$$

where

$$a(W) = F^{(0)} + (F^{(1)})' - W(F^{(0)})', \quad b(W) = F^{(0)}(F^{(1)})' - (F^{(0)})'F^{(1)}.$$

In Fig. 4.8 the eigenvalues $\lambda_{3,4,5,6}$ are plotted against the longitudinal mean energy W for several values of $E_T - \varepsilon_\nu$. Since the four eigenvalues $\lambda_{3,4,5,6}$ are real and distinct, each of them has a corresponding eigenspace of dimension one.

Concerning the eigenvalue $\lambda = 0$, we observe that whatever $\mathbf{n}$ we take the first and fourth rows of $\mathcal{A}^{(n)}$ are linearly independent, the second and third rows are proportional and similarly the last two rows since $\rho > 0$ and n_1 and n_2 cannot be both zero. We observe that

$$\det \begin{pmatrix} F^{(0)} & \rho(F^{(0)})' \\ F^{(1)} & \rho(F^{(1)})' \end{pmatrix} = \rho\, b(W).$$

The fact that the eigenvalues $\lambda_{3,4,5,6}$ are real implies that $b(W) > 0$ and therefore the rank of $\mathcal{A}^{(n)}$ is four which means that the eigenspace associated to $\lambda = 0$ has dimension two, leading to the hyperbolicity of the system (4.48).

In the one dimensional case one has only the eigenvalues $\lambda_{3,4,5,6}$ and again by similar computations hyperbolicity is recovered.

$$\lambda_{3,4,5,6} = \pm\sqrt{\left(2 \pm \sqrt{2}\right)\frac{W}{m^*}}$$

which are real and distinct provided $W > 0$ according to the previous case.

4.5.2 Hyperbolicity of the 3DEG subsystem

In a similar way we have for the 3DEG

$$\mathbf{U} = \begin{pmatrix} \rho \\ V^1 \\ V^2 \\ V^3 \\ W \\ S^1 \\ S^2 \\ S^3 \end{pmatrix}, \quad \mathcal{F}^{(0)} = n \begin{pmatrix} 1 \\ V^1 \\ V^2 \\ V^3 \\ W \\ S^1 \\ S^2 \\ S^3 \end{pmatrix}, \quad \mathcal{F}^{(1)} = n \begin{pmatrix} V^1 \\ F^{(0)} \\ 0 \\ 0 \\ S^1 \\ F^{(1)} \\ 0 \\ 0 \end{pmatrix}, \quad \mathcal{F}^{(2)} = n \begin{pmatrix} V^2 \\ 0 \\ F^{(0)} \\ 0 \\ S^2 \\ 0 \\ F^{(1)} \\ 0 \end{pmatrix}, \mathcal{F}^{(3)} = n \begin{pmatrix} V^3 \\ 0 \\ 0 \\ F^{(0)} \\ S^3 \\ 0 \\ 0 \\ F^{(1)} \end{pmatrix}$$

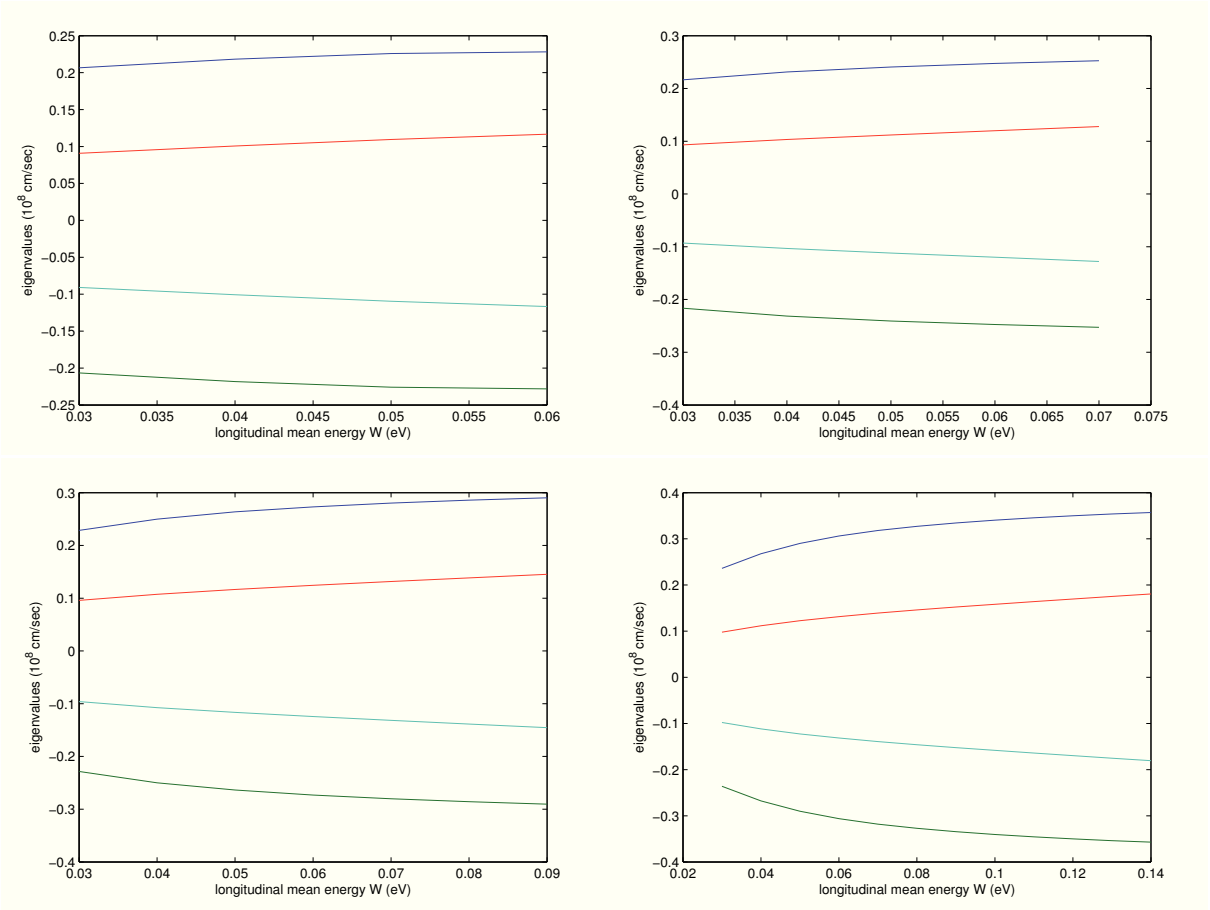

FIGURE 4.8: Plot of $\lambda_{3,4,5,6}$ versus the longitudinal mean energy for $E_T - \varepsilon_\nu = 0.125$ (upper left), 015 (upper right), 02 (bottom left), 03 (bottom right) eV. Note the range of the energy changes according to the discussion regarding λ_W.

and the Jacobian matrices are given by

$$\mathcal{A}^{(0)} = \begin{pmatrix} 1 & 0 & 0 & 0 & 0 & 0 & 0 & 0 \\ V^1 & n & 0 & 0 & 0 & 0 & 0 & 0 \\ V^2 & 0 & n & 0 & 0 & 0 & 0 & 0 \\ V^3 & 0 & 0 & n & 0 & 0 & 0 & 0 \\ W & 0 & 0 & 0 & n & 0 & 0 & 0 \\ S^1 & 0 & 0 & 0 & 0 & n & 0 & 0 \\ S^2 & 0 & 0 & 0 & 0 & 0 & n & 0 \\ S^3 & 0 & 0 & 0 & 0 & 0 & 0 & n \end{pmatrix},$$

$$\mathcal{A}^{(n)} = \sum_{i=1}^{2} n_i \mathcal{A}^{(i)} = \begin{pmatrix} \mathbf{n}\cdot\mathbf{V} & n_1 n & n_2\rho & n_3 n & 0 & 0 & 0 & 0 \\ n_1 F^{(0)} & 0 & 0 & 0 & n_1 n(F^{(0)})' & 0 & 0 & 0 \\ n_2 F^{(0)} & 0 & 0 & 0 & n_2 n(F^{(0)})' & 0 & 0 & 0 \\ n_3 F^{(0)} & 0 & 0 & 0 & n_3 n(F^{(0)})' & 0 & 0 & 0 \\ \mathbf{n}\cdot\mathbf{S} & 0 & 0 & 0 & 0 & n_1 n & n_2 n & n_3 n \\ n_1 F^{(1)} & 0 & 0 & 0 & n_1 n(F^{(1)})' & 0 & 0 & 0 \\ n_2 F^{(1)} & 0 & 0 & 0 & n_2 n(F^{(1)})' & 0 & 0 & 0 \\ n_3 F^{(1)} & 0 & 0 & 0 & n_3 n(F^{(1)})' & 0 & 0 & 0 \end{pmatrix},$$

where the prime denotes partial derivation respect to W. The equation

$$\det\left(\mathcal{A}^{(n)} - \lambda\mathcal{A}^{(0)}\right) = 0$$

gives the eigenvalues

$$\lambda_{1,2,3,4} = 0, \quad \text{with multiplicity } 4 \tag{4.52}$$

$$\lambda_{5,6,7,8} = \pm\sqrt{\frac{a(W) \pm \sqrt{a(W)^2 - 4b(W)}}{2}} \tag{4.53}$$

where, assuming the same notation of the previous case,

$$a(W) = F^{(0)} + (F^{(1)})' - W(F^{(0)})', \quad b(W) = F^{(0)}(F^{(1)})' - (F^{(0)})'F^{(1)}.$$

In Fig. 4.9 the eigenvalues $\lambda_{5,6,7,8}$ are plotted against the longitudinal mean energy W for several values of E_T. Since the four eigenvalues $\lambda_{5,6,7,8}$ are real and distinct, each of them has a corresponding eigenspace of dimension one.

Concerning the eigenvalue $\lambda = 0$, we use arguments similar to that used previously and, assuming $n_1 = 1, n_2 = n_3 = 0$, observe that

$$\det\begin{pmatrix} \mathbf{nV} & n_1 n & 0 & 0 \\ n_1 F^{(0)} & 0 & n_1 n(F^{(0)})' & 0 \\ \mathbf{nS} & 0 & 0 & n_1 n \\ n_1 F^{(1)} & 0 & n_1 n(F^{(1)})' & 0 \end{pmatrix} = n^3 b(W).$$

The fact that the eigenvalues $\lambda_{5,6,7,8}$ are real implies that $b(W) > 0$ and therefore the rank of $\mathcal{A}^{(n)}$ is four which means that the eigenspace associated to $\lambda = 0$ has dimension four, leading to the hyperbolicity of the system (4.48).

4.6 Energy-transport model

As seen in the previous section, the moment system closed wit MEP has a nice mathematical structure. However, from a computational point of view, it is still present some difficulty related in particular to the boundary conditions for the energy-flux and for the possible loss of regularity. We will give a formulation of energy-transport type which is more suited for a numerical integration.

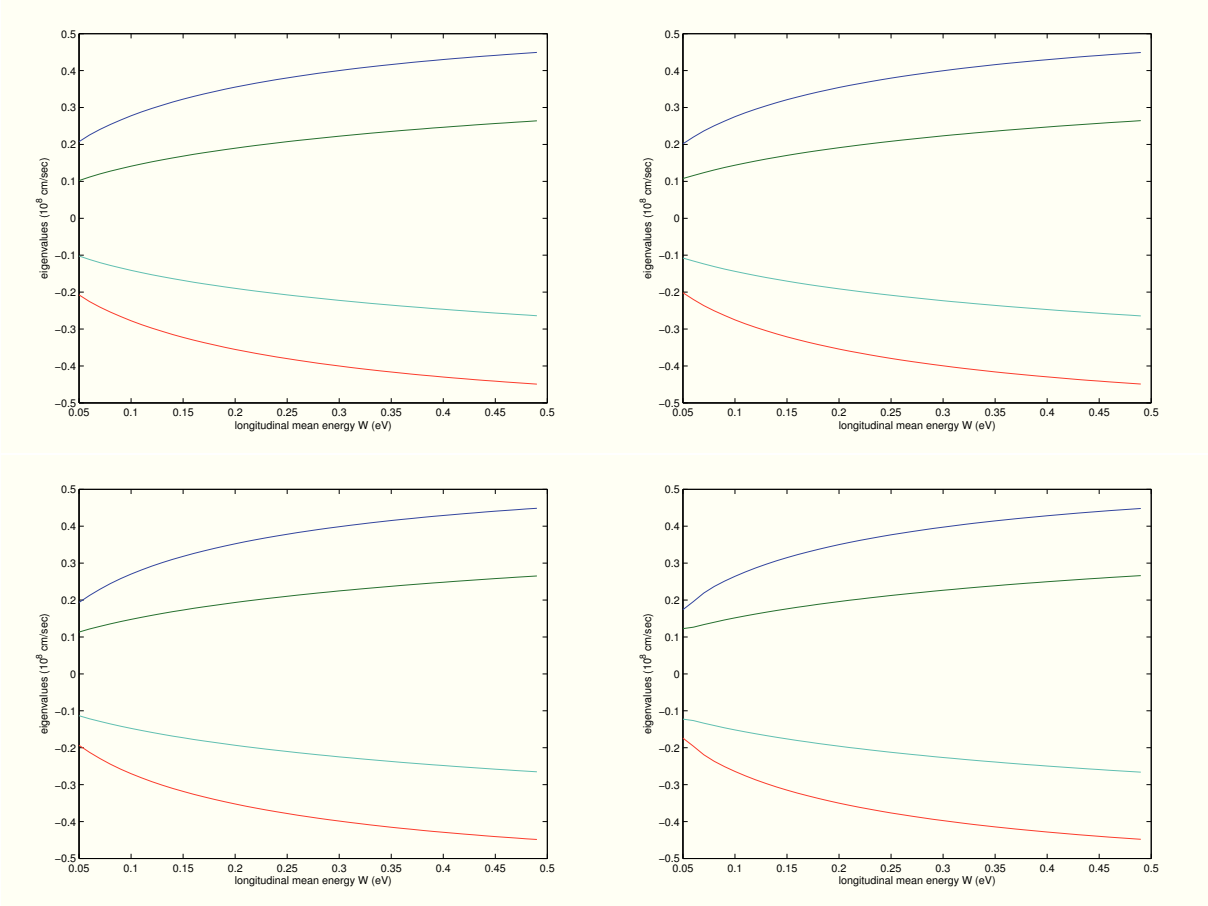

FIGURE 4.9: Plot of $\lambda_{3,4,5,6}$ versus the longitudinal mean energy for $E_T = 0.00$ (upper left), 0.10 (upper right), 0.20 (bottom left), 0.30 (bottom right) eV. Note the range of the energy changes according to the discussion regarding λ_W.

To derive an energy-transport model, let us assume as in [56, 59, 60] and according to the small anisotropy assumption that the following scaling holds

$$t = \mathcal{O}\left(\frac{1}{\delta^2}\right), \mathbf{r} = \mathcal{O}\left(\frac{1}{\delta}\right), \mathbf{V} = \mathcal{O}(\delta), \mathbf{S} = \mathcal{O}(\delta). \tag{4.54}$$

Then, by introducing this scaling into systems (4.25),(4.29) and equating to zero at the several orders in δ, one obtains again the balance equation for the superficial density and longitudinal mean energy in each subband along the balance equations of density and energy density for the 3DEG

$$\frac{\partial \rho^\nu}{\partial t} + \nabla_{\mathbf{r}_{||}} \cdot (\rho^\nu \mathbf{V}^\nu) + \rho^\nu L_0^\nu = \rho^\nu C_\rho^\nu(\mathbf{W}) \tag{4.55}$$

$$\frac{\partial (\rho^\nu \mathbf{W}^\nu)}{\partial t} + \nabla_{\mathbf{r}_{||}} \cdot (\rho^\nu \mathbf{S}^\nu) + \rho^\nu \mathbf{V}^\nu \cdot \nabla_{\mathbf{r}_{||}} \varepsilon_\nu + \rho^\nu L_1^\nu = \rho^\nu C_W^\nu(\mathbf{W}) \quad \nu = 1, 2, . \tag{4.56}$$

$$\frac{\partial n}{\partial t} + \nabla_{\mathbf{r}} \cdot (n\mathbf{V}) = nC_n(W) \tag{4.57}$$

$$\frac{\partial (nW)}{\partial t} + \nabla_{\mathbf{r}} \cdot (n\mathbf{S}) + n\mathbf{V} \cdot (q\mathbf{E}) = nC_W(W) \tag{4.58}$$

and the following constitutive equations for $\mathbf{V}^\nu$, $\mathbf{S}^\nu$, $\mathbf{V}$, $\mathbf{S}$

$$\nabla_{\mathbf{r}_{||}} \left(\rho^\nu F^{(0)\nu}\right) + \left(\rho^\nu G^{(0)\nu}\right) \cdot \nabla_{\mathbf{r}_{||}} \varepsilon_\nu = \rho^\nu C^\nu_{\mathbf{V}} \tag{4.59}$$

$$\nabla_{\mathbf{r}_{||}} \left(\rho^\nu F^{(1)\nu}\right) + \left(\rho^\nu G^{(1)\nu}\right) \cdot \nabla_{\mathbf{r}_{||}} \varepsilon_\nu = \rho^\nu C^\nu_{\mathbf{S}} \tag{4.60}$$

$$\nabla_{\mathbf{r}} \left(nF^{(0)}\right) + q\mathbf{E} \cdot \left(nG^{(0)}\right) = nC_{\mathbf{V}} \tag{4.61}$$

$$\nabla_{\mathbf{r}} \left(nF^{(1)}\right) + q\mathbf{E} \cdot \left(nG^{(1)}\right) = nC_{\mathbf{S}} \tag{4.62}$$

By rewriting the production terms of (4.59) and (4.60) in a compact form

$$\begin{pmatrix} C^\nu_{\mathbf{V}} \\ C^\nu_{\mathbf{S}} \end{pmatrix} = \begin{pmatrix} c^\nu_{11}(W^\nu) & c^\nu_{12}(W^\nu) \\ c^\nu_{21}(W^\nu) & c^\nu_{22}(W^\nu) \end{pmatrix} \begin{pmatrix} \mathbf{V}^\nu \\ \mathbf{S}^\nu \end{pmatrix} \tag{4.63}$$

$$\begin{pmatrix} C_{\mathbf{V}} \\ C_{\mathbf{S}} \end{pmatrix} = \begin{pmatrix} g_{11}(W) & g_{12}(W) \\ g_{21}(W) & g_{22}(W) \end{pmatrix} \begin{pmatrix} \mathbf{V} \\ \mathbf{S} \end{pmatrix} \tag{4.64}$$

with an obvious meaning of the coefficients $c^\nu_{ij}(W^\nu)$ and $g_{ij}(W)$, one gets a linear system with respect to $\mathbf{V}^\nu$, $\mathbf{S}^\nu$, $\mathbf{V}$, $\mathbf{S}$ which can be easily solved obtaining

$$\mathbf{V}^\nu = D^\nu_{11}(W)\nabla_{\mathbf{r}_{||}} \log \rho^\nu + D^\nu_{12}\nabla_{\mathbf{r}_{||}} W^\nu - D^\nu_{13}\nabla_{\mathbf{r}_{||}} \varepsilon_\nu \tag{4.65}$$

$$\mathbf{S}^\nu = D^\nu_{21}(W)\nabla_{\mathbf{r}_{||}} \log \rho^\nu + D^\nu_{22}\nabla_{\mathbf{r}_{||}} W^\nu - D^\nu_{23}\nabla_{\mathbf{r}_{||}} \varepsilon_\nu \tag{4.66}$$

$$\mathbf{V} = M_{11}\nabla_{\mathbf{r}} \log n + M_{12}\nabla_{\mathbf{r}} W - M_{13} q\mathbf{E} \tag{4.67}$$

$$\mathbf{S} = M_{21}\nabla_{\mathbf{r}} \log n + M_{22}\nabla_{\mathbf{r}} W - M_{23} q\mathbf{E} \tag{4.68}$$

where the coefficients D^ν_{ij} and M_{ij} are given by

$$D^\nu_{11} = \frac{c_{22}F^{(0)\nu} - c_{12}F^{(1)\nu}}{c^\nu}, \quad D^\nu_{12} = \frac{c_{22}(F^{(0)\nu})' - c_{12}(F^{(1)\nu})'}{c^\nu}, \quad D^\nu_{13} = \frac{c_{22}G^{(0)\nu} - c_{12}G^{(1)\nu}}{c^\nu}$$

$$D^\nu_{21} = \frac{c_{11}F^{(1)\nu} - c_{21}F^{(0)\nu}}{c^\nu}, \quad D^\nu_{22} = \frac{c_{11}(F^{(1)\nu})' - c_{21}(F^{(0)\nu})'}{c^\nu}, \quad D^\nu_{23} = \frac{c_{21}G^{(0)\nu} - c_{11}G^{(1)\nu}}{c^\nu}$$

$$M_{11} = \frac{g_{22}F^{(0)} - g_{12}F^{(1)}}{g}, \quad M_{12} = \frac{g_{22}M^{(0)'} - g_{12}F^{(1)'}}{g}, \quad M_{13} = \frac{g_{22}G^{(0)} - g_{12}G^{(1)}}{g}$$

$$M_{21} = \frac{g_{11}F^{(1)} - g_{21}F^{(0)}}{g}, \quad M_{22} = \frac{g_{11}F^{(1)'} - g_{21}F^{(0)'}}{g}, \quad M_{23} = \frac{g_{21}G^{(0)} - c_{11}G^{(1)}}{g}$$

with $c^\nu = c^\nu_{11}c^\nu_{22} - c^\nu_{12}c^\nu_{21}$ and $g = g_{11}g_{22} - g_{12}g_{21}$.

Equations (4.55)-(4.58) coupled with the Schrödinger-Poisson block along with the constitutive relations (4.65)-(4.68) represent our energy-transport model based on MEP (hereafter ET-MEP model) for the 2DEG\3DEG physical system. In the steady state case the original moment system and the ET-MEP model are equivalent at least for smooth solutions.

4.7 Mathematical properties of the ET-MEP model

In this section we analyse the mathematical structure of the ET-MEP model. As for the study of the hyperbolicity, the 2DEG and the 3DEG are treated separately.

4.7.1 2DEG ET-MEP subsystem

The main difference with respect to section 4.5 is that in the coefficients of the diffusion matrix the energy subbands ε_ν's and interaction integrals $G_{\nu\mu}$'s appear but they in general can be evaluated only numerically. To overcome the problem we consider two particular but significant cases where the solution of the Schrödinger equation is known [28, 63]: the infinite potential well, which is appropriate for a DG-MOSFET, and the triangular well, which is a reasonable approximation in the channel of a MOSFET.

In order to classify the ET equations, let us rewrite for each subband the system (4.55)-(4.56) as

$$\frac{\partial}{\partial t}\begin{pmatrix} \rho^\nu \\ \rho^\nu W^\nu \end{pmatrix} + \operatorname{div}\begin{pmatrix} (D_{11}^\nu - W^\nu D_{12}^\nu)\nabla\rho^\nu + D_{12}^\nu \nabla(\rho^\nu W^\nu) \\ (D_{21}^\nu - W^\nu D_{22}^\nu)\nabla\rho^\nu + D_{22}^\nu \nabla(\rho^\nu W^\nu) \end{pmatrix} + \text{r.t.} = \begin{pmatrix} 0 \\ 0 \end{pmatrix}$$

where r.t. stands for the remaining lower order derivative terms. We would like to show that the diffusion matrix

$$\hat{D}^\nu = \begin{pmatrix} D_{11}^\nu - W^\nu D_{12}^\nu & D_{12}^\nu \\ D_{21}^\nu - W^\nu D_{22}^\nu & D_{22}^\nu \end{pmatrix} \tag{4.69}$$

is negative definite, that is $\xi \cdot \hat{D}^\nu \xi < 0, \quad \forall \xi \in \mathbb{R}^2, \xi \neq (0,0)^T$. The elements of $\hat{D}^\nu$ indeed depend on the bottom of the subbands ε_ν and the interaction terms $G_{\nu\mu}$ through the envelope functions $\varphi_\nu(z)$, $\nu = 1, 2, 3, \ldots$.

- In the case of an infinite potential barrier, one has the explicit formulas

$$\varepsilon_\nu = \frac{\nu^2\pi^2\hbar^2}{2L_z^2 m^*}, \quad \varphi_\nu(z) = \sqrt{\frac{2}{L_z}}\sin\frac{\nu\pi}{L_z}(z - t_{ox}), \quad z \in [0, L_z], \quad \nu = 1, 2, \dots$$

  where L_z is the length of the confining direction

- In the case of a triangular potential well one has the explicit formulas [65]

$$\varepsilon_\nu = \hat{c}_\nu\varepsilon_0, \quad \varphi_\nu(z) = Ai\left(\frac{eFz - \varepsilon_\nu}{\varepsilon_0}\right), \quad z \in [0, L_z], \quad \nu = 1, 2, \dots$$

  where $eF = \frac{eV}{L_z}$ is the strength of the constant confining field, $\varepsilon_0 = \left[\frac{(eF\hbar)^2}{2m^*}\right]^{1/3}$ and $Ai(y)$ represents the Airy function of first type while the $\hat{c}_\nu$'s are its zeros with reverse sign. In particular we recall that $\hat{c}_1 = 2.338$, $\hat{c}_2 = 4.088$ and $\hat{c}_3 = 5.521$ [65].

By evaluating the eigenvalues of $\hat{D}^\nu$ with the previous expressions of the bottom energy and envelope functions of the first three subbands, one finds the results plotted in Fig.s 4.10 - 4.12. Of course additional subbands can be considered but as obtained in [26] the inclusion of more subbands is in many cases superfluous. For the relevant range of energy W^ν we have two distinct and real negative eigenvalues in each subband. Therefore *at least in the case of an infinite potential barrier or a triangular potential barrier, employing the first three subbands, the ET model is represented by two parabolic equations for each subband coupled to the Poisson equation in a suitable range of the longitudinal mean energy.*

4.7.2 3DEG ET-MEP model

Similarly to the 2DEG case, we rewrite the ET equations for the 3DEG as

$$\frac{\partial}{\partial t}\begin{pmatrix} n \\ nW \end{pmatrix} + \operatorname{div}\begin{pmatrix} (M_{11} - WM_{12})\nabla n + M_{12}\nabla(nW) \\ (M_{21} - WM_{22})\nabla n + M_{22}\nabla(nW) \end{pmatrix} + \text{r.t.} = \begin{pmatrix} 0 \\ 0 \end{pmatrix}.$$

Again one finds that the diffusion matrix

$$\hat{M} = \begin{pmatrix} M_{11} - WM_{12} & M_{12} \\ M_{21} - W^\nu M_{22} & M_{22} \end{pmatrix} \tag{4.70}$$

is negative definite, that is $\xi \cdot \hat{M} \cdot \xi < 0 \quad \forall \xi \in \mathbb{R}^2, \xi \neq (0,0)^T$, by a numerical inspection. The results are plotted in Fig. 4.13.

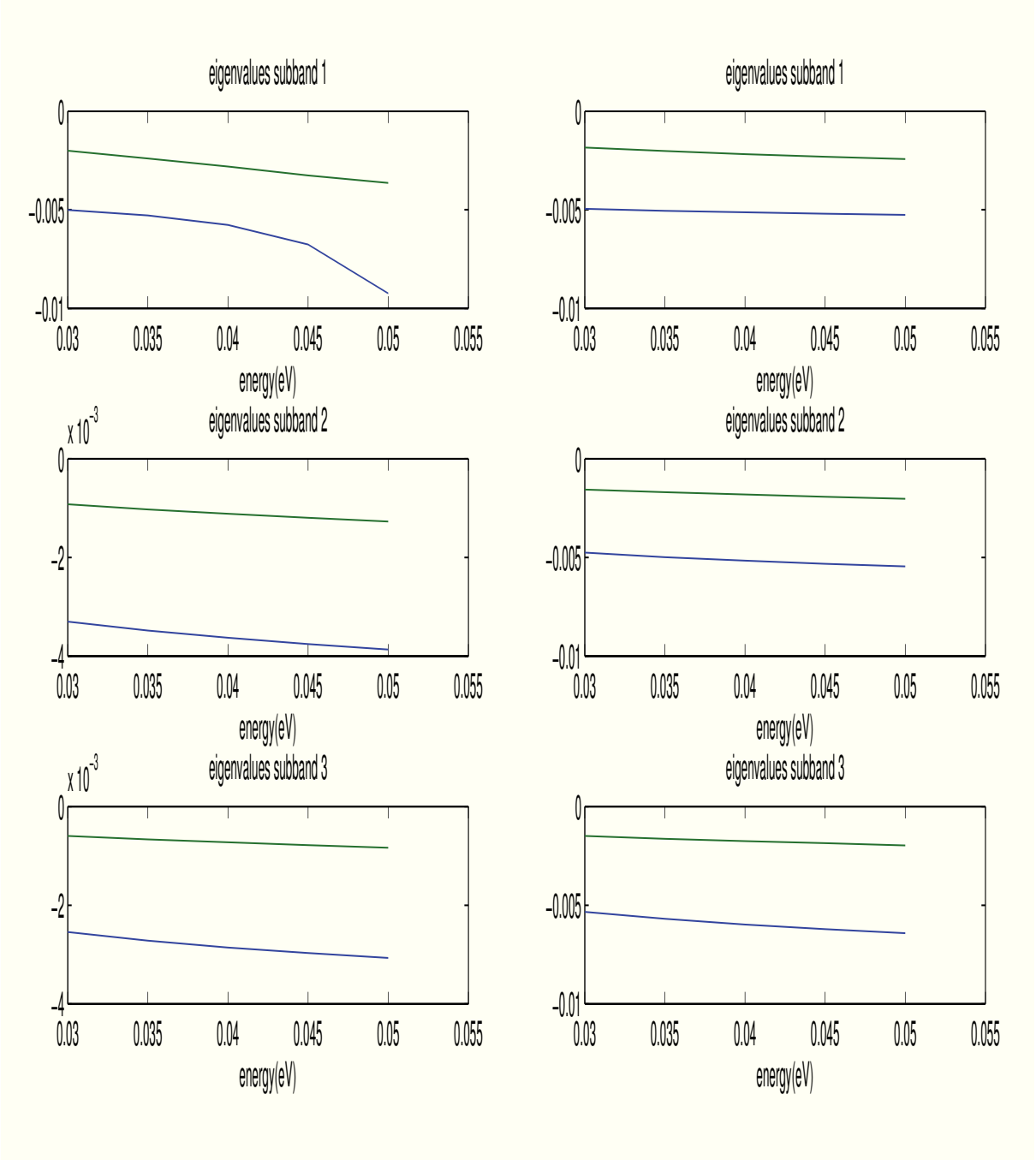

FIGURE 4.10: Eigenvalues of the matrix $\hat{D}^{\nu}$ for $\nu = 1, 2, 3$ versus the mean longitudinal energy. On the left column the case of the infinite potential well when $E_T - \varepsilon_\nu = 0.15$ eV and $L_z = 8$ nanometers. On the right column the case of the triangular potential well with $E_T - \varepsilon_\nu = 0.2$ eV , $L_z = 20$ nanometers and field strength $eF = 10$ eV/micron.

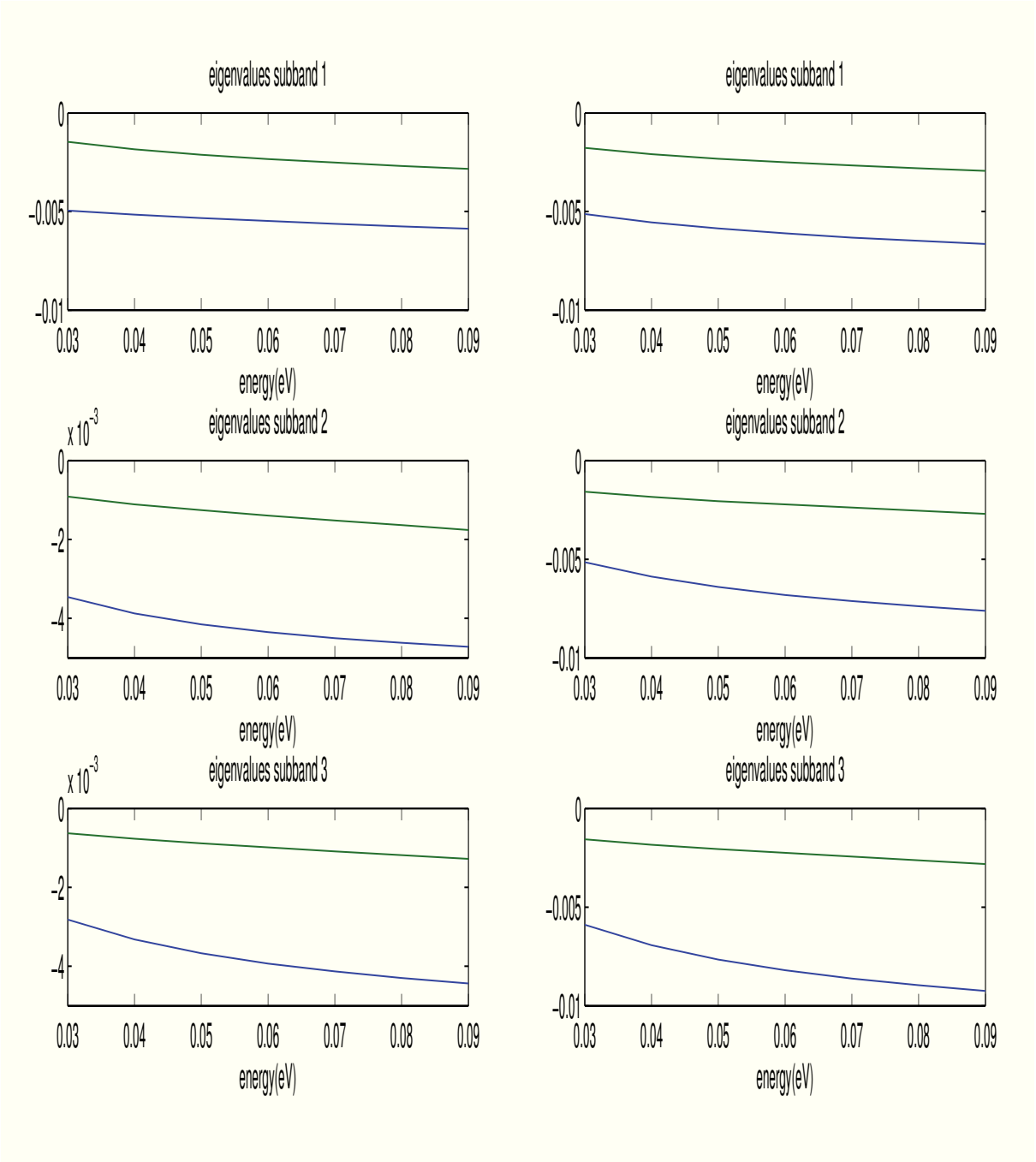

FIGURE 4.11: Eigenvalues of the matrix $\hat{D}^{\nu}$ for $\nu = 1, 2, 3$ versus the mean longitudinal energy. On the left column the case of the infinite potential well when $E_T - \varepsilon_\nu = 0.2$ eV and $L_z = 8$ nanometers. On the right column the case of the triangular potential well with $E_T - \varepsilon_\nu = 0.2$ eV , $L_z = 20$ nanometers and field strength $eF = 10$ eV/micron.

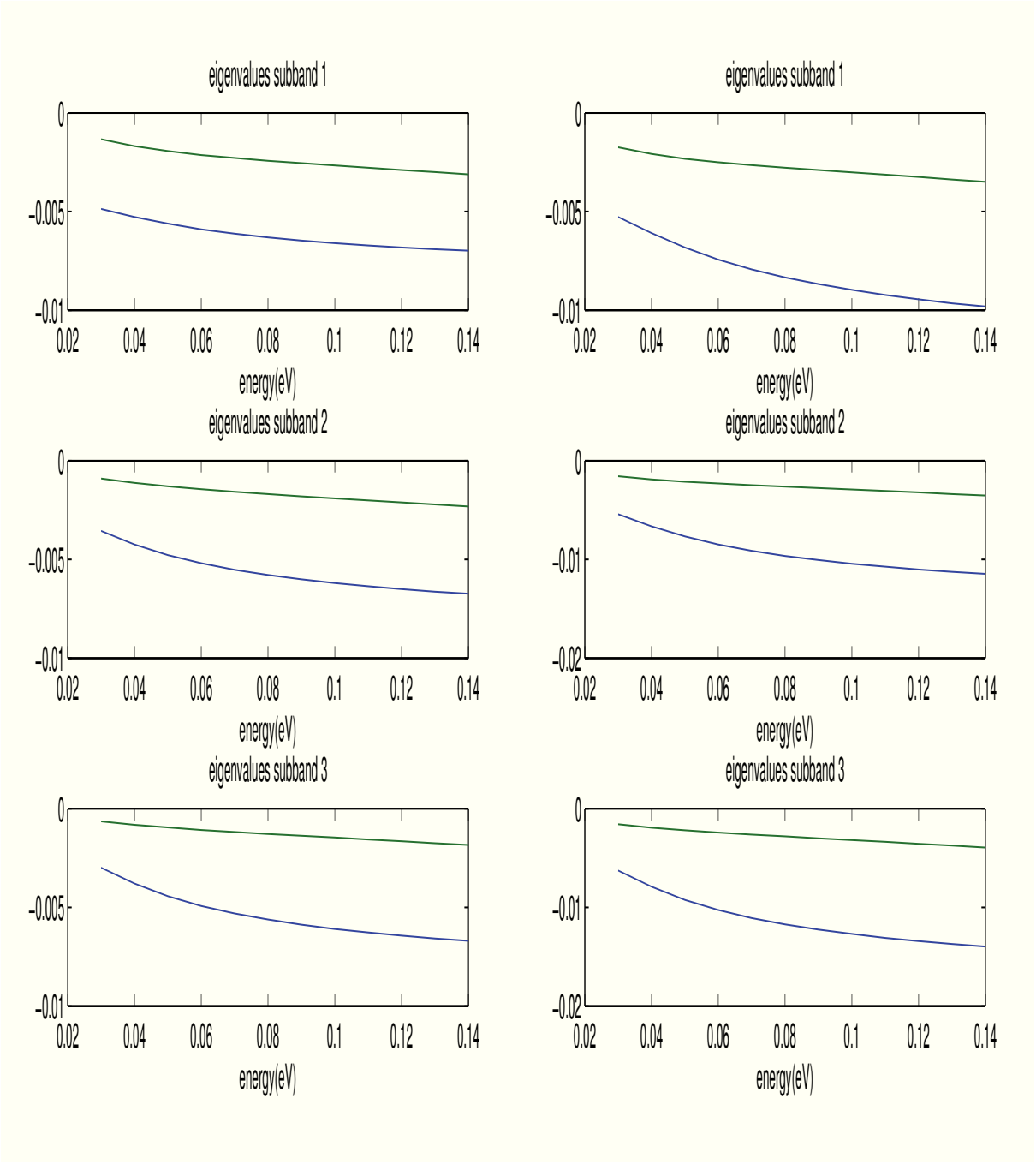

FIGURE 4.12: Eigenvalues of the matrix $\hat{D}^{\nu}$ for $\nu = 1, 2, 3$ versus the mean longitudinal energy. On the left column the case of the infinite potential well when $E_T - \varepsilon_\nu = 0.3$ eV and $L_z = 8$ nanometers. On the right column the case of the triangular potential well with $E_T - \varepsilon_\nu = 0.3$ eV , $L_z = 20$ nanometers and field strength $eF = 10$ eV/micron.

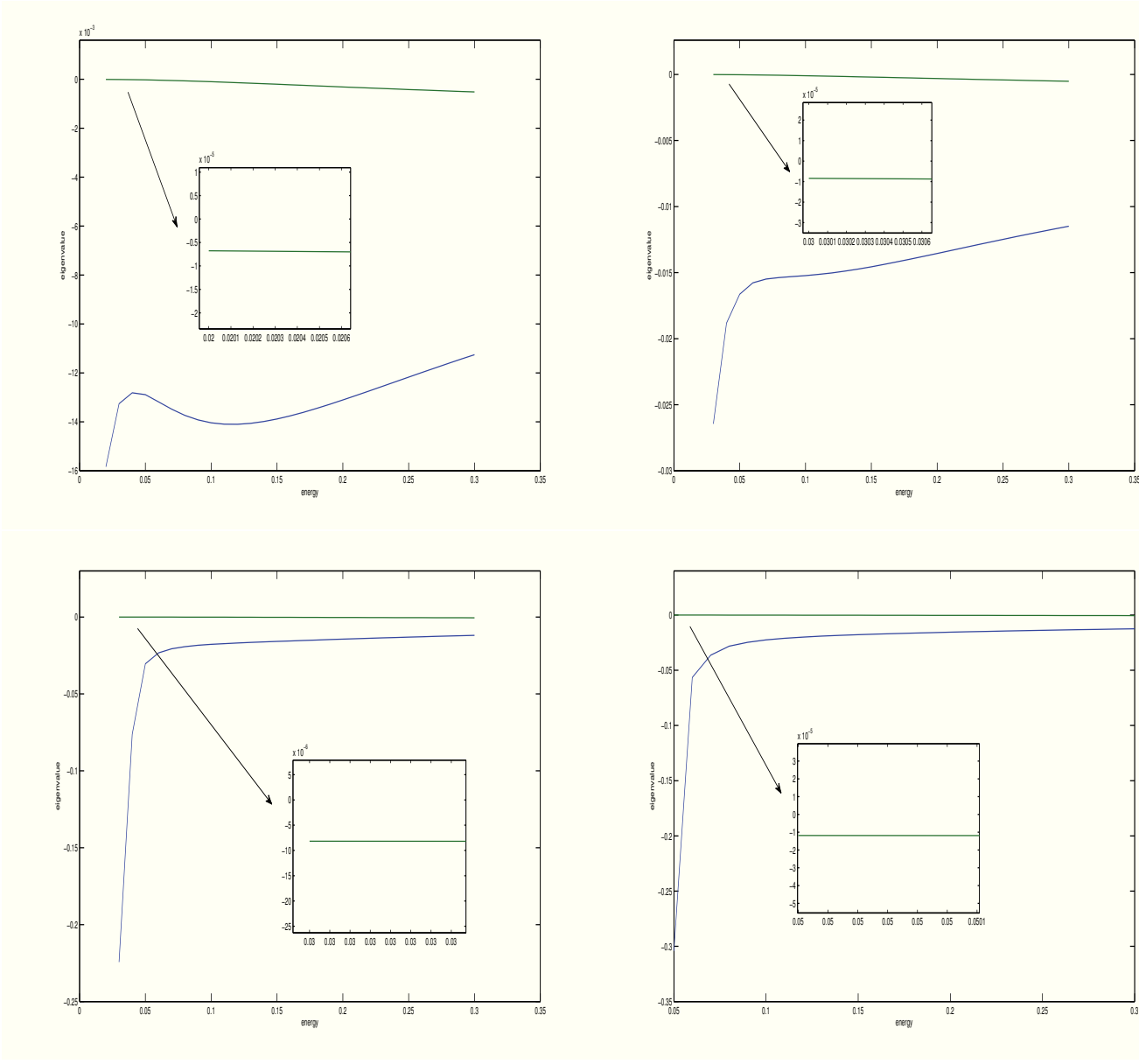

FIGURE 4.13: Eigenvalues of the matrix $\hat{M}$ versus the mean longitudinal energy for $E_T = 0.00$ (upper left), 0.10 (upper right), 0.20 (bottom left), 0.30 (bottom right) eV.

Appendix A

Closure relations for the parabolic case and physical parameters

In this Appendix, for the sake of self-consistency, we report the closure relations for the extra-fluxes and the production terms. Inserting expressions (3.5) into the constraints for the densities and the energies, one finds in polar coordinates

$$\rho^\nu = \int_0^{2\pi}\int_0^{+\infty} \exp\left(-\lambda^\nu - \lambda_W^\nu \frac{\hbar^2 k_{||}^2}{2m^*}\right) k_{||}\, dk_{||}\, d\phi,$$
$$\rho^\nu W^\nu = \int_0^{2\pi}\int_0^{+\infty} \frac{\hbar^2 k_{||}^2}{2m^*} \exp\left(-\lambda^\nu - \lambda_W^\nu \frac{\hbar^2 k_{||}^2}{2m^*}\right) k_{||}\, dk_{||}\, d\phi,$$

wherefrom $\lambda^\nu = -\log \dfrac{\hbar^2\,\rho^\nu}{2\pi m^* W^\nu}$ and $\lambda_W^\nu = \dfrac{1}{W^\nu}$.

Similarly, substituting (3.5) into the remaining constraints for the velocities and the energy-fluxes, one has

$$\lambda_{\mathbf{V}}^\nu = -\frac{3m^*}{W^\nu}\mathbf{V}^\nu + \frac{m^*}{(W^\nu)^2}\mathbf{S}^\nu, \quad \lambda_{\mathbf{S}}^\nu = \frac{m^*}{(W^\nu)^2}\mathbf{V}^\nu - \frac{m^*}{2(W^\nu)^3}\mathbf{S}^\nu.$$

Note the symmetry of the coefficients which reminds us of the Onsager [64] reciprocity conditions. The obtained distribution functions are used to get the needed closure relations for the fluxes and the production terms. For the fluxes we find

$$\mathbf{F}_{ij}^{(0)\nu} = \frac{1}{m^*}W^\nu\delta_{ij}, \quad \mathbf{F}_{ij}^{(1)\nu} = \frac{2}{m^*}(W^\nu)^2\mathbf{I},$$
$$\mathbf{G}_{ij}^{(0)\nu} = \frac{1}{m^*}\delta_{ij}, \quad \mathbf{G}_{ij}^{(1)\nu} = \frac{2}{m^*}(W^\nu)\mathbf{I},$$

with $\mathbf{I}$ the identity.

Concerning the production terms, for the acoustic phonon scattering one has

$$
\begin{aligned}
C_\rho^\nu &= \frac{2\pi m^*}{\hbar^2}\sum_{\mu=1}^{+\infty} C_{\nu\mu}\left[\frac{\rho_\mu}{\rho_\nu}\exp\left(-\frac{\Delta_{\nu\mu}+a_{\nu\mu}}{W^\mu}\right)-\exp\left(-\frac{a_{\nu\mu}}{W^\nu}\right)\right],\\
C_{\mathbf{V}}^\nu &= \frac{2\pi}{\hbar^2}\sum_{\mu=1}^{+\infty} C_{\nu\mu}\exp\left(\frac{-a_{\nu\mu}}{W^\nu}\right)\left[\lambda_{\mathbf{V}}^\nu\left(a_{\nu\mu}+W^\nu\right)+\lambda_{\mathbf{S}}^\nu\left(a_{\nu\mu}^2+2a_{\nu\mu}W^\nu+2(W^\nu)^2\right)\right],\\
C_W^\nu &= \frac{2\pi m^*}{\hbar^2}\sum_{\mu=1}^{+\infty} C_{\nu\mu}\left[\frac{\rho_\mu}{\rho_\nu}\exp\left(-\frac{\Delta_{\nu\mu}+a_{\nu\mu}}{W^\mu}\right)\left(a_{\nu\mu}+W^\mu\right)-\exp\left(-\frac{a_{\nu\mu}}{W^\nu}\right)\left(a_{\nu\mu}+W^\nu\right)\right],\\
C_{\mathbf{S}}^\nu &= \frac{2\pi}{\hbar^2}\sum_{\mu=1}^{+\infty} C_{\nu\mu}\exp\left(\frac{-a_{\nu\mu}}{W^\nu}\right)\left[\lambda_{\mathbf{V}}^\nu\left(a_{\nu\mu}^2+2a_{\nu\mu}W^\nu+2(W^\nu)^2\right)\right.\\
&\quad\left.+\lambda_{\mathbf{S}}^\nu\left(a_{\nu\mu}^3+3a_{\nu\mu}^2W^\nu+6a_{\nu\mu}(W^\nu)^2+6(W^\nu)^3\right)\right],
\end{aligned}
$$

where $\Delta_{\nu\mu}=\varepsilon_\nu-\varepsilon_\mu$, $a_{\nu\mu}=\max(0,\varepsilon_\mu-\varepsilon_\nu)$ and $C_{\nu\mu}=A^{(ac)}G_{\nu\mu}$.

For the non-polar optical phonon scattering one has

$$
\begin{aligned}
C_\rho^\nu &= \frac{2\pi m^*}{\hbar^2}\sum_{\mu=1}^{+\infty} D_{\nu\mu}N_{op}\left[\frac{\rho_\mu}{\rho_\nu}\left(\exp\left(\frac{\hbar\omega}{k_BT_L}-\frac{\Delta_{\nu\mu}^+ + a_{\nu\mu}^-}{W^\mu}\right)+\exp\left(-\frac{\Delta_{\nu\mu}^- + a_{\nu\mu}^+}{W^\mu}\right)\right)\right.\\
&\quad\left.-\exp\left(\frac{\hbar\omega}{k_BT_L}-\frac{a_{\nu\mu}^+}{W^\nu}\right)-\exp\left(-\frac{a_{\nu\mu}^-}{W^\nu}\right)\right],\\
C_{\mathbf{V}}^\nu &= \frac{2\pi}{\hbar^2}\sum_{\mu=1}^{+\infty} D_{\nu\mu}N_{op}\left[\lambda_{\mathbf{V}}^\nu\left(\exp\left(\frac{\hbar\omega}{k_BT_L}\right)\eta^{(1)}\left(\lambda_W^\nu,a_{\nu\mu}^+\right)+\eta^{(1)}\left(\lambda_W^\nu,a_{\nu\mu}^-\right)\right)\right.\\
&\quad\left.+\lambda_{\mathbf{S}}^\nu\left(\exp\left(\frac{\hbar\omega}{k_BT_L}\right)\eta^{(2)}\left(\lambda_W^\nu,a_{\nu\mu}^+\right)+\eta^{(2)}\left(\lambda_W^\nu,a_{\nu\mu}^-\right)\right)\right],\\
C_W^\nu &= \frac{2\pi m^*}{\hbar^2}\sum_{\mu=1}^{+\infty} D_{\nu\mu}N_{op}\left[\frac{\rho_\mu}{\rho_\nu}\left(\exp\left(\frac{\hbar\omega}{k_BT_L}-\frac{\Delta_{\nu\mu}^+}{W^\mu}\right)\eta^{(1)}\left(\lambda_W^\mu,a_{\nu\mu}^-\right)\right.\right.\\
&\quad\left.\left.+\exp\left(-\frac{\Delta_{\nu\mu}^-}{W^\mu}\right)\eta^{(1)}\left(\lambda_W^\mu,a_{\nu\mu}^+\right)\right)-\exp\left(\frac{\hbar\omega}{k_BT_L}\right)\eta^{(1)}\left(\lambda_W^\nu,a_{\nu\mu}^+\right)-\eta^{(1)}\left(\lambda_W^\nu,a_{\nu\mu}^-\right)\right],\\
C_{\mathbf{S}}^\nu &= \frac{2\pi}{\hbar^2}\sum_{\mu=1}^{+\infty} D_{\nu\mu}N_{op}\left[\lambda_{\mathbf{V}}^\nu\left(\exp\left(\frac{\hbar\omega}{k_BT_L}\right)\eta^{(2)}\left(\lambda_W^\nu,a_{\nu\mu}^+\right)+\eta^{(2)}\left(\lambda_W^\nu,a_{\nu\mu}^-\right)\right)\right.\\
&\quad\left.+\lambda_{\mathbf{S}}^\nu\left(\exp\left(\frac{\hbar\omega}{k_BT_L}\right)\eta^{(3)}\left(\lambda_W^\nu,a_{\nu\mu}^+\right)+\eta^{(3)}\left(\lambda_W^\nu,a_{\nu\mu}^-\right)\right)\right],
\end{aligned}
$$

where $a_{\nu\mu}^\mp=\max(0,\varepsilon_\mu-\varepsilon_\nu\mp\hbar\omega)$, $\Delta_{\nu\mu}^\pm=\varepsilon_\nu-\varepsilon_\mu\pm\hbar\omega$, $D_{\nu\mu}=A^{(no)}G_{\nu\mu}$ and

$$
\begin{aligned}
\eta^{(n)}(x,y) &= (-1)^n\, x\frac{d^n}{dx^n}\int_0^\infty e^{-x(t+y)}\,dt\\
&= x^{-1-n}\exp(-x\,y)\Gamma(n+1),\quad \text{for}\quad x>0,
\end{aligned}
$$

with Γ the gamma function.

TABLE A.1: Values of the physical parameters

m_e	electron rest mass	9.1095×10^{-28} g
m^*	effective electron mass	$0.32\ m_e$
T_L	lattice temperature	300 K
ρ	density	2.33 g/cm^3
v_s	longitudinal sound speed	9.18×10^5 cm/sec
Ξ_d	acoustic-phonon deformation potential	9 eV
ϵ_r	Si relative dielectric constant	11.7
ϵ_{r_O}	SiO_2 relative dielectric constant	3.9
ϵ_0	vacuum dieletric constant	8.85×10^{-18} C/V μm

TABLE A.2: Coupling constants and phonon energies for the inelastic scatterings in silicon

A	Z_f	$\hbar\omega$ (meV)	$D_tK(10^8$ eV/cm)
1	1	12	0.5
2	1	18.5	0.8
3	4	19.0	0.3
4	4	47.4	2.0
5	1	61.2	11
6	4	59.0	2.0

We remark that there are six types of non polar optical phonons (see Table A.2). The complete expression of the production terms is the sum of the contribution for each type of phonon. From the previous expressions it is straightforward to infer the elements c_{ij} appearing in the ET model for each subband.

Appendix B

Closure relations for the Kane case

By inserting the MEP distribution functions into the definitions of the fluxes and the production terms one gets the needed closure relations. Some relationships useful from a computational point of view are given in the Appendix C. For the *fluxes* we find

$$\mathbf{F}^{(i)\nu} = \frac{g(W^\nu)}{m^*}\left[\gamma_{1+i}(W^\nu,0) + \alpha\,\gamma_{2+i}(W^\nu,0)\right]\mathbf{I}, \qquad i=0,1, \tag{B.1}$$

$$\mathbf{G}^{(i)\nu} = i\,\mathbf{F}^{(0)\nu} + \frac{g(W^\nu)}{m^*}\left[\left(\frac{1}{\lambda_W^\nu}\right)^{i+1} - \zeta_{i+1}(W^\nu) - \alpha\,\zeta_{i+2}(W^\nu)\right]\mathbf{I}, \qquad i=0, \tag{B.2}$$

where $\mathbf{I}$ is the identity operator,

$$\gamma_n(x,y) := \int_0^\infty \frac{(t+y)^n}{1+2\,\alpha(t+y)}\exp\left[-\lambda_W(x)(t+y)\right]\,dt, \qquad n=0,1,\ldots, \tag{B.3}$$

defined for the values of y such that the integral there exists, and

$$\zeta_n(x) := \int_0^\infty \frac{2\alpha\,t^n}{(1+2\alpha t)^2}\exp\left(-\lambda_W(x)\,t\right)\,dt = -2\alpha\left(n\gamma_n(x,0) - \lambda_W\gamma_{n+1}(x,0)\right). \tag{B.4}$$

Concerning the production terms, for the *acoustic phonon scattering* one has

$$C^\nu_{W_{(i)}} = \frac{2\pi m^*}{\hbar^2}\sum_{\mu=1}^{+\infty} C_{\nu\mu}\left[\frac{\rho_\mu g(W^\mu)}{\rho_\nu}\exp\left(-\Delta_{\nu\mu}\lambda_W^\mu\right)B^{(i)}(W^\mu,a_{\nu\mu},\Delta_{\nu\mu}) - g(W^\nu)B^{(i)}(W^\nu,a_{\nu\mu},\Delta_{\nu\mu})\right], \tag{B.5}$$

$$C^\nu_{\mathbf{V}_{(i)}} = \frac{2\pi\,g\,(W^\nu)}{\hbar^2}\sum_{\mu=1}^{+\infty} C_{\nu\mu}\left\{\lambda^\nu_{\mathbf{V}}\left[\eta^{(1+i)}(W^\nu,a_{\nu\mu},\Delta_{\nu\mu})\right] + \lambda^\nu_{\mathbf{S}}\left[\eta^{(2+i)}(W^\nu,a_{\nu\mu},\Delta_{\nu\mu})\right]\right\}, \quad i=0,1, \tag{B.6}$$

where $W_{(0)} = \rho,\ W_{(1)} = W,\ \mathbf{V}_{(0)} = \mathbf{V},\ \mathbf{V}_{(1)} = \mathbf{S},\ \Delta_{\nu\mu} = \varepsilon_\nu - \varepsilon_\mu,\ a_{\nu\mu} = \max(0, \varepsilon_\mu - \varepsilon_\nu)$, and $C_{\nu\mu} = A^{(ac)} G_{\nu\mu}$. The functions $B^{(i)}$ are given by

$$B^{(i)}(x,y,z) := \int_0^\infty (t+y)^i \exp\left(-\lambda_W(x)\,(t+y)\right)\left(1+2\alpha(t+y)\left[1+2\alpha\,(t+y+z)\right]\right)\,dt$$

$$= \sum_{j=0}^{i} (-1)^j \exp\left(-\lambda_W(x)\,y\right) \begin{pmatrix} i \\ i-j \end{pmatrix} \left.\frac{\partial^j p\,(\lambda_W, y, z)}{\partial \lambda_W^j}\right|_{\lambda_W = \lambda_W(x)} y^{i-j}, \quad i = 0, 1, . \tag{B.7}$$

with

$$p\,(x,y,z) = \frac{8\alpha^2}{\lambda_W^3(x)} + \frac{4\alpha\,(1+\alpha\,(2y+z))}{\lambda_W^2(x)} + \frac{\left[1+2\alpha\,(2y+z)+4\alpha^2\left(y^2+yz\right)\right]}{\lambda_W(x)}.$$

The functions $\eta^{(n)}(x,y,z)$ are defined by

$$\eta^{(n)}(x,y,z) = (1+2\,\alpha\,z)\gamma_n(x,y) + (3\,\alpha + 2\,\alpha^2\,z)\gamma_{n+1}(x,y) + 2\,\alpha^2\gamma_{n+2}(x,y). \tag{B.8}$$

Regarding the *non-polar optical phonon scattering* one has

$$C^\nu_{W_{(i)}} = \frac{2\pi m^*}{\hbar^2} N_{op} \sum_{\mu=1}^{+\infty} D_{\nu\mu} \left\{ \frac{\rho_\mu}{\rho_\nu}\, g\,(W^\mu) \left[\exp\left(\frac{\hbar\omega}{k_B T_L} - \Delta^+_{\nu\mu}\lambda^\mu_W\right) B^{(i)}\left(W^\mu, a^-_{\nu\mu}, \Delta^+_{\nu\mu}\right) \right.\right.$$
$$\left. + \exp\left(-\Delta^-_{\nu\mu}\lambda^\mu_W\right) B^{(i)}\left(W^\mu, a^+_{\nu\mu}, \Delta^-_{\nu\mu}\right)\right] - g(W^\nu)\left[\exp\left(\frac{\hbar\omega}{k_B T_L}\right) B^{(i)}\left(W^\nu, a^+_{\nu\mu}, \Delta^-_{\nu\mu}\right)\right.$$
$$\left.\left. + B^{(i)}\left(W^\nu, a^-_{\nu\mu}, \Delta^+_{\nu\mu}\right)\right]\right\}, \tag{B.9}$$

$$C^\nu_{\mathbf{V}_{(i)}} = \frac{2\pi}{\hbar^2} N_{op}\, g\,(W^\nu) \sum_{\mu=1}^{+\infty} D_{\nu\mu} \left\{ \lambda^\nu_{\mathbf{V}} \left[\eta^{(1+i)}\left(W^\nu, a^-_{\nu\mu}, \Delta^+_{\nu\mu}\right) + \exp\left(\frac{\hbar\omega}{k_B T_L}\right) \eta^{(1+i)}\left(W^\nu, a^+_{\nu\mu}, \Delta^-_{\nu\mu}\right)\right]\right.$$
$$\left. + \lambda^\nu_{\mathbf{S}} \left[\eta^{(2+i)}\left(W^\nu, a^-_{\nu\mu}, \Delta^+_{\nu\mu}\right) + \exp\left(\frac{\hbar\omega}{k_B T_L}\right) \eta^{(2+i)}\left(W^\nu, a^+_{\nu\mu}, \Delta^-_{\nu\mu}\right)\right]\right\}, \qquad i = 0, 1, \tag{B.10}$$

where $a^\mp_{\nu\mu} = \max(0, \varepsilon_\mu - \varepsilon_\nu \mp \hbar\omega),\ \Delta^\pm_{\nu\mu} = \varepsilon_\nu - \varepsilon_\mu \pm \hbar\omega,\ D_{\nu\mu} = A^{(no)} G_{\nu\mu}$.

Appendix C

Useful computational relations

In this section some formulas which allow a fast evaluation of the functions $\gamma_n(x,y)$ are presented, along with the physical parameters present in the model. Recalling the definition

$$\gamma_n(x,y) := \int_0^\infty \frac{(t+y)^n}{1+2\,\alpha(t+y)} \exp\left[-\lambda_W(x)(t+y)\right]\, dt, \qquad n=0,1,\ldots, \tag{C.1}$$

and noting that

$$\gamma_n(x,y) = (-1)^n \frac{\partial^n}{\partial\,\lambda_W^n} \int_0^\infty \frac{1}{1+2\,\alpha(t+y)} \exp\left[-\lambda_W\,(t+y)\right]\, dt \Big|_{\lambda_W=\lambda_W(x)},$$

one has

$$\gamma_1(x,y) = -\frac{1}{2\alpha}\gamma_0(x,y) + \frac{\exp\left(-\lambda_W(x)\,y\right)}{2\alpha\lambda_W(x)},$$

and by recursion the following formula is obtained

$$\gamma_n(x,y) = \left(\frac{1}{2\alpha}\right)^{n+1}\gamma_0(x,y) + \frac{1}{2\alpha}\left(\sum_{i=0}^{n-1}\left(\frac{1}{2\alpha}\right)^{n-i}\sum_{k=0}^{i}\frac{i!}{k!}\frac{y^k}{\left(\lambda_W(x)\right)^{i-k}}\right)\frac{e^{-\lambda_W(x)y}}{\lambda_W(x)} \tag{C.2}$$

In particular, γ_0 can be expressed in terms of the exponential integral

$$E_n(x') := \int_1^\infty \frac{\exp\left(-x'\,t\right)}{t^n}\, dt, \quad n=0,1,\ldots.$$

as

$$\gamma_0(x,y) = \frac{1}{2\alpha}\exp\left(\frac{\lambda_W(x)}{2\alpha}\right) E_1\left(\frac{\lambda_W(x)}{2\overline{y}}\right),$$

with $\overline{y} = \dfrac{\alpha}{1+2\alpha y}$.

We remark that there are six types of non polar optical phonons (see Table A.2). The complete expression of the production terms is the sum of the contribution for each type of phonon. From the previous expressions it is straightforward to infer the elements c_{ij} appearing in the ET model for each subband.

Bibliography

[1] C. Kittel: Introduction to Solid State Physics 8th edition, John Wiley & Sons (2005)

[2] A. Jungel: Transport Equations for Semiconductors, Springer (2009)

[3] C. Jacoboni: Theory of Electron Transport in Semiconductors, Springer (2010)

[4] J.J. Sakurai: Meccanica Quantistica Moderna, Zanichelli (1996)

[5] Datta, S.: Quantum Phenomena, Vol. VIII of the Modular Series on Solid State Devices. Addison-Wesley Publishing (1989)

[6] Datta, S.: Electronic Transport in Mesoscopic Systems. Cambridge University Press (1999)

[7] Polizzi, E., Ben Abdallah, N.: Subband decomposition approach for the simulation of quantum electron transport in nanostructures. J. Comput. Phys. **202(1)**, 150–180 (2004)

[8] Galler, M., Schuerrer, F.: A deterministic Solver to the Boltzmann-Poisson System Including Quantization Effects for Silicon-MOSFETs, in: Progress in Industrial Mathematics at ECMI 2006, Series: Mathematics in Industry, Springer 531-536 (2008)

[9] Ben Abdallah, N., Caceres, M.J., Carrillo, J.A., Vecil,F.: A deterministic solver for a hybrid quantum-classical transport model in nanoMOSFETs. J. Comp. Phys. **228**, 6553 (2009)

[10] Romano, V.: Nonparabolic band hydrodynamical model of silicon semiconductors and simulation of electron devices. Math. Meth.

[11] Mascali, G., Romano, V.: Si and GaAs mobility derived from a hydrodynamical model for semiconductors based on the maximum entropy principle. Physica A **352**, 459-476 (2005)

[12] Mascali, G., Romano, V.: A hydrodynamical model for holes in silicon semiconductors: The case of non-parabolic warped bands. Math. and Comp. Mod. **53(01-2)**, 213–229 (2011)

[13] Jüngel, A.: Transport Equations for Semiconductors, Lect. Notes in Phys. 773. Springer (2009)

[14] Nishibara, S., Suzuki, M.: Hierarchy of semiconductor equations: relaxation limits with initial layers for large initial data, MSJ Memoirs 26. Mathematical Society of Japan (2011)

[15] Ren, Z.: Nanoscale MOSFETs:Physics, Simulation, and Design. PhD thesis, Purdue University, West Lafayette (2001)

[16] Blokhin, A., Tkachev, D.: Local-in-time well-posedness of a regularized mathematical model for silicon MESFET. Zeitschrift fr Angewandte Mathematik und Physik (ZAMP) **61 (5)**, 849–864 (2010)

[17] Romano, V.: 2D numerical simulation of the MEP energy-transport model with a finite difference scheme. J. of Computational Physics, **221** 439 (2007)

[18] M.V. Fischetti and S.E. Laux "Monte Carlo study of electron transport in silicon inversion layers", Physical Review B, **48** (1993)

[19] Mascali, G., Romano, V.: Hydrodynamic subband model for semiconductors based on the maximum entropy principle. IL NUOVO CIMENTO C **33**, 155 (2010)

[20] Mascali, G., Romano, V.: A non parabolic hydrodynamical subband model for semiconductors based on the maximum entropy principle. Mathematical and Computer Modeling **55 (3-4)** (2012)

[21] Jaynes, E. T.: Information Theory and Statistical Mechanics. Phys. Rev. B **106**, 620 (1957)

[22] Jaynes, E. T.: Probability theory, the logic of science, Cambridge University Press (2010)

[23] Shannon, C.E.: A mathematical theory of communication, Bell System Technical Journal, **27**, 379-623 (1948)

[24] Mascali, G., Romano, V.: Simulation of Gunn Oscillations with a Non-Parabolic Hydrodynamical Model Based on the Maximum Entropy Principle. Compel **24(1)**, 35–54 (2005)

[25] La Rosa, S., Mascali, G., Romano, V.: Exact maximum entropy closure of the hydrodynamical model for Si semiconductors: the 8-moment case. SIAM J. Appl. Math. **70**, 710 (2009)

[26] Camiola V.D., Mascali G., Romano V. "Numerical simulation of a double-gate MOSFET with a subband model for semiconductors based on the maximum entropy principle. Continuum Mechanics and Thermodynamics" **70**, 710 (2011)

[27] Camiola V.D., Mascali G., Romano V. "Simulation of a double-gate MOSFET by a non-parabolic energy-transport model for semiconductors based on the maximum entropy principle ", to appear in MCM (2012)

[28] Datta, S.: Quantum Phenomena, Vol. VIII of the Modular Series on Solid State Devices. Addison-Wesley Publishing (1989)

[29] Datta, S.: Electronic Transport in Mesoscopic Systems. Cambridge University Press (1999)

[30] Ando, T., Fowler, A. B., Stern, F.: Electronic properties of two-dimensional systems. Rev. Mod. Phys. **54**, 437–672 (1982)

[31] Polizzi, E., Ben Abdallah, N.: Self-consistent three dimensional models for quantum ballistic transport in open systems. Phys. Rev. B **66**, 245301-1–245301-9 (2002)

[32] Degon, P., Jüngel, A., Pietra, P.,: Numerical discretization of energy-transport models for semiconductors with non-parabolic band structure. SIAM J. Sci. Comput. **22**,986-1007 (2000)

[33] Polizzi, E., Ben Abdallah, N.: Subband decomposition approach for the simulation of quantum electron transport in nanostructures. J. Comput. Phys. **202(1)**, 150–180 (2004)

[34] Galler, M., Schuerrer, F.: A deterministic Solver to the Boltzmann-Poisson System Including Quantization Effects for Silicon-MOSFETs, in: Progress in Industrial Mathematics at ECMI 2006, Series: Mathematics in Industry, Springer 531-536 (2008)

[35] Ben Abdallah, N., Caceres, M.J., Carrillo, J.A., Vecil,F.: A deterministic solver for a hybrid quantum-classical transport model in nanoMOSFETs. J. Comp. Phys. **228**, 6553 (2009)

[36] De Falco, C., Gatti, E., Lacaita, A., Sacco, R.: Quantum-corrected drift-diffusion models for transport in semiconductor devices. J. Comp. Physics **204**, 533 (2004)

[37] C. de Falco, C., Jerome, J. W., Sacco, R.: Quantum Corrected Drift–Diffusion Models: Solution Fixed Point Map and Finite Element Approximation. J. Comp. Phys., **228**, 1770-1789 (2009).

[38] Ben Abdallah, N., Méhats, F.,Vauchelet, N.: Diffusive transport of partially quantized particles: existence, uniqueness and long-time behaviour. Proc. Edinb. Math. Soc. **2 (49)**, 513–549 (2006)

[39] Muscato, O, Di Stefano, V.: Hydrodynamic modeling of silicon quantum wires. J. Comp. Electr. **11**, 45-55, (2012), DOI 10.1007/s10825-012-0381-3

[40] Bonilla, L L., Barletti, L., Alvaro, M.: Nonlinear electron and spin transport in semiconductor superlattices. SIAM J. Appl. Math. **69(2)**, 494513 (2008).

[41] Anile, A.M., Mascali, G.: Theoretical foundations for tail electron hydrodynamical models in semiconductors. Applied Mathematics Letters, **14 (2)**, 245–252 (2001)

[42] G. D. Mahan, Many Particles Physics, Kluwer Academic/Plenum Publishers (2000).

[43] H. J. W. Haug and A.-P. Jauho, Quantum Kinetics in Transport and Optics of Semiconductors, Springer (2008).

[44] Wang, J., Polizzi, E., Lundstrom, M.: A three dimensional quantum simulation of silicon nanowire transistors with the effective-mass approximation. J. Appl. Phys. **96**, 2192–2203 (2004)

[45] Chen, D., Wei, G.-W.: Modeling and simulation of electron structure, material interface and random doping in nano-electronic devices. J. Comp. Phys. **229**, 4431–4460 (2010)

[46] Markowich, P., Ringhofer, C. A., Schmeiser, C.: Semiconductor Equations. Springer, Wien (1990)

[47] Jüngel, A.: Transport Equations for Semiconductors, Lect. Notes in Phys. 773. Springer (2009)

[48] Romano, V.: Quantum corrections to the semiclassical hydrodynamical model of semiconductors based on the maximum entropy principle. J. Math. Phys. **48**, 123504 (2007)

[49] Fischetti, M. V.: Master equation approach to the study of electronic transport in small semiconductor devices. Phys. Rev. B **59**, 4901–4917 (1999)

[50] Wu, N.: The Maximum Entropy Method. Springer-Verlag, Berlin (1997)

[51] Anile, A. M., Romano, V.: Non parabolic band transport in semiconductors: closure of the moment equations. Continuum Mech. Thermodyn. **11**, 307 (1999)

[52] Romano, V.: Non parabolic band transport in semiconductors: closure of the production terms in the moment equations. Cont. Mech. Thermodyn. **12**, 31 (2000)

[53] Anile, A. M., Muscato, O., Romano, V.: Moment equations with Maximum Entropy closure for carrier transport in semiconductor devices: validation in bulk silicon. VLSI DESIGN, **10**, 335-354, (2000)

[54] Muscato, O., Romano, V.: Simulation of submicron silicon diodes with a non-parabolic hydrodynamical model based on the maximum entropy principle. VLSI DESIGN, **13**,273-279, (2001)

[55] Mascali, G., Romano, V.: Hydrodynamical model of charge transport in GaAs based on the maximum entropy principle. Cont. Mech. Thermodyn. **14**, 405 (2002)

[56] Mascali, G., Romano, V.: Si and GaAs mobility derived from a hydrodynamical model for semiconductors based on the maximum entropy principle. Physica A **352**, 459-476 (2005)

[57] Mascali, G., Romano, V., Sellier, J.M.: MEP parabolic hydrodynamical model for holes in silicon semiconductors. NUOVO CIMENTO DELLA SOCIETA ITALIANA DI FISICA B, **120(2)**, 197–215 (2005)

[58] Muscato, O.: Validation of an Extended Hydrodynamic model for a submicron *npn* Bipolar Junction Transistor. Physica A, **365**(2) pp. 409–428, (2006)

[59] Mascali, G., Romano, V.: A hydrodynamical model for holes in silicon semiconductors: The case of non-parabolic warped bands. Math. and Comp. Mod. **53(01-2)**, 213–229 (2011)

[60] Romano, V.: Nonparabolic band hydrodynamical model of silicon semiconductors and simulation of electron devices. Math. Meth. Appl. Sciences **24**, 439-471 (2001)

[61] Junk M., Romano v.: Maximum entropy moment system of the semiconductor Boltzmann equation using Kanes dispersion relation. Continuum Mech. Thermodyn. 17: 247267 (2005)

[62] La Rosa, S.: Hydrodynamical Models for Si Semiconductors Based on the Maximum Entropy Principle, PhD Thesis (2008)

[63] Lundstrom, M.: Fundamentals of Carrier Transport. Cambridge University Press (2000)

[64] Muscato, O.: The Onsager reciprocity principle as a check of consistency for

[65] Davies, J.H.: The physics of low-dimensional semiconductors, Cambridge University Press (200)

[66] Majorana A., Muscato O., Milazzo C.,: Charge transport in 1D silicon devices via Monte Carlo simulation and Boltzmann Poisson solver. COMPEL **23**(2), 410-425 (2004)

[67] Müller, I., Ruggeri, T.: Rational Extended Thermodynamics. Springer

[68] Jou, D., Casas-Vazquez, J., Lebon, G.: Extended Irreversible